UiT The Arctic University of Norway

Faculty of Science and Technology

Department of Geoscience

Reconstruction of the Kråknes landslide event, Alta.

Stina Mari Pettersen

GEO-3900 *Master's thesis in Geology, May 2021.*

Abstract

On June 3rd, 2020 a major quick clay landslide occurred at Kråknes in Alta municipality, Northern Norway. The landslide event destroyed eight buildings and was estimated to be 650 meters wide and 40 meters high. Two days later, another landslide occurred, this time causing the old E6 road above the previous landslide area to slip out towards the sea. People lost cabins and other valuable possessions, but there were no casualties.

Landslide events in sensitive clay along the Norwegian coastline pose a threat to coastal communities and infrastructure and have frequently caused fatalities and damage throughout recent history. To avoid and prepare for potential landslide disasters, it is crucial to study and understand the development of sensitive clay landslides. In this study, the Kråknes landslide in Alta, Northern Norway has been reconstructed based on field observations, geotechnical data and numerical modeling in DAN3D to gain insight into the sequence of events and better understand and prepare for potential landslide events in the future.

The results show that the topography and stratigraphy of Kråknes make the area unstable and sensitive to external forces due to alternating permeable and impermeable layers in a moderately dipping fjord sequence created by the ice sheets during deglaciation and exposed by isostatic uplift. This stratigraphy provides good conditions for groundwater flow and the creation of highly sensitive clay and weak layers when exposed to excess pore pressure. Human activity has further increased the instability through loading of fill material during the construction of a cabin in 2015. After heavy amounts of snowfall during winter season 2019/2020, hydrometric data show that the ground was up to 100% saturated due to snowmelt in the days prior to the landslide. The high amounts of meltwater caused an increase in the pore water pressure in the already unstable study area and initially triggered the landslide event.

Two scenarios on how the landslide event occurred are proposed and simulated in DAN3D, where one is initiated below sea level and the other is initiated above sea level. Based on the results, it is concluded that the landslide was triggered on land as a progressive landslide, which continued to retrogress backward and laterally in several slabs. The rapid deposition

of landslide mass on the seafloor initiated an underwater slide, which later caused further retrogression on land due to lack of support from the buttressing mass in front.

The expansion of residential areas and infrastructure below the marine limit can cause drastic changes in the stability of areas with sensitive clay. With the ongoing climate change we see today, the shifts in temperature and rain and snow patterns may increase the amount of groundwater compared to previous years. In fjords, the stratigraphies' ability to feed already unstable slopes with high amounts of groundwater should therefore be examined closely before constructions are made that could create weak layers and shear bands.

Acknowledgments

Finally, five years of school and hard work have come to an end.

First of all, I would like to thank my supervisor Louise M. Vick for all her guidance and feedback throughout this process. I appreciate how you have shared your knowledge and motivated me along the way. I would also like to thank Anders Bjørdal (NVE) for taking the time to show us around the study area and sharing his photos, videos and knowledge of the landslide area. A special thanks to student colleague Torgrim Sandnes for a fun week in Alta during fieldwork and our many discussions throughout the year.

A very special thanks go to my family for their support and motivating words through many years of school. I am particularly grateful for how you all have taken extra care of Emrik the last year so I could focus extra on school and work. We are both very fortunate and beyond grateful to have you.

I also have to thank my fellow students for many unforgettable memories through five years of rocks, thin sections, field trips, reports, coffee breaks, beers, etc. I will cherish them forever!

Last but not least, I have to thank Kenneth, for letting me focus on school for five years while you have worked your ass off to pay the bills while renovating the house and being the best dad and boyfriend. I could not have done it without you!

Stina Mari Pettersen

Tromsø, May 2021.

Table of Contents

Abbreviations

ASCII   American Standard Code For Information Interchange

asl   above sea level

bsl   below sea level

DAN3D   Dynamical Analysis in 3D

DEM   Digital Elevation Model

GIS   Geographical Information System

LGM   Last glacial maximum

LL   Liquid Limit

ML   Marine Limit

NGI   Norwegian Geotechnical Institute

NGU   Geological Survey of Norway

NVE   Norwegian Water Resources and Energy Directorate

PL   Plastic Limit

SVV   Norwegian Public Roads Administration

SL   Shrinkage Limit

YD   Younger Dryas

1 Introduction

Quick clay landslides are initiated when sensitive clay is disturbed, such as by erosion or overloading, causing the initial firm clay structure to collapse and liquefy. Landslides with sensitive clay or quick clay are a significant environmental challenge in Norway. They are capable of destroying buildings and infrastructure, making them an economical and societal threat. About 5,000 km^2 of Norway is covered in marine clay deposits, and it is estimated that 20% of these areas consist of highly sensitive or quick clay (Kalsnes et al., 2014).

Reconstructing previous landslide events is essential for the understanding and prediction of future landslides. However, the information from older landslide events is often missing or unreliable (Oven et al., 2019). Reconstructing recent landslide events provides insight into the failure and runout mechanisms and makes it easier to obtain new information that can later help predict the outcome of potential landslides.

On June 3rd, 2020, a major quick clay landslide occurred at Kråknes in Alta municipality, Northern Norway. The landslide event destroyed eight buildings and was estimated to be 650 m wide and 40 m high. Two days later, another landslide event occurred, this time causing the old E6 road above the previous landslide area to slip out towards the sea (Figure 1). People lost cabins and other valuable possessions, but there were no casualties. The event was preceded by extraordinary volumes of snowmelt and clear signs of instability prior to the landslide. Questions arose regarding the trigger of the slope failure and whether it was human-induced or natural. Questions also arose regarding the sequence of events and initial failure point, as material was removed from both above and below sea level. This thesis was conducted concurrently with masters student Torgrim Sandnes. While Sandnes investigated the causes of instability and geotechnical conditions, this thesis rather focuses of the sequence of events and landslide characteristics. The work was also conducted at the same time as a national consortium investigated the landslide. This consortium was composed of experts from official bodies and consultants. Some of the data was supplied by the investigation team, but this work can be considered academic and independent of their findings.

Figure 1 The Kråknes landslide area on June 7th, 2020 (Photo courtesy of Anders Bjoerdal, NVE).

1.1 Objectives

The objective of this thesis was to reconstruct the landslide events which occurred at Kråknes between 3-6th June 2020. This was done by mapping the landslide characteristics, deposits and topography, and determining the sequence of events and landslide propagation properties.

The main research questions answered in this thesis are:

1. How did the landslide occur, and what was the sequence of events leading up to and during the sliding?
2. What is the volume of the failed landslide masses, and where did it initiate (above or below sea level)?
3. How has the landscape changed since the event, and what does the new landscape tell us about the landslide characteristics (e.g., exposed sliding surfaces, drainage pathways, etc.)?

The tasks undertaken in this thesis to answer the research questions included:

- Mapping of the landslide area and sediments in the field.

- Analysis of lidar and bathymetry data from before and after the event to reconstruct the landslide events above and below the water level.
- Analysis of geotechnical data to determine factors that promote instability.
- Construct cross-sections through the landslide area based on field observations and geotechnical data for a deeper understanding of the site conditions.
- Conduct runout modeling of the landslide above and below water level with Dan3D for back analysis.

1.2 Geographical setting and climate

Kråknes is located in the western part of the municipality of Alta, a city in Troms and Finnmark County in Northern Norway (Figure 2). It is 125 km NE of Tromsø, situated on the major Altafjord system, 70°01'40.6" N and 23°03'52.9" E. It is a west-facing beach area in the northern part of the Talvik peninsula. The area is a glacial landscape with an average 1:6 slope towards the northwest and the beach zone (Corner et al., 1990; Waldeland, 2020). About 40 km east of Kråknes, the 249 km long Alta river meets the Alta fjord with the 5 km wide Alta delta (Askheim, 2020). This is one of several watercourses in the area.

The landslide occurred at Flatstrand, a lower-lying beach about 400 m long surrounded by the higher elevated Storhaugen (100 m asl) in the east and the Vintersetnes water (167.5m asl) in the south. Kråkvikdalen (valley) is in the southeast and shapes the upslope area above Flatstrand (Figure 2). Surface water drains from the surrounding mountains into Kråkvikdalen, where it subsequently drains towards Flatstrand. Before the landslide occurred, there were eight cabins and one permanent inhabitant at the site (Figure 3A). Small tractor roads connect the building to the Kråknes Road, which is the main road in the area. The former E6 road used to pass through Kråknes (Now Kråknes Road), but was realigned through a tunnel further east between 2013-2016. In Figure 3, the study area from both before and after the landslide event can be seen.

The climate varies throughout Troms and Finnmark County. Along the coast, it is predominantly a maritime climate. The winters tend to be mild, while the summers are cool. The warmest month is July, when the average temperature is around 14°C. July is also the month

with the most rainfall, with an average amount of 32.8 mm, while the yearly amount is 270.8 mm. The coldest month is February, with temperatures down to -7°C (CustomWeather, 2020).

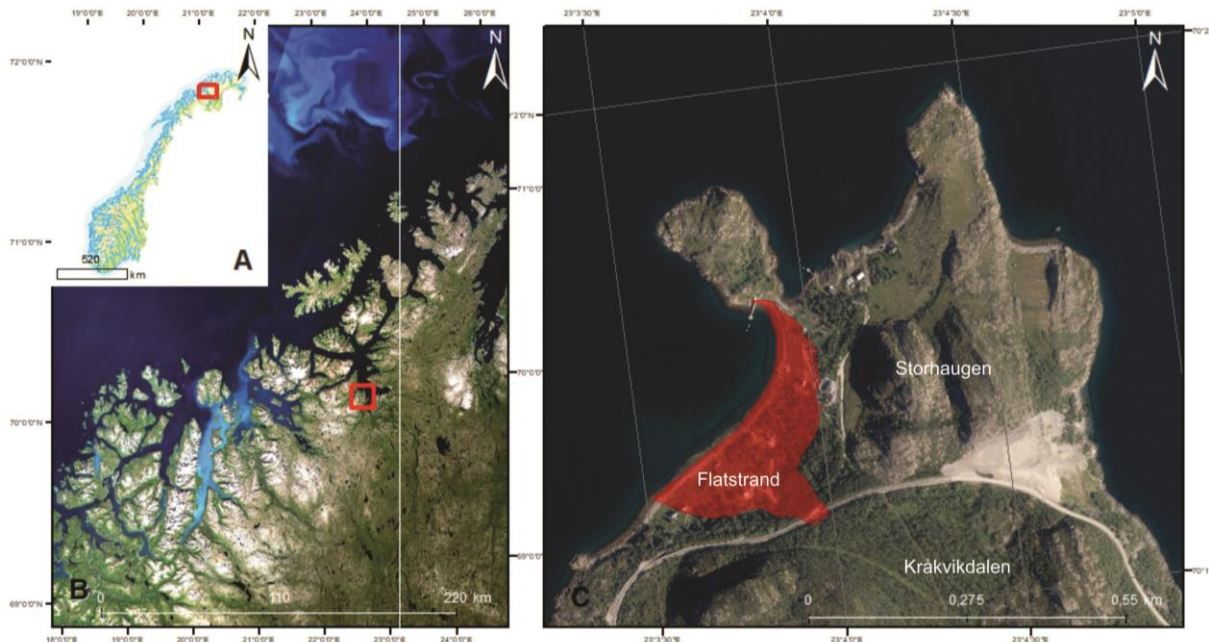Figure 2) Map of Norway with the Alta area marked by a red square B) Orthographic image of Troms and Finnmark County, the Kråknes peninsula indicated by the red square. C) Orthographic photo of Kråknes from 2018. The red polygon indicates the landslide area (obtained from Kartverket, 2018)
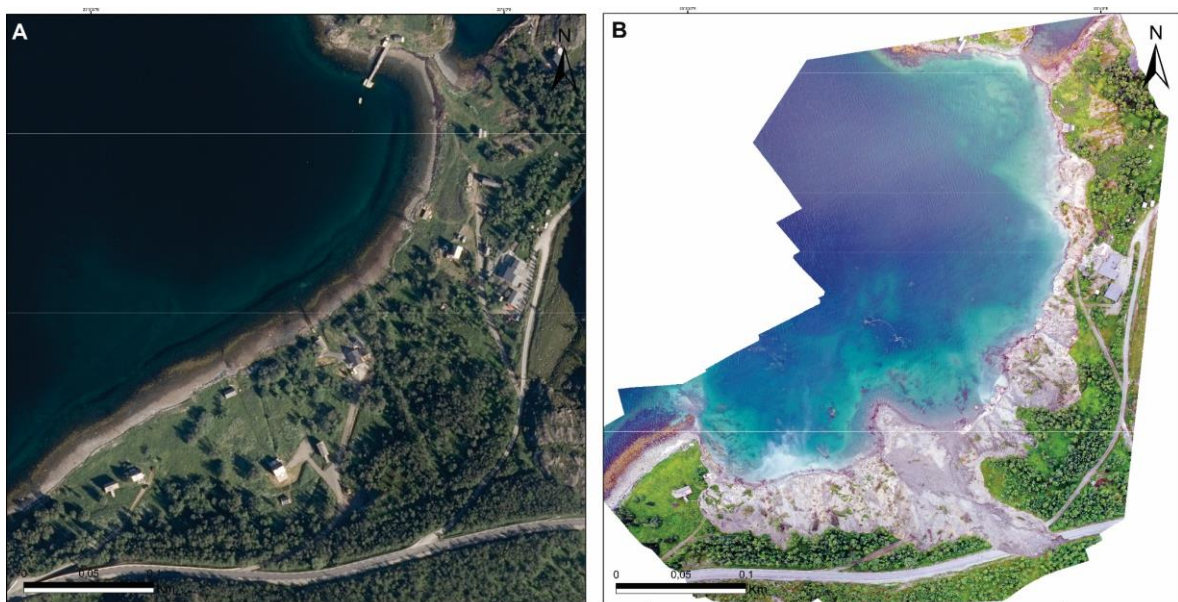

Figure 3 A) The study area before the landslide (Kartverket, 2018). B) The study area after the landslide.

1.3 Previous events in Troms and Finnmark

Due to the paraglacial setting of northern Norway, sensitive glaciomarine sediments are abundant around the coastline. Several landslide events in sensitive clay have occurred in areas close to Kråknes (Figure 4) and are briefly described below.

Figure 4 Locations of different landslide events in sensitive clay that have occurred close to Kråknes.

1.3.1 Indre Sokkelvik and Sørkjosen

A quick clay landslide occurred in Indre Sokkelvik, Nordreisa municipality in 1959. During road construction six months prior to the landslide event, a 7.5 m heigh embankment fill was placed close to the shore, which caused the area to become unstable. The landslide event was later triggered due to high amounts of rainfall and meltwater in the area that increased the pore pressure in the ground. A total of 17 out of 29 inhabitants along the bay in Sokkel-vika were taken by the landslide, and 9 of them perished (L'Heureux et al., 2017). Figure 5 shows the 12 m high and 600 m long landslide scarp after the event. The landslide also triggered a tsunami that caused waves up to 5 m heigh to hit Sørkjosen, 5 km away from Indre Sokkelvik (Furseth, 2013). A similar landslide event happened again 60 years later in Sørkjosen, three km south of Indre Sokkelvik. This landslide event started when a newly built pier disappeared into the fjord after intense rainfall (Austefjord, 2016). A road was destroyed in the event, but there were no casualties (Aspaker, 2019).

Figure 5 Picture of the landslide scar in the northernmost part of Sokkelvik captured in 1959 (L'Heureux et al., 2017).

1.3.2 Lyngseidet

Another recent landslide event happened at Lyngseidet in Lyngen municipality in 2010. The landslide event started in the tidal zone and retrogressed backward over several days. It was found to be triggered by unsanctioned filling during constuction. The landslide evolved over time, where several buildings, construction vehicles, cars, and parts of the highway slid out into the ocean. Up to 1000 m^3 of landslide masses slid out and left a bowl-shaped scarp (Figure 6). One resident was taken in his house, but later rescued from his attic by helicopter. A new highway was later established through the slide area, and security measures were made for the inhabitants in the area (Hoseth et al., 2014).

Figure 6 Quick clay landslide at Lyngseidet in 2010 (Hoseth et al., 2014)

1.3.3 Store Lerresfjord

In March 1975, a sensitive clay landslide occurred in Store Lerresfjord in Alta county. The event was initiated on the shoreline before it triggered a sub-marine landslide in the fjord. Several people were caught in the landslide and there were three casualties. The landslide caught a fish farm in the debris and dragged it from the beach zone towards the middle of the fjord (Furseth, 2013).

1.3.4 Kviby

In July 2010, a sensitive clay landslide occurred in Kviby in Altamunicipality. Kviby is located on the opposite side of Altafjorden from Kråknes. The landslide occurred after heavy rainfall in the area. Five acres of land were destroyed and three residential buildings lost road connection. The high amounts of rainfall which triggered the slide also triggered rockfall which impacted a road in Store Lerresfjord, 45 kilom away (NVE, 2020).

1.4 Geological background

1.4.1 Bedrock

In the northwestern part of Finnmark, Precambrian bedrock is covered by Caledonian thrust nappes. The thrust nappe has been uplifted and eroded, allowing the Precambrian basement to be exposed in the Alta-Kvænangen tectonic window (Ramberg et al., 2013). The peninsula in which Kråknes is located is within the Alta-Kvænangen window, and consists of bedrock from the Kvenvikformation in the lower Raipas Group. The Kvenvik formation is dominated by metabasalt with areas of metagabbro, basaltic tuff and tuffite (Figure 5A). South and west of Kråknes, there is the presence of dolomite and limestone that is stromatolite-bearing and has layers of siltstone, which is part of the lower Kvenvik greenschist belt (Zwaan & Gautier, 1980). The Kvenvikformation is mapped in detail by Zwaan and Gautier (1980) south of Kråknes. Here the foliation strikes NNW-SSE. Current lidar data suggests that this trend spans the area around Kråknes. The layering is cut by other faults oriented E-W and ENE-WSW (Indrevær, 2020) (Figure 5B). These trends are consistent with large normal faults mapped in the Altafjord (Koehl et al., 2019). In Figure 7A and B the bedrock and interpreted structures are mapped.
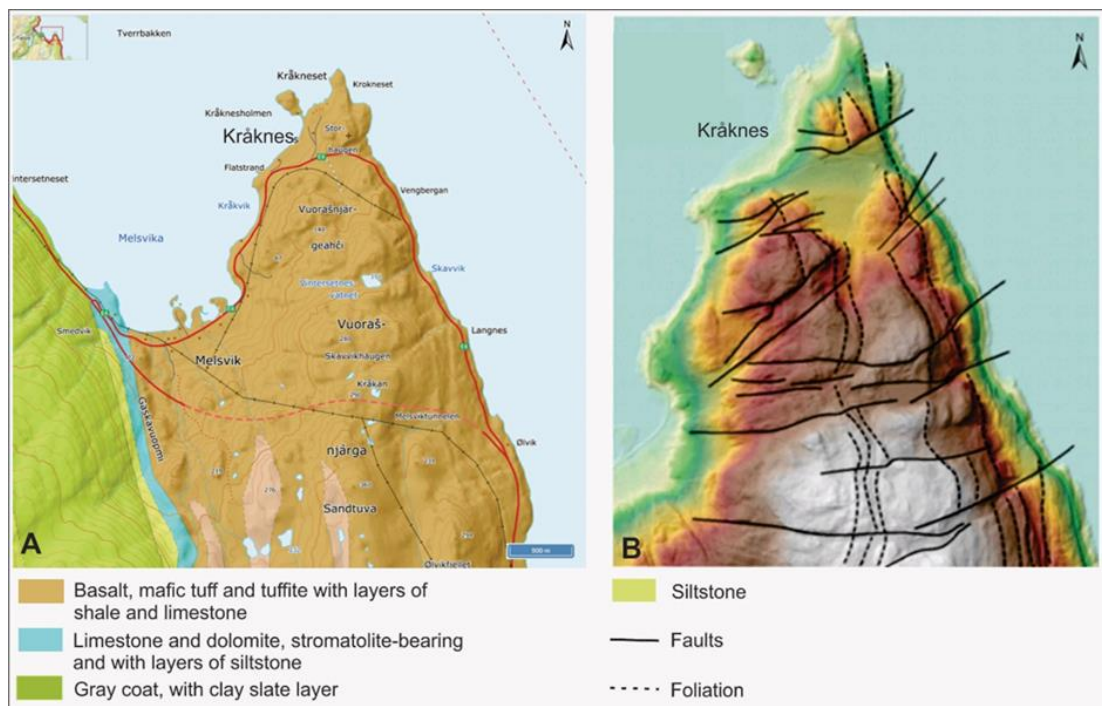

Figure 7 A) Bedrock lithology in the study area (NGU, 2015a). B) Bedrock structures in the study area from lidar-data (Indrevær, 2020).

1.4.2 Quaternary geology

Knowing the Quaternary geology in the study area is essential to understand the landscape and deposits present today. Marine clay is a glaciomarine sediment that is common in Scandinavia because of processes and formations that occurred during the Quaternary period from 2.6 million years ago until present time. From the beginning of the Quaternary period until 11 600 years ago, there were several cycles of dramatic climate change on earth. The climate cycles varied between cold glacial periods and warmer interglacial periods that characterize the Quaternary period (Ramberg et al., 2013).

The last glaciation

During the last glacial cycle, the Fennoscandian Ice Sheet united with the Barents Sea Ice Sheet and reached its possible maximum around 22 000-19 000 years ago north of the study area. Around 17 000 years BP, the ice sheet started to retreat rapidly in the west, and about 15 000 years BP, the southern Barents Sea was completely ice-free (Vorren & Laberg, 1996).

The most recent glaciation (the Weichselian) took place between 117 000 and 11 500 years ago. This is the glacial cycle that is responsible for most of the quaternary features and depositional landforms that are found in Norway today (Ramberg et al., 2013). A significant amount of land in the Northern hemisphere was covered by glaciers up to several times during this period. The most extensive distribution of glaciers happened 18 000 years ago during the last glacial maximum (LGM) when the edge of the Fennoscandian Ice Sheet reached from the continental shelf outside Norway through Denmark, Germany and into Poland, and then through the Baltic states into European Russia (Lowe & Walker, 2015) (Figure 7A).

A significant period of ice retreat occurred between 15 000 and 12 000 years ago, at which point most of the Norwegian coast was considered ice-free. The ice advanced again until 11 500 years ago, during the Younger Dryas (YD). Large YD end moraines were deposited at the ice-margin and represent a temporary break in the melting process or the maximum extent of the glacier at the time (Figure 6B). The melting of the ice sheet continued, and 10 000 years ago the ice sheet had melted away entirely (Sigmond et al., 2013).
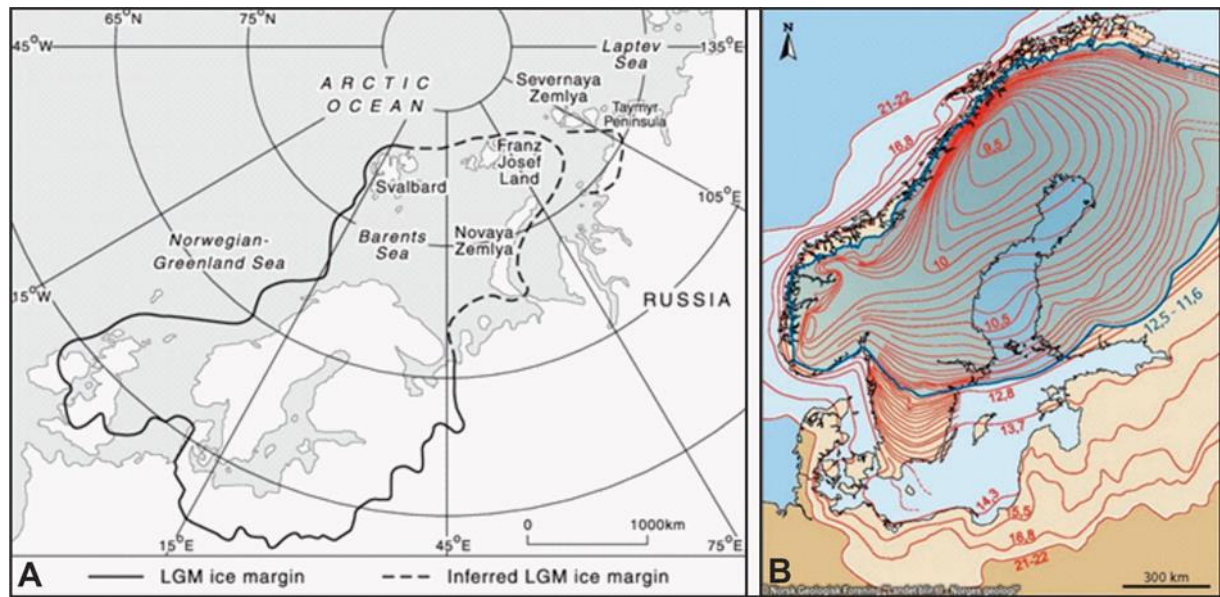
Figure 8 A) Map showing the Eurasian ice sheet during LGM (Illustrated by Siegert and Dowdeswell 2004 as detailed by Svendsen et al. 1999.) B) Map of Scandinavia showing the edge of the Fennoscandian ice sheet during deglaciation. The numbers indicate the age in a thousand calendar years. The 12.5-11.6 line marks the outer limit of the ice sheet during YD (Ramberg et al. 2013).

Local deglaciation

Three significant deglaciated ice-marginal position of the Fennoscandian Ice Sheet has been dated at the coast of Finmark based on dated ice-deposits and raised shoreline features (Marthinussen 1961; Sollid et al. 1973; Landvik et al. 1998). These indicate three glacial stages: the Porsanger stage at 14 000 years BP, the Reppafjord stage at 13 000 years BP, and the YD at 11 500 years BP(Landvik et al., 1998; Romundset et al., 2011, 2017). Kråknes is located north of the YD end moraine, suggesting that the YD stage most likely never reached Kråknes (Figure 9) which implies that Kråknes became ice-free between 13 000 and 11 500 years ago. The direction of movement of the ice around the study area is interpreted based on furrows (erosion tracks) and drumlins and indicates an N-NW movement of ice towards Kråknes (Figure 10). As the ice withdrew, the sea level rose due to isostatic adjustment. When the ice melted, the continent started to rise to compensate for the loss of weight from the ice. The relative sea-level fell, bringing glacier deposits from the marine environment asl. The uplift is still ongoing today, and the land rises about 2 mm per year in the area (Romundset et al., 2011).
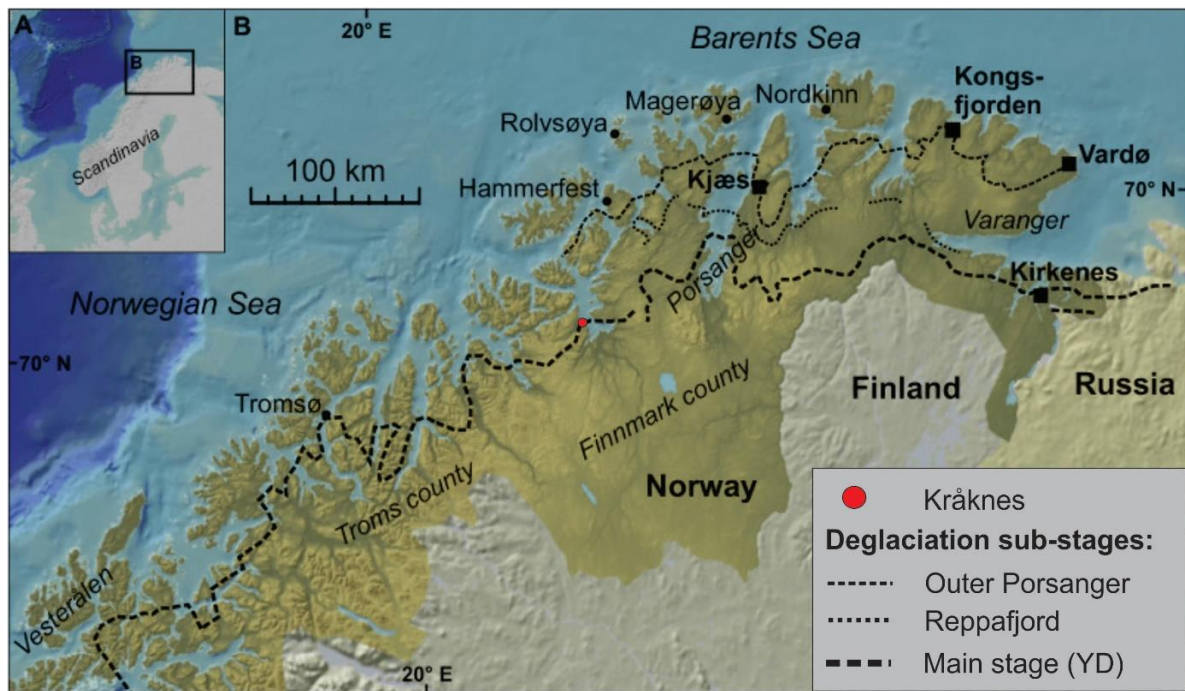
Figure 9 Map of the main deglaciation sub-stages of the Fennoscandian Ice Sheet in Northern Norway. Kråknes is located within the red circle B) Map of where the Fennoscandian Ice Sheet and the Barents Sea Ice Sheet united. (Figure by Romundset et al., 2017 , based on Solid et al. 1973 and Olsen et al., 1996)
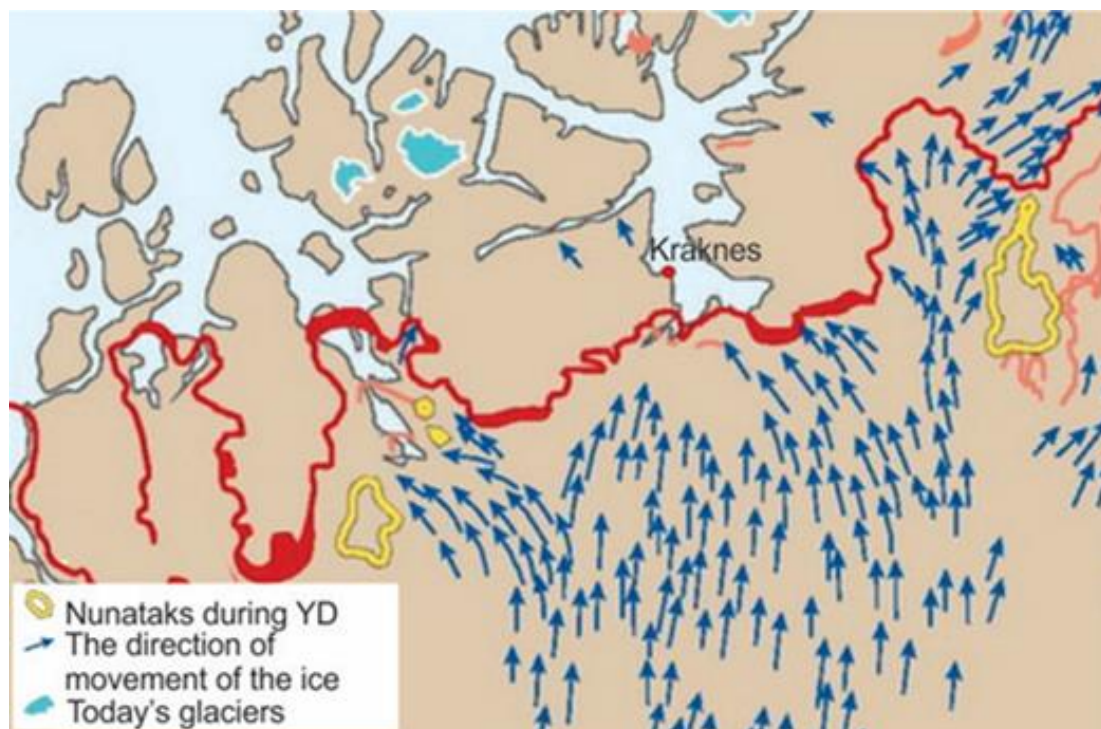
Figure 10 The blue arrows indicate the direction of movement of the ice in the study area. The red line is the YD main stage and the yellow line shows the nunataks during YD (Modified from Ramberg et al., 2013).

1.4.2.1 Marine Limit

The marine limit (ML) marks the highest sea level since deglaciation. The marine limit defines a typical upper limit for fine-grained marine deposits, including sensitive clay due to periods of large amounts of sedimentation from glacial discharge (Hansen et al., 2014). A common stratigraphy below the marine limit in a fjord valley consists of bedrock covered by glacial deposits and bedding of clay with layers of sand and silt. The bedded clay can be covered by beach deposits or deltaic and fluvial deposits (Figure 11). In Norway, the marine limit varies in different locations- it is higher in elevation today in areas where ice was thickest during the last glacial period. In Østlandet, it is 220 m asl, while in Troms and Finnmark, it is about 90 m asl (Wiig et al., 2019). Based on beach deposits on the peninsula, the marine limit at Kråknes is estimated to be about 70 m asl (Marthinussen, 1960) (Figure 12).
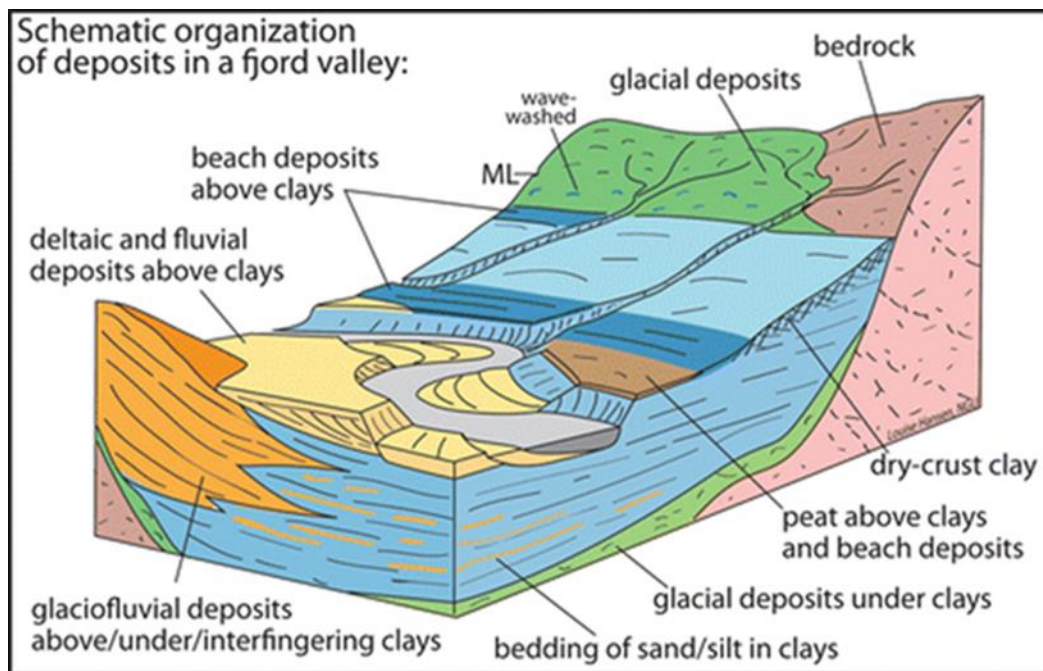
Figure 11 Common deposits in a fjord valley beneath the marine limit (Hansen et al., 2014).

Quaternary deposits at Kråknes

In figure 12, the quaternary deposits at Kråknes are mapped by NGU (2015b). Here the deposits are roughly separated but show the main materials in the study area before the landslide occurred. Sea and fjord deposits are dominant in the landslide area, with exposed bedrock and moraine material south and southwest of Kråknes. The blue dashed line marks the marine limit at 70 m asl. West of Kråknes, areas with aeolian and glaciofluvial deposits are

mapped. The mapping prior to the landslide did not incorporate glaciomarine sediments at Kråknes. The map was completed at a 1:50K scale, so it is not unexpected that areas of potential sensitive clay are missed. It has now been updated to show large sections of marine sediments (blue polygons, Figure 12).
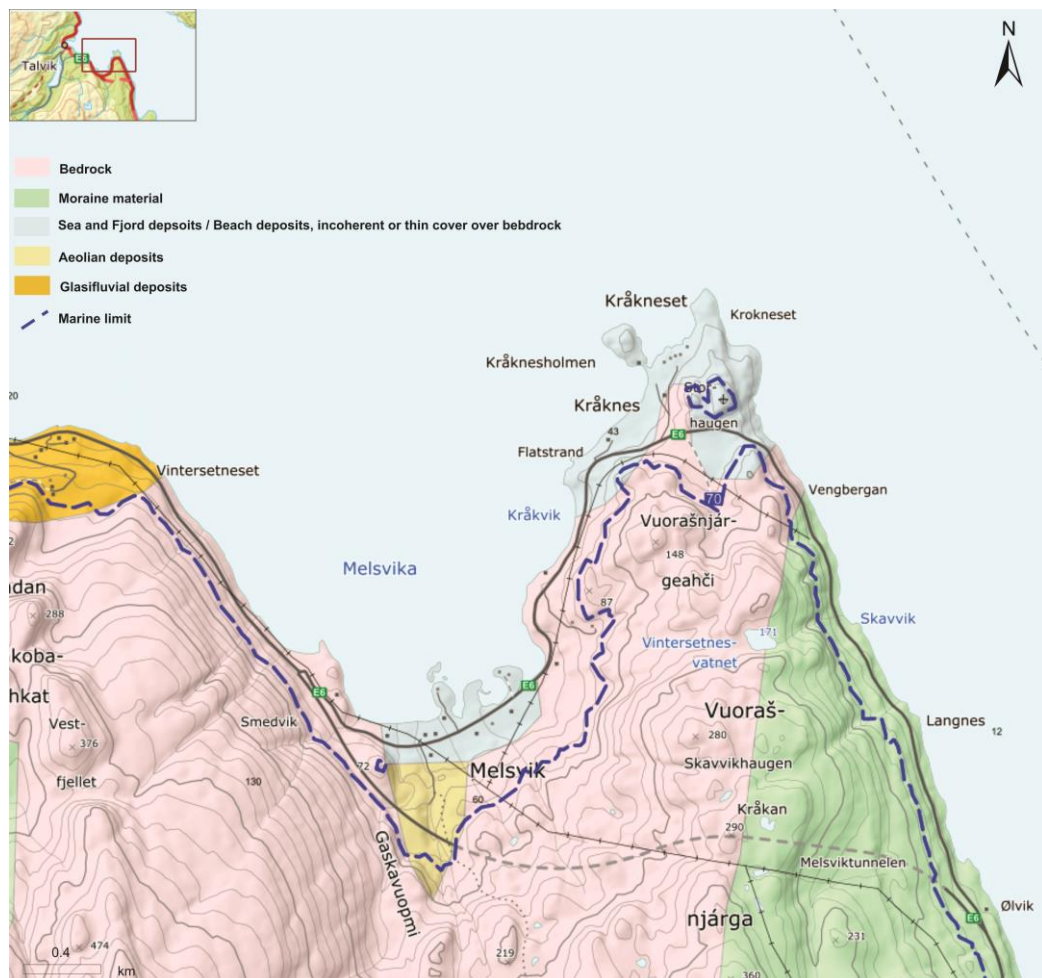
Figure 12 Updated map of quaternary deposits as Kråknes (NGU, 2015a).

1.4.3 Landscape development

Beach deposits and beach ridges are commonly found between the marine limit and today's sea level in Finnmark due to deposition from the ice sheet as it withdrew southward during the last ice age. Beach deposits and beach ridges were developed by wave and frost erosion on the bedrock and glacial deposits as the relative sea-level fell from the marine limit to today's level. Stronger storms and waves acted to develop the raised shorelines at Kråknes. A beach ridge at 25 m.a.s.l may correspond to the Tapes shoreline, created during the Tapes transgression in the mid-Holocene and is thought to be around 28 m.a.s.l in the Alta area

13

(Corner et al., 1990; Romundset et al., 2011). The quaternary deposits and the stratigraphy in the study area will be described closer in chapter 4.1.

1.4.4 Mapping of sensitive clay

The landscape development in and around Alta creates good conditions for sensitive clay to be found above sea level in the area today (see chapter 2.1.2). In 2009-2011, mapping of areas with sensitive clay was carried out by NVE in Alta municipality as part of a national risk assessment project to prevent disasters such as the Kråknes landslide. Several places in Alta municipality are identified as potential sensitive clay areas. The areas are classified with a risk class from one-five based on topography, geotechnical conditions, hydrological criteria, and the consequences a potential landslide would have on infrastructure and human life. One is the lowest and five is the highest risk class (NGI, 2011). A report from NGI in 2011 concluded that areas around Kråknes: Storvik, Melsvik, and Talvik, are medium and high-risk areas of sensitive clay slides based on the classification system (Figure 13) (NGI, 2011). However, Kråknes itself has not been mapped for potential quick clay risk.
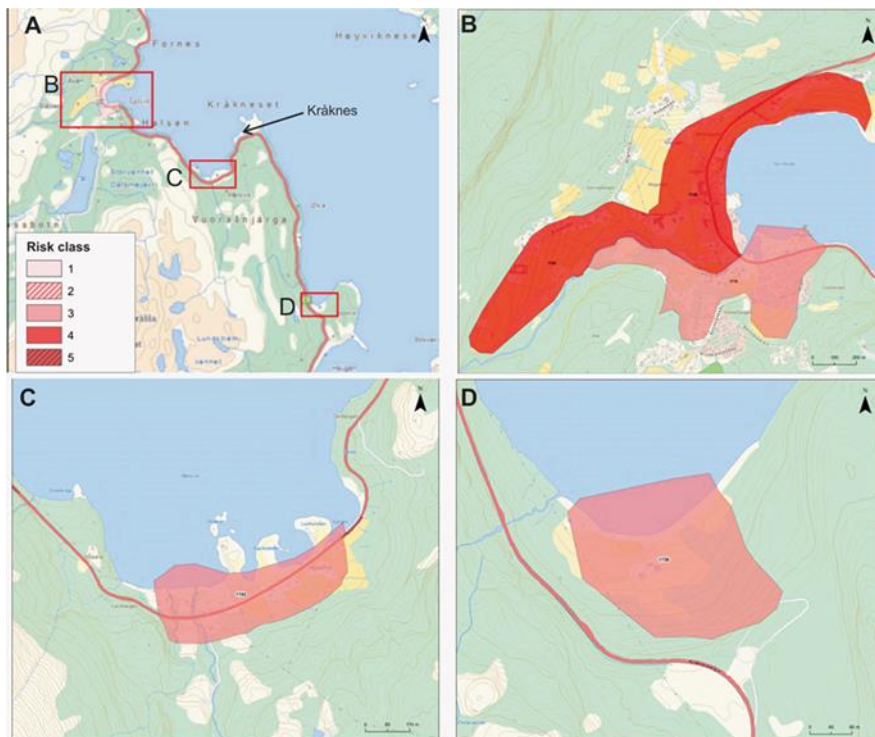

Figure 13 A) Areas mapped for sensitive clay by NGI close to the study area. B) The risk class mapped at Talvik C) Melsvik D) Storvik (All pictures from NGI, 2011).

2 Theory and background

This section looks at the theoretical background of clay and landslides to better understand the sequence of events and triggering mechanisms at Kråknes

2.1 Clay

2.1.1 What is clay?

Clay is sediment composed of solid particles that make up a skeleton with voids that are filled with gas or liquid or a combination of both. The particles are clay minerals formed by the chemical weathering of feldspars and mica (Raade, 2020). Chemical weathering is a process where bedrock dissolves when it is in contact with acidic water and biological processes that increase the amount of carbon dioxide and humus in soil (Sigmond et al., 2013). The most common clay minerals are kaolinite, illite (hydro mica), smectite, or chlorite. The amount and type of clay mineral present depend on the climate, source material, drainage conditions, and vegetation in the area. In a cold environment like in Norway, the most common clay mineral is illite, made of crushed bedrock enriched with mica (Raade, 2020; Rankka et al., 2004).

The crystal structure and chemical component of the clay is determined by the clay mineral. All clay minerals are built up from layers of silica along with aluminum hydroxide or magnesium hydroxide (Rankka et al., 2004). Silica has a tetrahedral molecular geometry with one silicon ion (Si^{4+}) in the middle, surrounded by four oxygen ions (O^{2+}). Both aluminum and magnesium hydroxide have octahedral coordination, with an aluminum or magnesium cation (Al^{3+}/Mg^{2+}) surrounded by hydroxide ions (OH^-)(Nesse, 2012). What type of clay mineral is formed can be determined by how the networks are stacked on top of each other. Figure 14 shows the structural compositions of different common clay minerals.
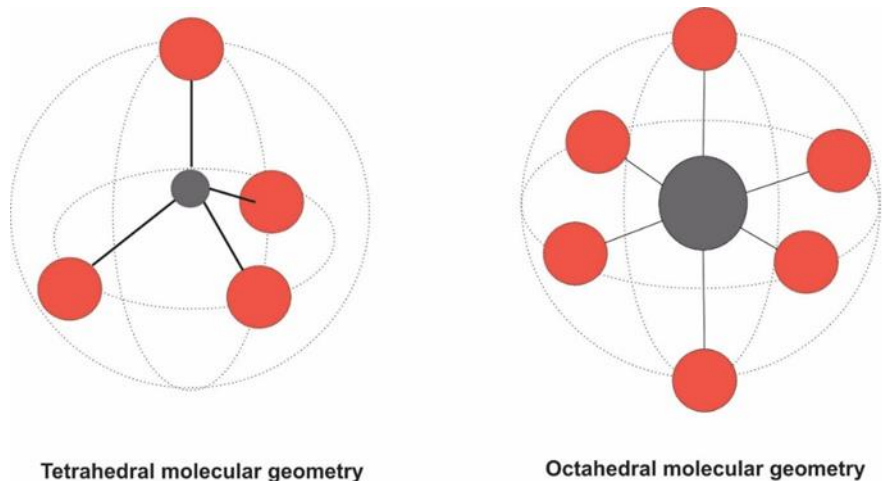
Figure 15 Tetrahedral molecular geometry and octahedral molecular geometry. In both Figures, the cations are represented in grey. In the tetrahedral geometry, the cation is surrounded by oxygen ions marked in red. In the octahedral geometry, the cations are surrounded by hydroxide marked in red—Figures inspired by Ophardt (2003).
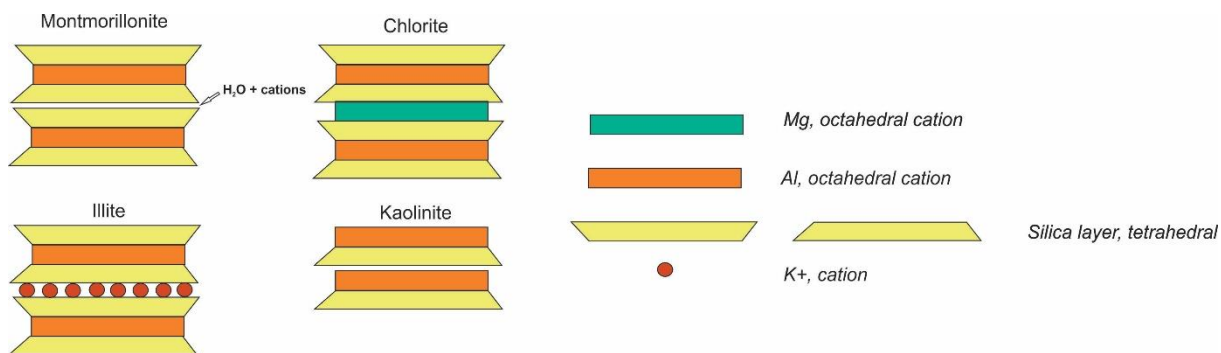
Figure 14 Illustration of the network stacking of different clay minerals (Inspired by Mitchell and Soga 2005).

The clay particle in the marine environment

A clay particle is defined by a diameter of 0.002 mm or less (2 μ). For a soil to be classified as clay, at least 30% of the soil mass needs to consist of clay-sized particles. Because of the small size of clay particles, the force of gravity is insignificant on them, and they are influenced by the electrical forces acting on their surface (Terzaghi et al., 1996). Particles with the same charge repel from each other, while particles with the opposite charge are attracted. When clay particles co-exist with water in a system, there is a constant reaction between the two. Ions from water replace weakly bounded ions in the clay particle, causing the more extended surface in the mineral to be negatively charged. The surface then attracts positively charged kations (such as K^+) from its surroundings and provides a strong bonding between the layers when the water content is low. However, not all these positive ions neutralize this negatively charged surface. Instead, they stay in the system as precipitated salt

(Mitchell & Soga, 2005). This gives the clay a "house of card" structure as seen in Figure 17A. The clay particles have a random arrangement with a lot of pore space between the grains, while the precipitated salt in the pore space glues the clay particles together (Nelson, 2015).

2.1.2 Formation of Quick Clay

Quick clay is a particular type of clay that loses its firmness and becomes completely liquid when it is loaded or disturbed. These properties are derived from its formation. Quick clay is predominantly formed in marine clay, deposited at sea and in the fjords during the last de-glaciation by meltwater from glaciers. As the ice withdrew, the landmasses started to rise to compensate for the lost weight from the ice, and marine clay was brought up asl (Figure 15) (Wiig et al., 2019). The salty porewater normally has a 3.5% salt content that makes strong electrochemical forces between the clay particles and gives the marine clay a stable "house of card" structure as described above (Figure 17A). When fresh groundwater from surrounding heights are transported towards the sea, the salt in the uplifted marine clay is washed out and quick clay is formed (Janbu et al., 1993; Wiig et al., 2019)(Figure 16).
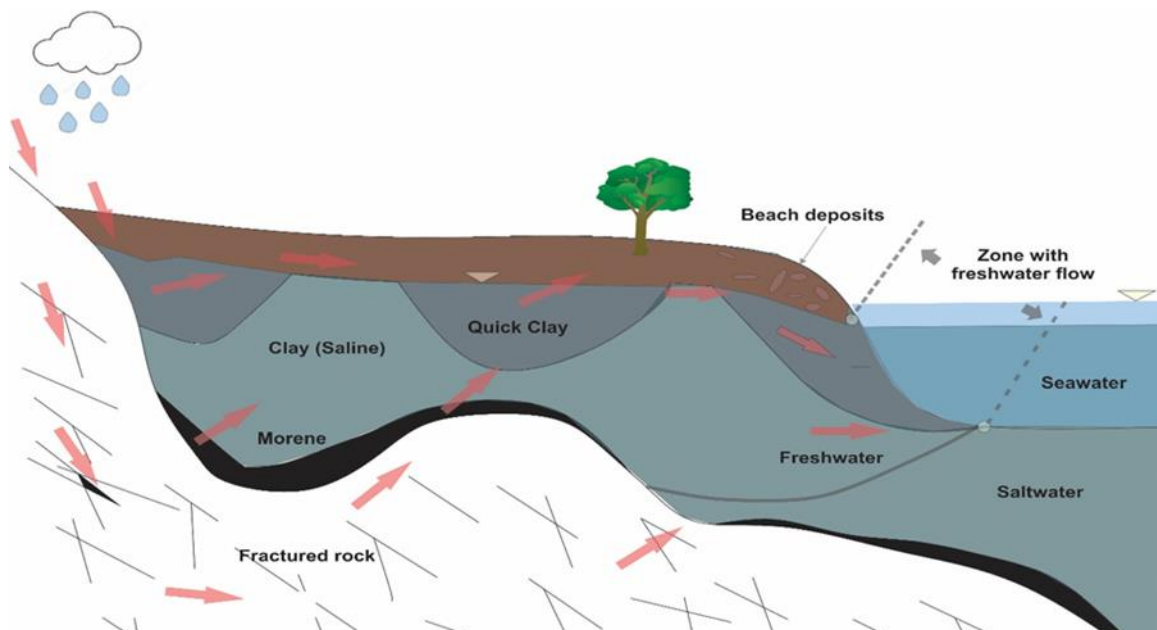

Figure 16 Illustration of how groundwater flows through Marin clay over time and creates pockets of quick clay (Inspired by Wiig et al. 2019). The red arrows indicate the flow direction.

Figure 17B illustrates the structure of quick clay where the loss of salt leaves negatively charged ions to create strong resisting forces between the clay particles. Because the salt normally glues the clay particles together, the loss of them makes the clay structure fragile and more sensitive. The small clay particles make clay a very compact sediment, and therefore the leaching of salt is a long process that is greater in areas with higher amounts of groundwater flow. Layers of coarser material within the clay, such as silt or sand, may accelerate the leaching process because of greater grain size and pore spaces, which give better conditions for groundwater flow (Janbu et al., 1993).
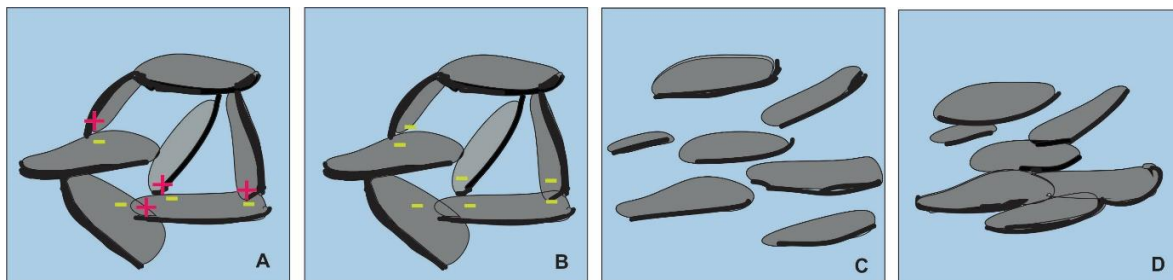
Figure 17 1 A) House of card structure of clay minerals with a negatively charged surface that attracts kations. B) The salte/kations are washed out of the pores, and the structure is susceptible. C) The clay structures have collapsed after being disturbed. D) Clay particles stirred together after a collapse (Recreated from Reite et al. 1999).

When the unstable quick clay is disturbed by external influences, such as loading or erosion, the structure will collapse (See chapter Why do landslides occur?2.2.2). Figure 17C shows a low viscosity clay with a collapsed clay structure and a surplus of pore water. After the collapse, the quick clay is stirred, and clay particles move closer into a more stable structure (Figure 17D) (Reite et al., 1999).

2.1.3 Typical occurrence of clay

The occurrence of sensitive or quick clay is connected to fjords in areas that have a history of glaciation during the Quaternary period. It can be found in marine clay beneath the marine limit. It is essential to express that not all marine clay becomes quick clay, but smaller pockets or lenses of quick clay can be formed inside the marine clay. They occur as mentioned in areas where the groundwater flow is high, such as in valleys or steep slopes near rivers and lakes (Janbu et al., 1993). It is estimated that 5000 km^2 of Norway consists of marine clay, where 20% of it is sensitive or quick clay (NGU, 2015b). Sensitive clay and quick clay are also commonly found in Sweden, Finland, Canada, and the northern USA because of the unique glaciomarine setting with ice withdrawal and isostatic uplift (Brenner et al., 1981).

2.1.4 Geotechnical characteristics of sensitive clay

To understand the mechanisms of landslides in sensitive clay it is important to know the geotechnical properties and physical behavior of the clay. Some important geotechnical terms and factors that are used to describe and classify sensitive clay are discussed here.

Clay can either be drained or undrained. Drained is when water is allowed to drain freely in the pores. Undrained is when water cant flow in or out of the soil, and therefore the clay behavior depends on the rate of loading or unloading. When clay is remolded, its natural structure is disturbed or modified, causing an increase in its shear strength. The **shear strength** is the maximum magnitude of the external forces the soil can sustain before it fails. The forces acting on the soil area called **shear stress** (Mitchell & Soga, 2005).

Sensitivity (S_t) is a term that defines the ratio of the undrained shear strength of a material that it is still intact (s_u), over the ratio of the undrained shear strength of the remolded clay (s_{ur}) with the same water content. It is in other words, the measure of the difference in soil properties from the intact soil to the remolded soil (L'Heureux et al., 2014) (Figure 18).

Figure 18 Highly sensitive clay in intact condition (left) and in fully remoulded state (right) (Thakur & Nigussie, 2014).

NVE classifies a clay with remolded shear strength less than 2.0 kPa and sensitivity greater than 15 as a brittle clay. The brittle clay is then categorized as either sensitive or quick clay based on the remolded shear strength (Gebremedhin, 2013). The definition of sensitive and quick clay is inconsistent in different literature and varies in different countries. In Norway, the clay is categorized as quick when the remolded shear strength is less than 0.5 kPa and has a sensitivity of 30 or more. If the remolded shear strength is between 0.5-2.0 kPa, it is categorized as sensitive clay. In Sweden, the remolded shear strength has to be less than 0.4 kPa and the sensitivity value of more than 50 for the clay to be classified as quick clay (Jean-Sébastien L'Heureux et al., 2014).

The Atterberg limits are used to identify, describe and classify cohesive soils and are used as an assessment to describing their mechanical properties (Mitchell & Soga, 2005). The Atternerg limits are the water content (w) in which the soil changes character behavior from consistency, solid, plastic, and liquid. The plasticity limit and the liquid limit are the two limits associated with the plasticity of a soil (Figure 19). The liquid limit (LL) is the percentage of water content when the soil changes from plastic to liquid and usually ranges from 35 to 45%. The plasticity limit (PL) is the percentage of water content when the soil goes from plastic to semi-solid consistency and usually ranges between 20-25% (Aarhaug, 1992). The shrinkage limit (SL) is when the soil changes from semi-solid to solid. The use of the Atterberg limits is generally accepted practice in soil mechanics. However, Bjerrum (1954) points out that a significant number of Norwegian clays have lower plasticity or Atterberg limits than what would be expected based on their grain size distribution. This is because leaching of marine clay (See chapter 2.1.2) reduces the salt content in the pore water, which again reduces the Atterberg limits and results in increased sensitivity. Therefore, it should be noted that the Atterberg limit may apply to some Norwegian clays but may fail in others.
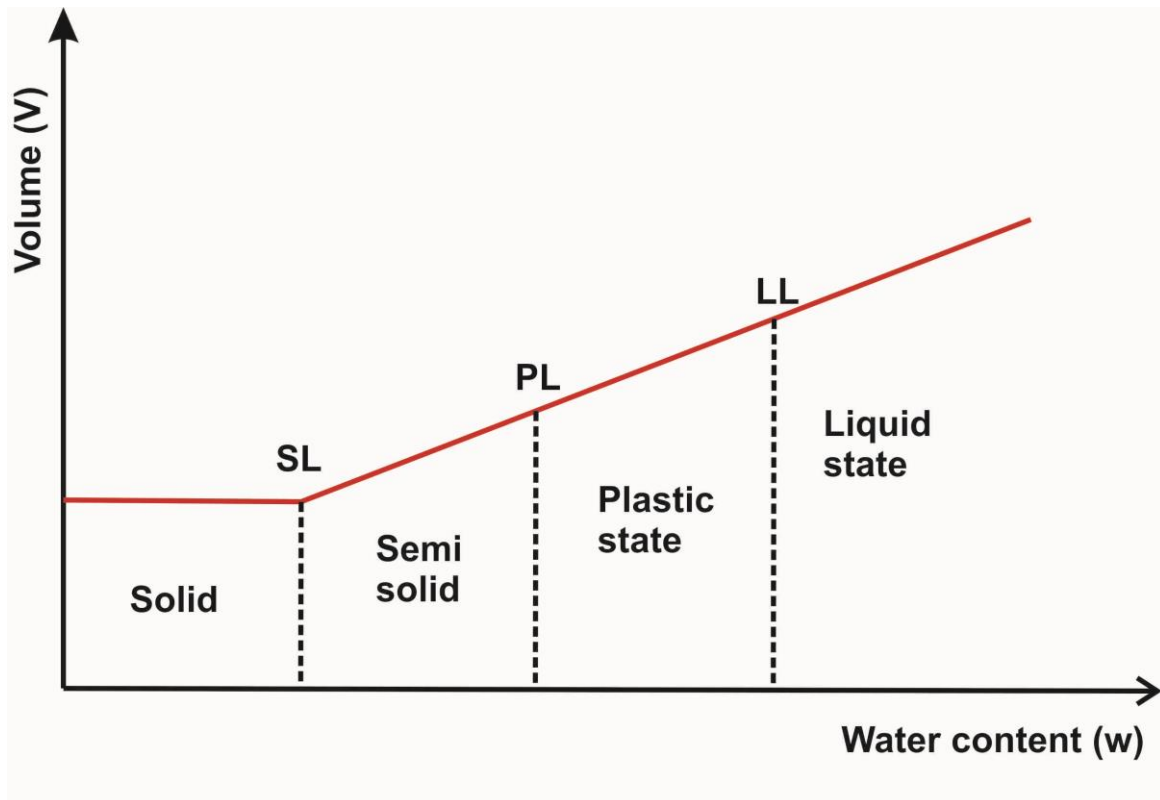
Figure 19 The Atterberg limits of soil. With the shrinkage limit (SL), Plastic limit (PL) and Liquid limit (LL).

Plasticity index (I$_P$) is a measure of the plasticity of the soil and is an indication of the soil's capability to change shape without changing its volume. It defines the range of moisture content in which the soil remains plastic and is the difference between the liquid limit and the plastic limit (PI=LL-PL). 1 gives the limited values for the plasticity index in Norwegian clay (Aarhaug, 1992).

Table 1 The limits of plasticity index in Norwegian soils.

PLASTICITY INDEX	PLASTICITY
I$_P$ < 10	Low plasticity
10 < I$_P$ < 20	Medium plasticity
I$_P$ > 20	Very high plasticity

Liquidity index (I_L) is a ratio calculated from the difference of water content, plastic limit and plasticity index. It normalizes the water content relative to the plastic limits (Mitchell & Soga, 2005). A logarithmic relationship between the liquidity index and the sensitivity can be seen in Figure 20A, where the reduction of salt content decreases the liquidity index and increases the sensitivity.
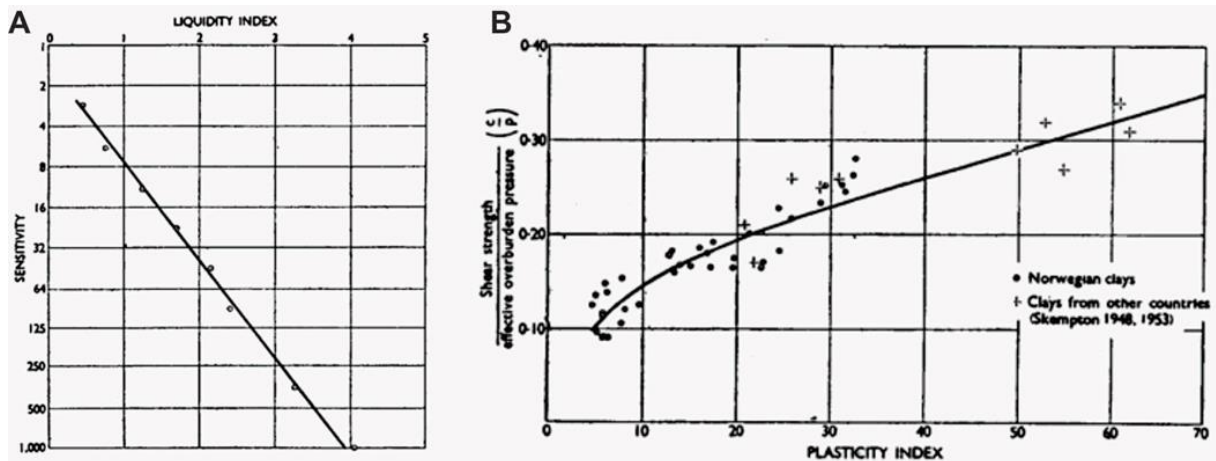
Figure 20 A)The relation between the sensitivity and the liquidity index in Norwegian marine clay (Bjerrum, 1954). B) The relationship between the shear strength and the plasticity index in clay soils (Skempton, 1948, 1953;Bjerrum, 1954).

Figure 20B show the correlation between the plasticity limit and the value of normalized shear strength, which shows that the leaching of salt gives a reduction in normalized shear strength (Bjerrum, 1954). Sensitive clays are related to their sensitivity and liquid limit, and the majority of highly sensitive clays have a water content larger than the liquid limit (w > LL). If w/w_L > 1, it characterizes open void structures that allow sensitive clay to be metastable in nature. Such clays are considered to be susceptible to flow slides when their liquidity index value is more than 1.2 (Burland, 1990; Thakur & Nigussie, 2014).

2.1.5 Catastrophic quick clay disasters in Norway

In Norway, there have been several sensitive clay disasters throughout the years. Some of these disasters are known worldwide because of their severe consequences. Two of these disasters are briefly described below.

The Rissa landslide

One of the most famous landslide disasters in Norway is the Rissa landslide, which occurred in Trondelag in 1978. The landslide event was initiated by a 700 m^3 fill mass that was placed by the shore of Lake Botnen. The landslide caused between five and six Mm^3 of clay to slide out into the sea, leaving a five km long back scarp. The slide mass also caused a three-meter high tsunami wave to hit the opposite side of the lake, causing material damage to the community of Leira (NGI, 1981). The disaster destroyed a total of 20 houses and farms and led to one fatality, making it Norway's most massive landslide event in the 20th century (Gregersen, 1981). This landslide event is very well documented as it was the first ongoing quick clay landslide ever to be filmed (NGI, 1981).

Figure 21 The Rissa landslide (Gregersen, 1981).

The Verdal landslide

The biggest landslide event to ever happen in Norway was in 1983 in Verdal, Northern-Trondelag (Figure 22). The landslide occurred in spring, after large amounts of rain and snowfall consistently during the prior autumn and winter. A mass of 55 Mm^3 of sensitive clay failed, causing a total of 112 fatalities as well as killing a large number of farm animals (Sigmond et al., 2013). The landslide mass moved downwards into a low lying area, where it spread across c. 9 km^2. An additional four people lost their lives after the landslide event due to related illnesses, such as pneumonia and lungs filled with clay (Walberg, 1993).

Figure 22 Picture of a farm destroyed by the 1983 Verdal landslide (Walberg, 1993).

2.2 Landslides

2.2.1 Definition of landslides

Landslides are defined as the downhill movement of rock, soil, and organic material and the landform that is created by the movement (Highland & Bobrowsky, 2008). For a landslide to occur, the force of gravity must exceed the internal strength of the material (shear strength) or friction of the material on the slope. The risk of a potential landslide occurring is usually increased if the water is added to material on a slope (Highland & Bobrowsky, 2008; WGS, 2017).

There are several types of slope movements and different types of material associated with the term landslide, but for sensitive clay the main types of landslides are flows and spreads. Flow slides are considered the most relevant landslide type in Scandinavia and can be divided into five different categories (L'Heureux et al., 2014):

I. **Debris flow**: a rapid mass movement of a combination of rock, soil, organic material, water and air, and has less than 50% of fine material (Figure 23A). These types of flows are usually triggered by surface-water flow.

II. **Debris avalanche**: a combination of very rapid and extremely rapid debris flows(Figure 23B).

III. **Earthflow**: a flow of fine-grained material or clay-bearing rocks, they occur under saturated conditions on moderate slopes and leave an "hourglass" shape (Figure 23C).

IV. **Mudflow**: a type of earth flow in which material is saturated enough to flow. The material consist of at least 50% sand-, silt- and clay-sized particles.

V. **Creep**: a slow, steady and gradual downward movement of soil and/or rock that forms a slope (Figure 23D). The shear stress in the material produces permanent deformation but is not significant enough to produce shear failure.

VI. **Lateral spreads:** occurs on gentle slopes or flat terrain (Figure 23E). They are caused by liquefication, where loose cohesionless sediments are transformed from solid into a liquified state. These spreads are usually triggered by rapid ground such as earthquakes but can also artificially be induced. When coherent material such as bedrock or soil rest on a liquified material, the upper layers may fracture and be extended, which causes them to rotate, subside, translate or liquify and flow. In several cases, a combination of these types occurs. In fine-grained material on shallow slopes, lateral-spreading happens progressively, where there is an initial failure in one area that spreads rapidly (L. Highland, 2004).
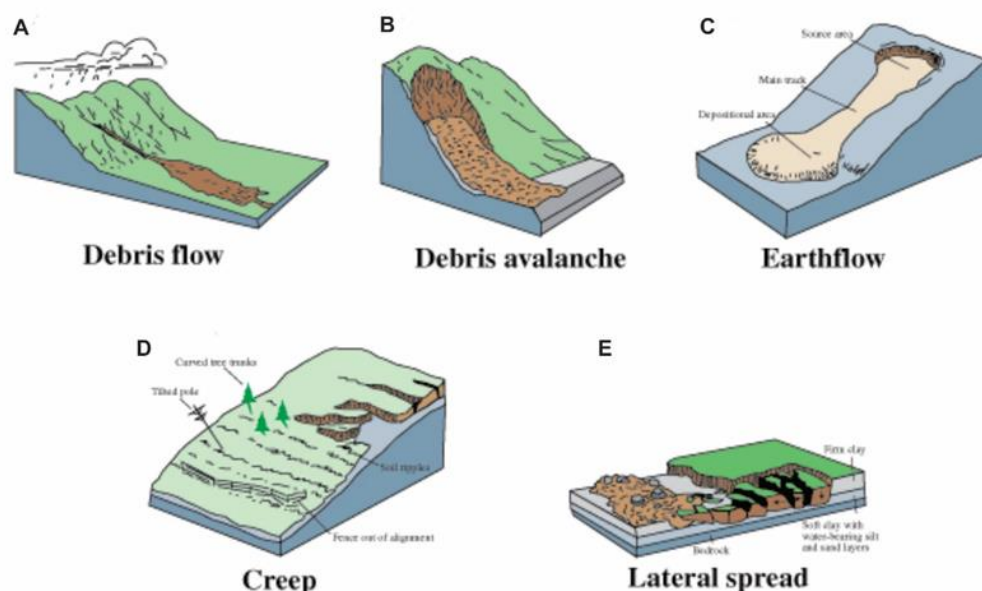

Figure 23 Different types of flows and spreads (Modified from L. Highland, 2004).

2.2.2 Why do landslides occur?

For a landslide to occur, the driving forces along a critical plane in a slope need to exceed the shear strength of the material. This can happen by increasing the driving forces or reducing the shear strength of the material. The shear stress in sensitive and quick clay is already close to the maximum shear strength, and minor mechanical forces can trigger a landslide (Bæverfjord et al., 2014). There is often a combination of several factors that causes landslide to occur and they can be divided into predetermined factors and triggering factors (L'Heureux et al., 2014). The predetermined factors are related to the properties of the sediment and make a slope or area sensitive to external influences. The triggering factor is the external influence that causes a landslide in the unstable area to occur and are often short events caused by natural processes or human activity (Masson et al., 2010). Different destabilizing factors are listed in Table 2.

Table 2 Different factors that can cause landslides (Highland & Bobrowsky, 2008; Masson et al., 2010).

Predetermined factors	Triggering factor by natural processes	Triggering factors by human activity
- Weak layers - Pore pressure - Water content - Topography - Deposition processes - Erosion channels - Gas and gas hydrates - Seepage	- Tidal water - Waves - Tectonic processes - Gas and gas hydrates - Erosion from rivers and streams - Ocean currents - Earthquakes	- Blasting - Fillings - Building - Change in drainage systems - Digging - Changes in river course or dams

A common cause of landslides is saturation of the slope. The presence of water lowers the strength of a material and reduces friction, making it less resistant to gravity. In saturated soils, there is a reduction of shear strength due to the buoyancy force exerted by water, and in unsaturated soil, there is a reduction of soil suction (Bogaard & Greco, 2016). Saturation occurs from intense rainfall, snowmelt, pipe leakage, changes in groundwater level, and change in surface water level along coastlines, lakes, rivers and such (Highland & Bobrowsky, 2008). The groundwater flow can be increased by weaker zones in the bedrock, such as in permeable faults. There can also be groundwater flow between the surface of the bedrock

and the more permeable sediment above. In areas with dolomite/chalk, groundwater flow can also be present in karst pipes (Indrevær, 2020).

Humans also contribute to the occurrence of landslides as cities and towns are expanded. According to NVE, 70-80% of landslides in sensitive clay are caused by human activity (Bæverfjord et al., 2014). Examples include undercutting at the bottom or loading on top of a slope, changing or disturbing drainage patterns, and removing vegetation. The Rissa Land-slide is an example of overloading the slope. In earthquake-affected areas, the landslides can be triggered by the vibrations as well as liquefaction of susceptible sediments and dilation of soils due to shaking of the ground (Highland & Bobrowsky, 2008). Earthquakes are, however, not a common triggering mechanism in Scandinavia because of the low magnitudes of earth-quakes events there.

Weak layers

In the stratigraphy, there can be layers that consist of sediments that have a significantly lower shear strength than the surrounding sediments. These layers can follow the stratigra-phy and may span continuously in a big area. Under critical circumstances, the weak layer may become the sliding surface of a failure. A combination of high-resolution bathymetry, geotechnical data, and seismic reflections are methods that can be used to identify weak lay-ers. A weak layer can be a thin clay layer or a thick band with multiple layers. Under certain conditions, layers of sediments with little or no cohesion can also act as weaker layers. Sand and gravel layers have a more open structure compared to cohesive soils, which allows gas hydrates to be accumulated. When pore pressure is increased in these layers, the gas within these layers may be forces to flow out of the sediment and cause the layer to collapse. Lay-ers of sand and gravel can also function as a channel of flow if the surrounding sediments are less permeable or impermeable. The water flow will reduce and the effective shear strength in the layer and can also exceed its shear strength. In submarine landslides, weaker layers can be found in different types of sediments that are listed above. The main effect of these different sediments is that there is an increase in pore pressure and/or a reduction in strength (Locat et al., 2014). Weaker layers can either be inherited, meaning that their weakness is derived from the sediments depositional properties, or they can be induced by

external factors. Strain softening is an example of this and is likely required for progressive failures in many types of sediments (Leroueil et al., 2012; Locat et al., 2014).

Effective stress and pore pressure

Pore pressure proves to be an essential factor in the stability of a slope. When the pore pressure is increased, the vertical effective shear stress is reduced and consequently, the frictional resistance and shear strength is also reduced. A general mathematic description proposed by Bishop is given in equation 1 where σ is the total normal stress, σ' is the effective stress, u_a is the atmospheric pressure, χ is the Bishop's coefficient which is a function of the soils degree of saturation (χ = 1 for saturated soils, χ ≤1 in unsaturated soils) (Bogaard & Greco, 2016).

$$\sigma' = \sigma - u_a + \chi(u_a - u_w)$$
(Eq. 1)

Due to internal friction and cohesion between soil particles, the shear stress can transmission through the soil. This leads to the Mohr-Coulomb failure criterion that defines the soils shear strength limit (τ_{lim}) given in equation 2, where c' is the effective cohesion and ϕ' is the internal friction angle (Bogaard & Greco, 2016).

$$\tau_{lim} = c' + \sigma'tan\phi'$$
(Eq. 2)

When the pore pressure is large enough to carry the weight of the overlying layer, a failure occurs. For failure mechanisms like this, the failure can occur in almost horizontal slopes. Excess pore pressure occurs when liquid within a layer is prevented from flowing into an area with lower potential by less permeable layers. Excess pore pressure can also occur due to rapid deposition or flows in coarser-grained material that is deposited below finer-grained sediments that are impermeable.

Figure 24 illustrates different factors affecting the slope stability in a fjord system. In the illustrated example, there is translational sliding in the regional event beds that are softer and more sensitive than the surrounding sediments. The low permeability in the beds causes a decrease in the effective stresses in the surrounding deposits and decreases the slope stability.

.

Pre-conditional factors such as heavy rainfall or snowmelt give unfavorable groundwater conditions, and an external factor such as human activity may then trigger a landslide that retrogresses from the fjord to the shore. With the presence of quick clay pockets, the landslide can potentially extend far inland with significant consequences (L'Heureux et al., 2012). Imperative conditions for this to happen are a prehistoric clay-slide activity in the catchments and a low to moderate dipping fjord where the event beds are able to accumulate (Hansen et al., 2011).
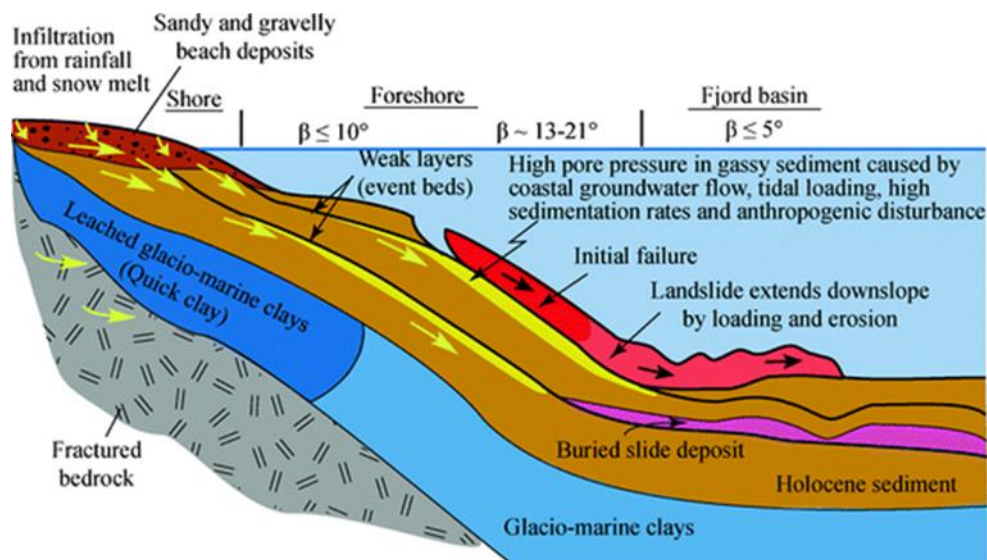
Figure 24 Different factors of slope stability form an example inTrondheimsfjorden, Norway (L'Heureux et al., 2012).

2.2.3 Consequences of landslides

Landslides can have a devastating impact on communities and human lives by destroying property, infrastructure, commercial structures and lifelines such as water or electrical lines. These damages can have a substantial economic impact and in the worst case, lead to casualties (Highland & Bobrowsky, 2008).

The remarkable thing about sensitive clay landslides is the fact that they can be triggered in almost flat terrain by initially small forces. They can begin to occur in a blink of an eye, while other clay landslides often evolve over time (Bæverfjord et al., 2014; Wiig et al., 2019). This

makes it hard to predict a coming landslide event and leaves little or no time for evacuation after a landslide is triggered.

As the population rises, so does the need to build more residential areas and commercial structures. In the construction industry today, risk evaluation and risk assessment are necessary for areas where landslides potentially can occur, such as in areas with sensitive clay. Risk assessment in areas of sensitive clay in Norway is based on "engineering scores" based on the geology, topography and local conditions, as well as possible worst-case consequences for people, infrastructure and properties (Kalsnes et al., 2014). For more details, see chapter 1.2.3.1.

2.2.4 Different types of landslides

A landslide can develop progressively or retrogressively. Soil slides retrogress when the back scarp/crown incrementally moves up-slope in a series of failures (Figure 25). The landslides move up-slope until the soil masses in the back scarp becomes stable. The landslide can propagate up to several hundreds of m backward or sideways in several slabs from the initial landslide. Each of the slabs fail as they lose support when the buttressing mass below is removed.
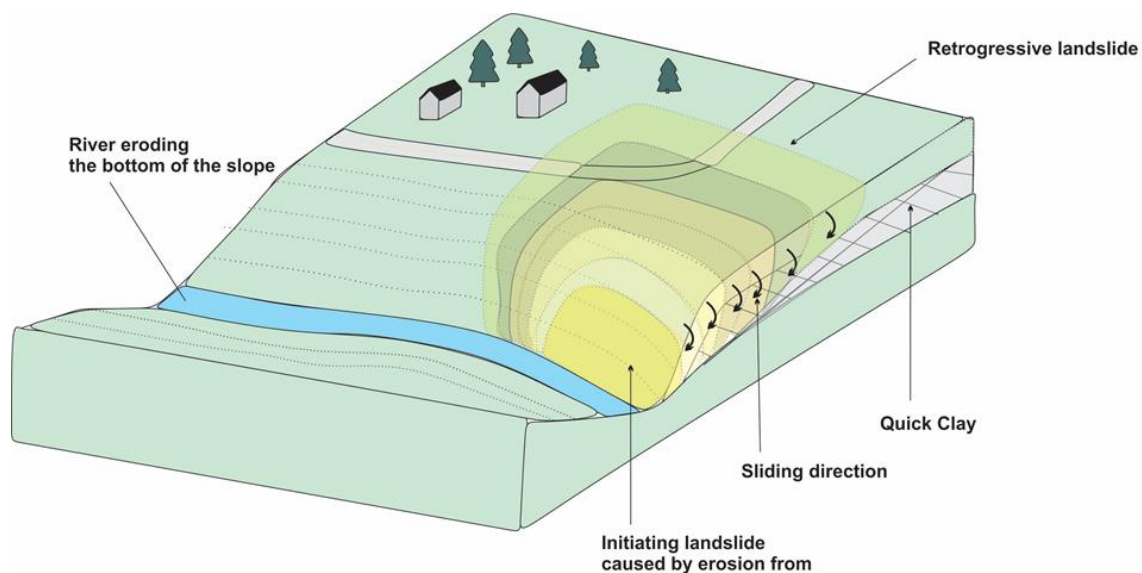

Figure 25 Retrogressive land slide (Inspired by Wiig et al., 2019).

If a retrogressive landslide occurs in sensitive clay, it often leaves a pear-shaped landslide pit, and if the material does not become completely liquid a stair-shaped or saw-shaped morphology may appear. It often occurs due to erosion, digging or filling placed on a slope. This process continues until a stable back scarp is formed or there is no sensitive clay left (Wiig et al., 2019). Several authors suggest that for retrogressive landslides in sensitive clays to occur, the remolded strength of the clay must be less than 1.0 kPa and the liquidity index (I_L) more than 1.2 (Lebuis et al., 1983; L'heureux, 2012; L'Heureux et al., 2014; Thakur et al., 2014; Strand et al., 2017) and only if the sensitivity is minimum 30 kPa (L'heureux, 2012).

When a progressive landslide occurs, the landslide masses develop successively along a sliding plane and all the landslide masses slide out together. In sensitive clay a progressive landslide may occur when the material is exposed to strain-softening, where the strain exceeds the peak strength and causes a permanent reduction in shear strength (Figure 26).
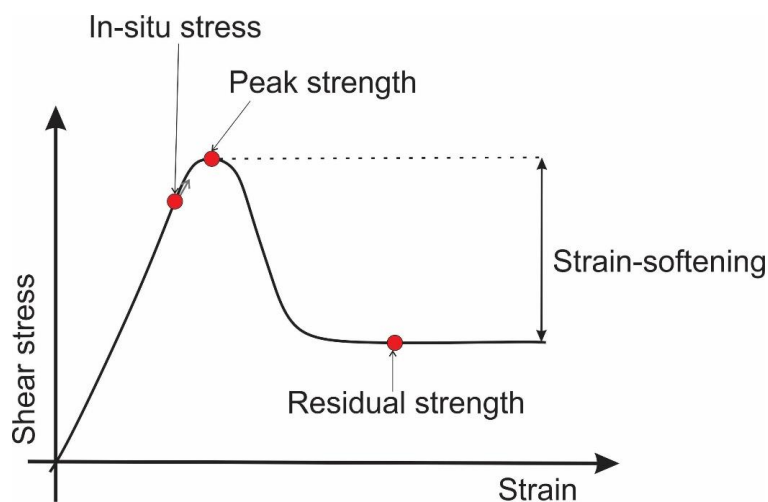
Figure 26 The relationship between stress and strain in strain-softening (Inspired by Wiig et al., 2019).

The reduced shear strength causes a chain reaction within the material where the overload moves from one point to another as the material loses its shear strength (Wiig et al., 2019). Eventually, a sliding plane is developed and the landslide masses slide out simultaneously along the sliding plane. A progressive landslide can have its initial development from the back of the slope and develop downslope (Figure 27A), or it can develop from the foot of the slope and propagate upslope in the opposite direction of the sliding masses (Figure 27B). The development, slope and depth of the sliding plane determine if the landslide developed retrogressively or as an upslope/backward progressive slide.
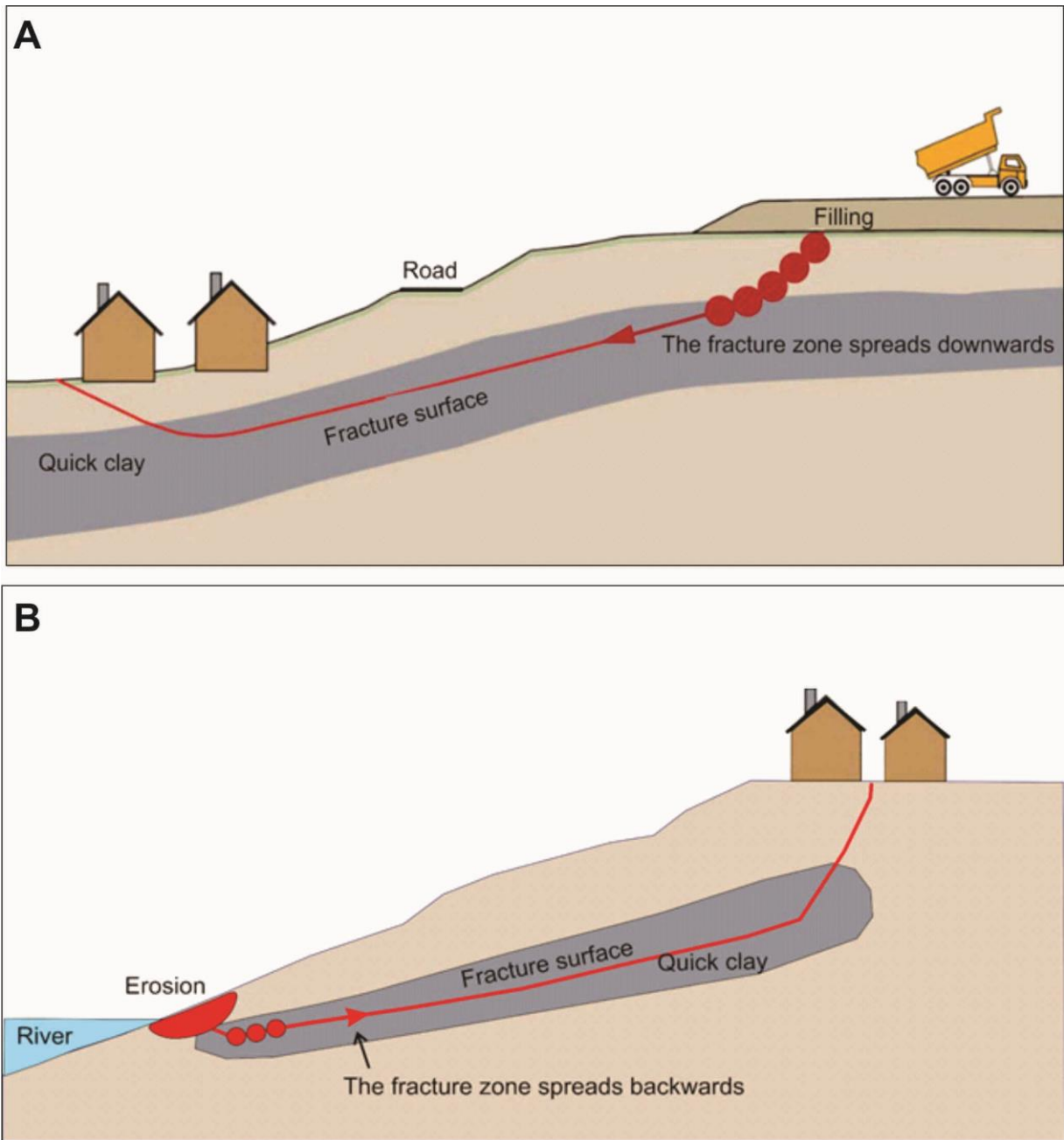
Figure 27 A) Progressive landslide where the fracture is iniitated at the top of the slope and spreads forward (Inspired ny NVE, 2019). B) Progressive landslide where the fracture is initiated at the foot of the slope and spreads backwards (Inspired by NVE, 2019 and Wiig et al., 2019).

2.2.5 Run-out areas

The run-out area in a landslide of sensitive clay is dependent on the type of landslide and the

length of the release area of the landslide (L'heureux, 2012). The length of retrogression is

connected to the mobility of landslide debris. In sensitive clay landslides, the mobility in-
creases with the mobilized volume of sediment per unit weight (Vol/W_{avg}). The physical and
mechanical properties of the sensitive clay and the environment they are in, is also contrib-
uting factors to the run-out distance. This explains the difference in run-out distance in Nor-
way and Canada, where Norwegian landslides often have a greater run-out distance com-
pared to Canadian landslides. Sensitive clay landslides in Norway often occur in areas close
to the shore where the debris can flow into the bottom of the fjord. In these cases, the low
permeability of the clay may cause water to be entrapped between the landslide masses and
the slope and causes a reduction in friction in the base of the landslide. This results in hydro-
planing and a longer run-out distance (Mazzanti & Bozzano, 2009; L'heureux, 2012) (Figure
28). When a critical velocity of 5 to 6 m/s is reached, hydroplaning tends to lift the front part
of the flow, reducing the shearing resistance at the base of the flow and therefore causing a
longer run-out distance (Locat & Lee, 2002).
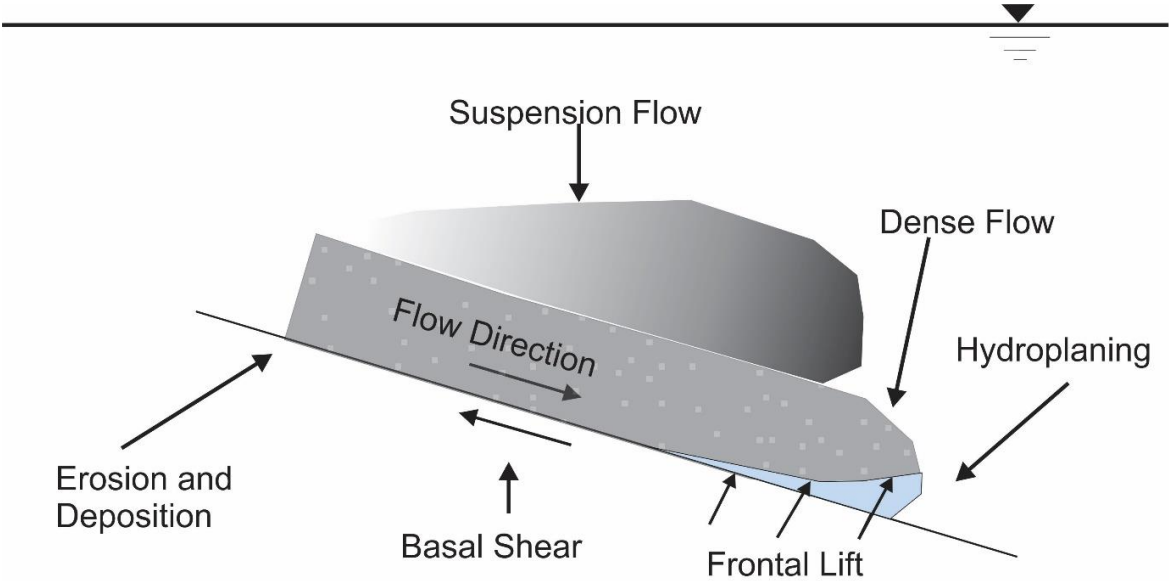
Figure 28 Schematical figure showing the potential frontal uplift of the dense flow that causes hydroplaning. Basal shear stress in the opposite direction of the flow direction leads to erosion and deposition. (Inspired by Locat   & Lee, 2002).

For risk assessment, there are methods to try and predict the outcome of a potential
landslide in areas with sensitive clay. The release area for retrogressive landslides can be de-
cided by the 1:15-method which is commonly used for mapping in Norway (Jean-Sébastien
L'Heureux & Solberg, 2013). This method is based on the relationship between the height of

the slope (H) and the length of the release area (L). Studies of former historical landslides show that 90 % of the landslides would stop when H/L would get close to 1:15 (L'heureux, 2012; Jean-Sébastien L'Heureux & Solberg, 2013; Wiig et al., 2019). This method is only relevant for landslides where the sensitive clay layer continues backward and are not hindered, such as by ravines and protruding bedrock. However, there are studies that show more extensive retrogression than what is suggested for this method.

When the length of the release area is decided, then the run-out length (L$_u$) of the landslide can be calculated based on empirical relations. The length of run-out distance is calculated from the foot of the slope of the release area (Figure 29). For retrogressive landslides in channeled terrain, the run-out distance is three times the length of the release area, while for retrogressive landslides in open terrain, the run-out distance is 1.5 times the length of the release area. Figure 30 illustrates the empirical relations for the run-out in channelized and open terrain, where L is the length of the release area, B is the with of the release area, B$_u$ is the width of the run-out area and L$_u$ is the run-out distance (Strand et al., 2017).
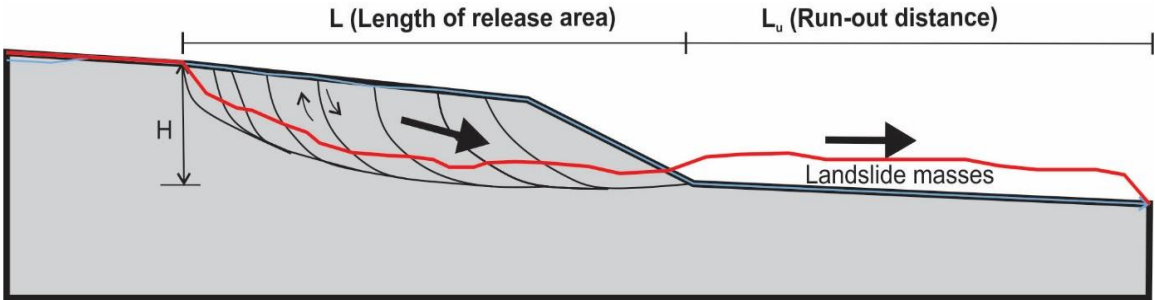
Figure 29 Sketch of a retrogressive landslide area where the length of the release area (L), the run-out distance of the landslide masses (L$_u$), and the height of the landslide (H) can be seen. The light blue line represents the terrain before the landslide occurred and the red line represents the terrain after the landslide occurred. (Inspired by and modified from Wiig et al., 2019).
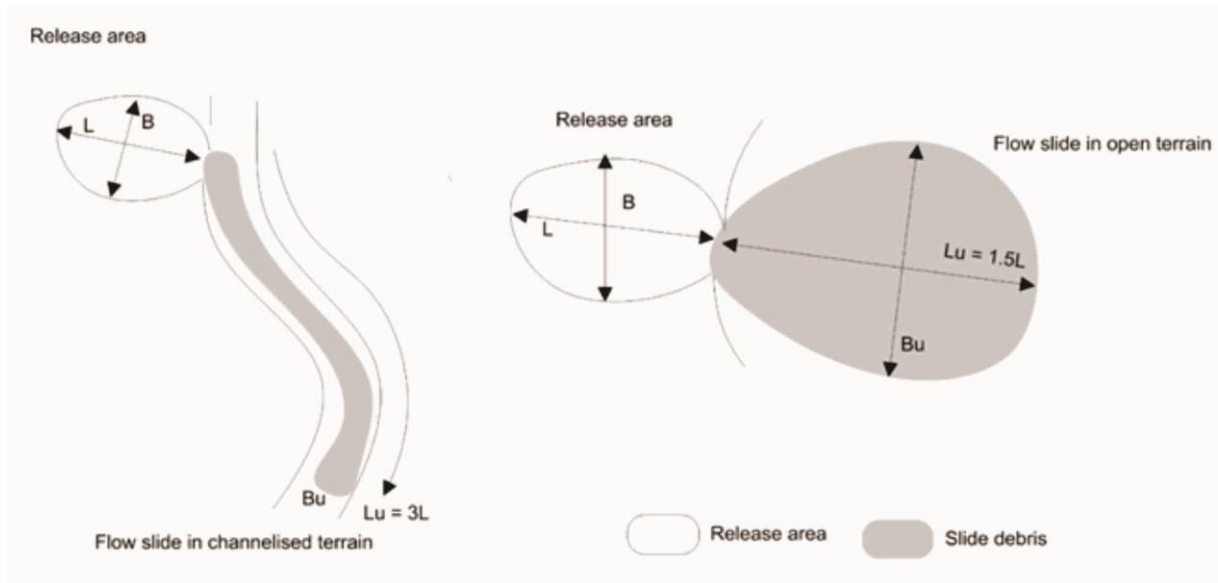
Figure 30 Run-out distance of retrogressive landslides in channelized terrain and open terrain (Strand et al., 2017).

3 Methods

3.1 Spatial data

Orthophotos from 2018 were retrieved from the Norwegian Mapping Authority (Kartverket, 2018) before they were put into a graphical information system (GIS) using the ArcMap 10.5 software and projected in the ESRI 1989 UTM Zone 35N coordinate system. Digital elevation models (DEM-files) from before and after the landslide event were provided by NVE and resampled to 1 m resolution by Louise Vick (UiT). The DEM-files were then put into ArcMap 10.5 and hillshaded. The hillshaded DEM files were overlaid by 1 m contours of bathymetric (DXF format) and lidar data to create a topography map. The bathymetric data is made of two different measurements from Kartverket (The Norwegian Mapping Authority) with different resolutions. The shallower parts are 1 m grid from 2004 and the deeper areas are of 5 m grid from 1998. The pre-landslide terrain is mainly based on Lidar data from 2004 (1 m grid) (Gylland et al., 2021). The post-landslide bathymetry and topography were measured by GeoNord Survey team in the days prior to the landslide event.

3.2 Fieldwork

On June 15th, 2020, a tour around the landslide area was given by Anders Bjordal in NVE and the National Coast Guard made it possible to get a view of the landslide from a boat. The more detailed fieldwork was done in the period from July 27 -31, 2020, with student colleague Torgrim Sandnes and supervisor Louise Vick. Mapping of the study area was done with the use of the Clino app on Apple iPads. Orientation measurements were done in the Clino app and compared to measurements by a geological compass to ensure the measurements' accuracy. Soil samples were collected, and the different soil types were interpreted in the field based on the guidelines for field classification and description of soils and rocks provided by The New Zealand Geotechnical Society (New Zealand Geotechnical Society, 2005). Large parts of the study area were not accessible because of the hazard risk. Therefore, several soil classifications within the landslide area are based on pictures from a distance or up-close drone photos. Drone photos and videos were taken by Louise Vick on July 28th, 2020, with a DJI Mavic 2 Pro drone featuring a Hasselblad L1D-20c camera.

Measurements of foliation, joints, beddings etc., from field work, were displayed and interpreted in Dips, projected with equal angle and in the lower hemisphere. A mosaic orthophoto of the landslide area post-failure was created from the drone photos taken during fieldwork. The mosaic was put together on dronedeploy (Dronedeploy, 2020) by Torgrim Sandnes. Additional drone photos and videos from the days of the landslide event and July 7th, 2020, were provided by Anders Bjørdal from NVE.

3.3 Geotechnical testing

The geotechnical testing in this study was done by Multiconsult AS in June 2020. They used a hydraulic bore rig (GT605 type) to collect the bore samples used for geotechnical testing (Figure 31). Appendix A shows the drill locations and the core samples. Laboratory testing was done by Multiconsults geotechnical laboratory in Tromsø. The different geotechnical tests are briefly described below.

Figure 31 Hydraulic bore rig used to collect bore samples by Multiconsult. Photo courtesy Anders Bjordal (NVE).

3.3.1 Field methods

All field methods are based on field guidelines as described by Statens Vegvesen (1997).

Total sounding is a method that combines rotary-pressure sounding and bedrock drilling and includes rotation, ramming and flushing methods. This rotary-pressure sounding method is

used to determine the soil types and the stratification of the sediments. It is done by inserting a rod with a standard tip into the ground with constant speed and rotation. The bedrock drilling helps indicate the depth to the bedrock and records the different properties throughput layers and is performed by drilling a spliceable rod and a carbide drill bit into the ground.

A cone penetration test with pore water pressure measurement (CPTU) was used to identify the permeability in the subsurface. The results are used to help determine mechanical properties of the soils, such as shear strength, deformation and consolidation param. The method is performed by pressing a cylindrical probe with a conical tip into the ground with a constant penetration speed.

Samples were collected in the field to test them in the laboratory. The samples were collected by mechanical hub drilling to collect disturbed bag samples. This is done by using a boring rig that bores down to 5-20 m depth and collects the sample in a hollow rod. A cylinder/ block sampling was used to collect undisturbed samples. These samples are taken by a piston, which collects a 60-100 cm long cylinder sample and pulls it up to the surface, where it is sealed and transported to the laboratory.

3.3.2 Lab tests

In the lab, grain distribution analyses were done for some of the collected samples. This is done by dry and wet sieving for grain fractions that have a diameter of more than 0.064 mm. For fine-grained fractions, the grain size is determined by using a hydrometer. A hydrometer measures the change in relative density of a mixture of soil and water as the soil particles sink. This is done by placing the hydrometer in a tall liquid-filled glass cylinder and pouring the fine soil fractions into the liquid. The results from the hydrometer is then put into Stokes law to calculate the maximum diameter of the soil particles. The results of these grain size distribution analyses are presented in a grain-size distribution plot, which can be used to classify the soil, its compressibility and risk of frost heave.

Odometer tests are used to determine the soil's deformation properties in some of the samples. This is performed by inflicting a given force on a sample of the material and by that registering the one-dimensional axial deformation of the material. This test is either done under a constant rate of strain or constant pore pressure ratio (Statens vegvesen, 2014).

Triaxial tests are performed on undisturbed cylinder samples to find different shear stress param. The cylindric sample is built into a rubber membrane and placed into a pressure cell where it is inflicted with either isotropic or anisotropic stress until the material fractures. The imposed stress resembles the subsurface stress under undrained conditions (Statens vegvesen, 2014). The results of the test are plotted in graphs and tables, such as stress plotted against deformation.

3.4 DAN3D

To model and reconstruct the landslide event the DAN3D software has been used. DAN3D is a numerical model of unsteady flow exclusively developed for rapid flow analysis. The purpose of DAN3D (dynamic analysis in 3D) is to model the post-failure motion of known cases so that the behavior of possible future events can be predicted (O. Hungr, 1995). The DAN3D software was developed by Hunger and McDougall and is based on the concept of "equivalent fluid," which is a semi-empirical approach defined by Hungr (McDougall & Hungr, 2004). The equivalent fluid is a hypothetical material that replaces the real heterogeneous and complex moving mass. However, the bulk properties of the equivalent fluid is still approximate to the behavior of the original moving mass. The concept of an equivalent flow is shown in Figure 32, where a homogeneous "apparent fluid" replaces the sliding mass. The apparent fluid has properties that give a similar external shape and mean velocity as the original mass. The selected rheology determines the velocity.
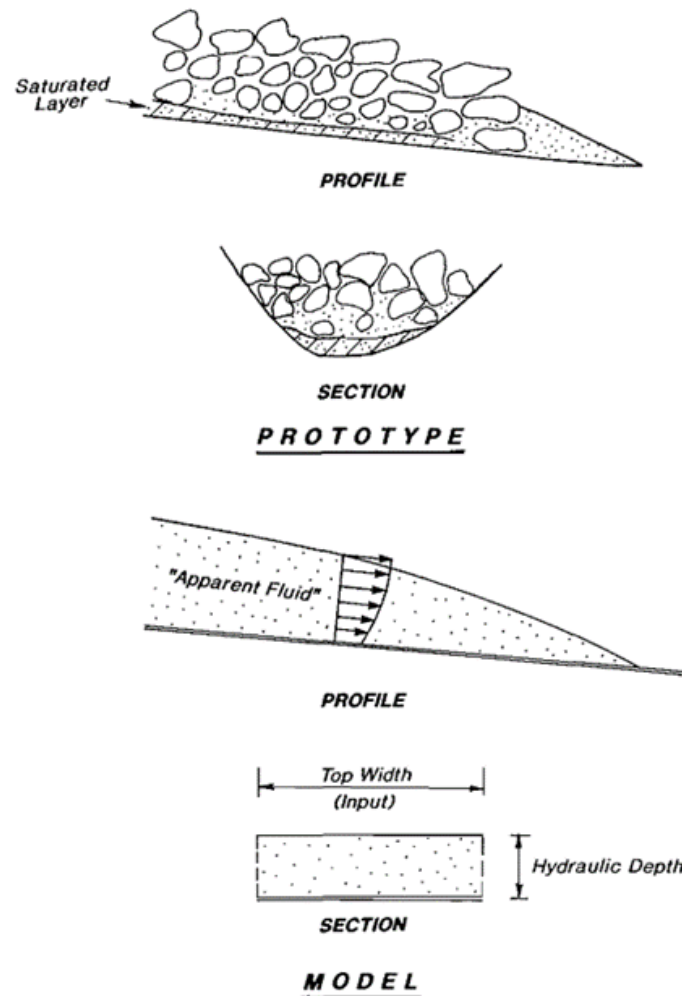
Figure 32 The slide mass is replaced by a homogeneous apparent fluid (O. Hungr, 1995).

In the model, the total volume of the sliding mass is divided into several elements called "smooth particles." Each smooth particle has a finite volume that only increases due to material entrainment. The position of the particles is indicated by the reference columns as simplified in Figure 33. Given the volume and location of each particle at a certain time, the depth and depth gradient is possible to estimate at that reference column.

Numerical integration of the momentum balance equations is what determines the instantaneous accelerations of a column. The local flow velocity will then be updated and the columns change their position in a short amount of time (Figure 33). For fore details on the different equations, see McDougall & Hungr (2004).

$$h_i = V_i W_{ii} + V_j W_{ij}$$
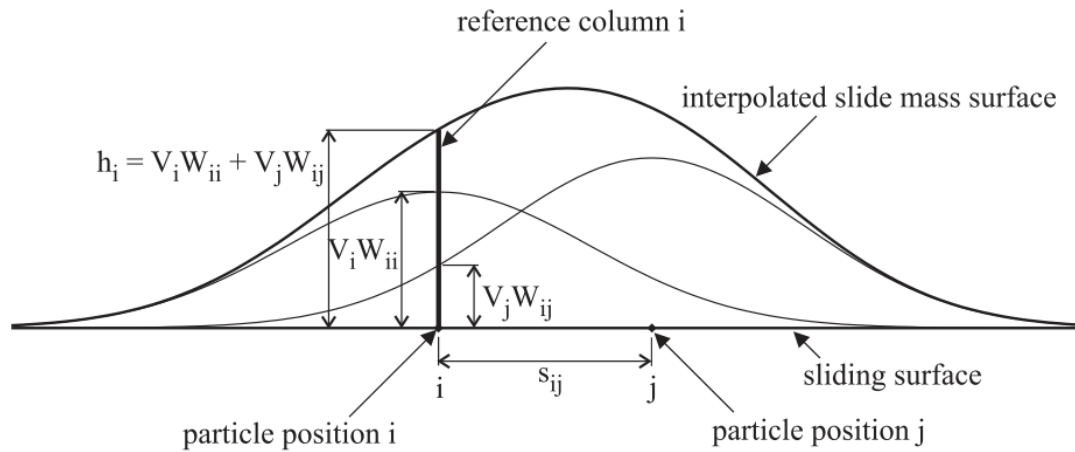
Figure 33 Simplified interpretation of the smoothed particle hydrodynamics. Here the particles are illustrated as bell-shaped objects (McDougall & Hungr, 2004)*.*

In DAN3D the calculation of the landslide acceleration is based on the gravitational forces that drive the motion down the slope (Figure 34). The opposite component of the gravitational force is the basal resistance force. The model also takes into account the internal pressure gradients caused by inclination at the top surface and momentum expended entraining path. The simulation is controlled by the param that govern the basal rheology, which along with the topography and the geology, is used to calculate the basal resisting force (Aaron et al., 2016). In DAN3D, there are five different rheologies that can be implemented, and these are briefly described below (Hungr & McDougall, 2009).
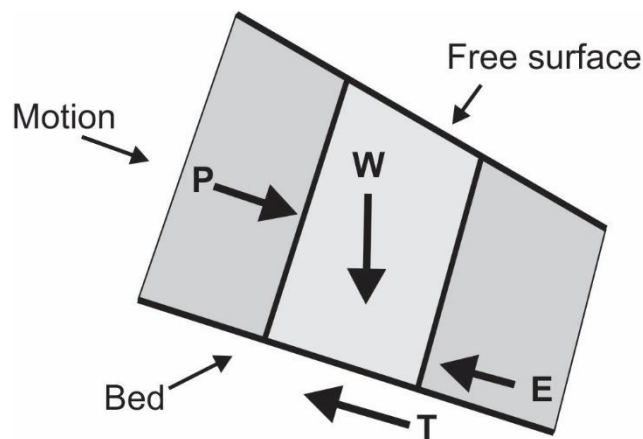
Figure 34 Illustration of the forces that act on a block of material in DAN3D. W is the weigth of the material, T is the basal resistance, E is the inertial resistance caused by entrainment, and P is the internal force (Inspired by Aaron et al. 2016).

I. **Plastic Flow** relates to a pseudo-static motion of liquefied soil and assumes that the base shear resistance is equivalent to a constant yield strength value:

$$\tau = -c \qquad\qquad\qquad (Eq.\ 3)$$

II. **Bingham model**: combines plastic and viscous behavior and has a threshold yield strength where it behaves as a rigid material above and a viscous material below. The following equation is used to determine the basal share resistance:

$$\tau^3 + 3\left(\frac{\tau_{yield}}{2} + \frac{\mu_{bingham}}{h}v\right)\tau^2 - \frac{\tau_{yield}}{2} = 0 \qquad\qquad (Eq.\ 4)$$

Where τ_{yield} is the the bingham yield and $\mu_{bingham}$ is the bingham viscosity.

III. **Frictional base resistance** is the difference between the normal stress and the pore fluid pressure at the base.

$$\tau = -\sigma'z(tan\phi) \qquad\qquad\qquad (Eq.\ 5)$$

Where φ is the dynamic basal friction angle.

IV. **Voellmy resistance model** combines frictional and turbulent behavior.

$$\tau = -\sigma'zf\left(\frac{phv^2}{\xi}\right) \qquad\qquad\qquad (Eq.\ 6)$$

Where f is the friction coefficient and ξ is the turbulence parameter.

V. **Newtonian flow** is the function of the velocity and viscosity parameter. Given by:

$$\tau = \frac{3V\mu}{H_\xi} \qquad\qquad\qquad (Eq.\ 7)$$

Where V is the velocity of the sliding mass and μ is viscosity.

For geotechnical analysis, the Plastic flow and Bingham model is most appropriate and will therefore be used to simulate the Kråknes landslide event. However, based on previous work it should be noted that the DAN3D software needs further development for cohesive rheologies, especially the Bingham model (Issler et al., 2013).

3.4.1 Input data

Two different files are necessary to provide in order to do a simulation in the DAN3D software. This includes digital terrain models in ASCII format of the landslide path (path topography file) and the depth of the release area (source depth) (Figure 35). The path topography represents the surface of the sliding mass and the source depth file is the vertical depth of

the initial sliding mass. In addition, an erosion map can be made if more than one material is used in the simulation, but this has not been done in this study. Both the path topography file and the source depth file were created from DEM-files provided by NVE. The DEM-files were converted to GRID-files and appropriately shaped according to the DAN3D-user manual (O. Hungr, 2010) in ArcMap and Surfer Golden Software. See Appendix B for more detailed information on how the different files were created.

Figure 35 Grid File Assignment in DAN3D.

The param used in DAN3D is the material properties and the control param. Material properties needed to run the model includes unit weight, shear strength, viscosity, type of material (rheology), friction and internal friction angle (Figure 36). These material properties were based on the geotechnical data provided by Multiconsult (Appendix A) and are listed in table 4. For the Bingham rheology it is necessary to put in the viscosity of the material. The viscosity was estimated from the liquidity index(I_L) in an equation proposed by Locat and Demers based on laboratory tests of Canadian sensitive clays (Eq.8).

$$\eta = (\frac{9.27}{I_L})^{3.33} \text{ mPa S.} \qquad\qquad (Eq.\ 8)$$

Canadian sensitive clays defer from Norwegian sensitive clays as discussed in Chapter 2 and highlighted by L'Heureux (2012), but as there are no corresponding Norwegian sensitive clay studies, these estimations were used for the Kråknes landslide.
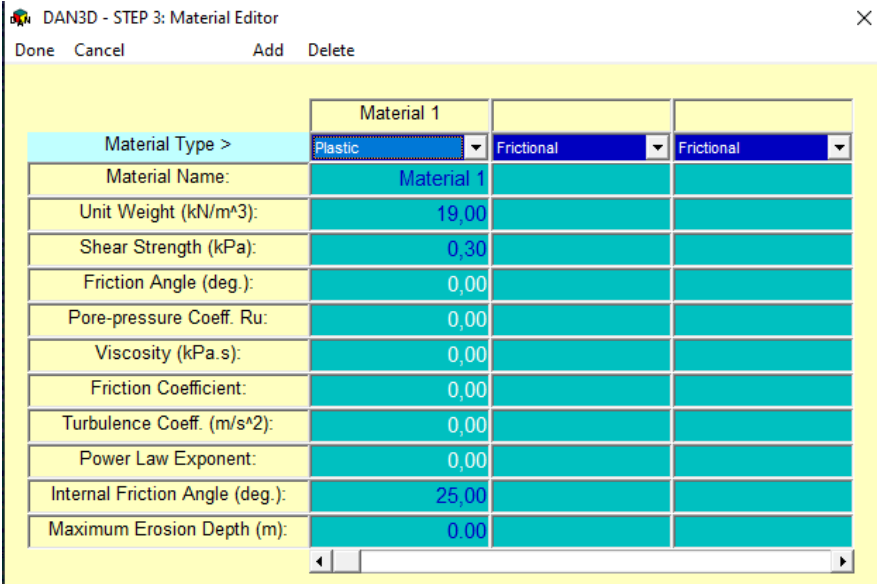

Figure 36 Different material properties to put in DAN3D.which properties that need to be filled in depends on the rheology.

Table 3 Material properties in DAN3D for the Kråknes landslide

Rheology	Plastic and Bingham
Unit weight (Kn/m³)	19
Shear strength (kPa)	0,3
Viscosity (Kpa.s)	0,00043
Internal friction angle (degree)	20°

Several authors have tested DAN3D on landslides in sensitive clay (Gebremedhin, 2013; Issler et al., 2013; V Thakur, Nigussie, et al., 2014; Gebreslassie, 2015) with varying results. The run-out distance from the DAN3D software on previous work seems to be more realistic than the output velocities provided by the model. It is clear that the software has some issues when simulating flows in sensitive clay and especially quick clay, but this is also an issue

for most numerical models that have been tested and compared to DAN3D by the same authors. In this study, the main goal is to reconstruct the Kårknes landslide event based on provided data, and for this purpose the DAN3D is considered usable. However, how some of the flaws in the model may affect the results are briefly described below:

1. The software can not model a slide developing retrogressively, and therefore the whole landslide is modeled as an instantaneous release. The movements of the entire mass spread at a lower rate than what a smaller part of the mass would do and may affect the simulated run-out distance.

2. The model does not account for the effect of the remolding of sensitive clay. Steps have been made to account for this in the Bingham fluid, where an exponential softening is assumed (De Blasio et al., 2003). However, this approach needs further improvement.

3. Multiple layers of different sensitivity are not accounted for. A quick clay slide can also involve amounts of both non-sensitive and less sensitive clays. An example of this is the Rissa landslide, where layers of clay were strong enough to stay intact as it rafted for hundreds of m (Issler et al., 2013).

4. The model does not consider hydrodynamic and buoyance effects in a subaqua failure (Issler et al., 2013) and can therefore reduce the simulated run-out distance compared to reality if there is subaerial movement.

4 Results

This chapter will present results of the investigation of the landslide area through stratigraphy and morphology mapping. Different sections of the landslide area will be presented as detailed outcrop descriptions, as well as other observations and data that have impacted the study area, such as hydrometrology and human activity. Results from the modeling in DAN3D will be illustrated and described and compared to empirical models used for risk assessment.

4.1 Description of the landslide area

This section describes the geomorphology of the Kråknes landslide area based on images taken and fieldwork conducted in the days following the landslide. Much of the description may not apply now due to the reworking of debris and small slides from the scarps. Figure 37 shows the study area and its major features used as reference points during the description of the study area.

Figure 37 The study area described in this section. The red line is the back scarp.

The landslide area occupies most of the beach at Kråknes. The landslide area is around 600 m wide from the southwest to the northeast. At the west is the water of Altafjord, and at the east rock of the Tålvik peninsula. A dome of rock, Storhaugen, frames the landslide on the northeastern side and reachs 80 m asl. Framing the landslide immediately at the east is the former E6-road (Now Kråknes Road). The geomorphology of the landslide area is shown in Figure 38. Within the landslide area is a well-exposed (up to 10 m high) back scarp facing west-northwest with a dip of 40-60°. From the foot of the back scarp to the waterline is a flat (slope angle) beach area which slopes gradually into the fjord. Within the landslide area (i.e. between the back scarp and waterline) are deposits of landslide debris, vegetation and remains of the houses that were caught in the landslide. Rotated blocks of soil that are intact can be seen within the debris and along the shore are two smaller scarps. Thin streams of water and sediments can be seen seeping from the back scarp, draining through the land-slide area and into the sea. Some of the seepages come from soil pipes that can be seen in the back scarp.

The landslide area has been divided into sections A, B, C and D (Figure 38) to provide a higher resolution description of the study area in subsequent sections.
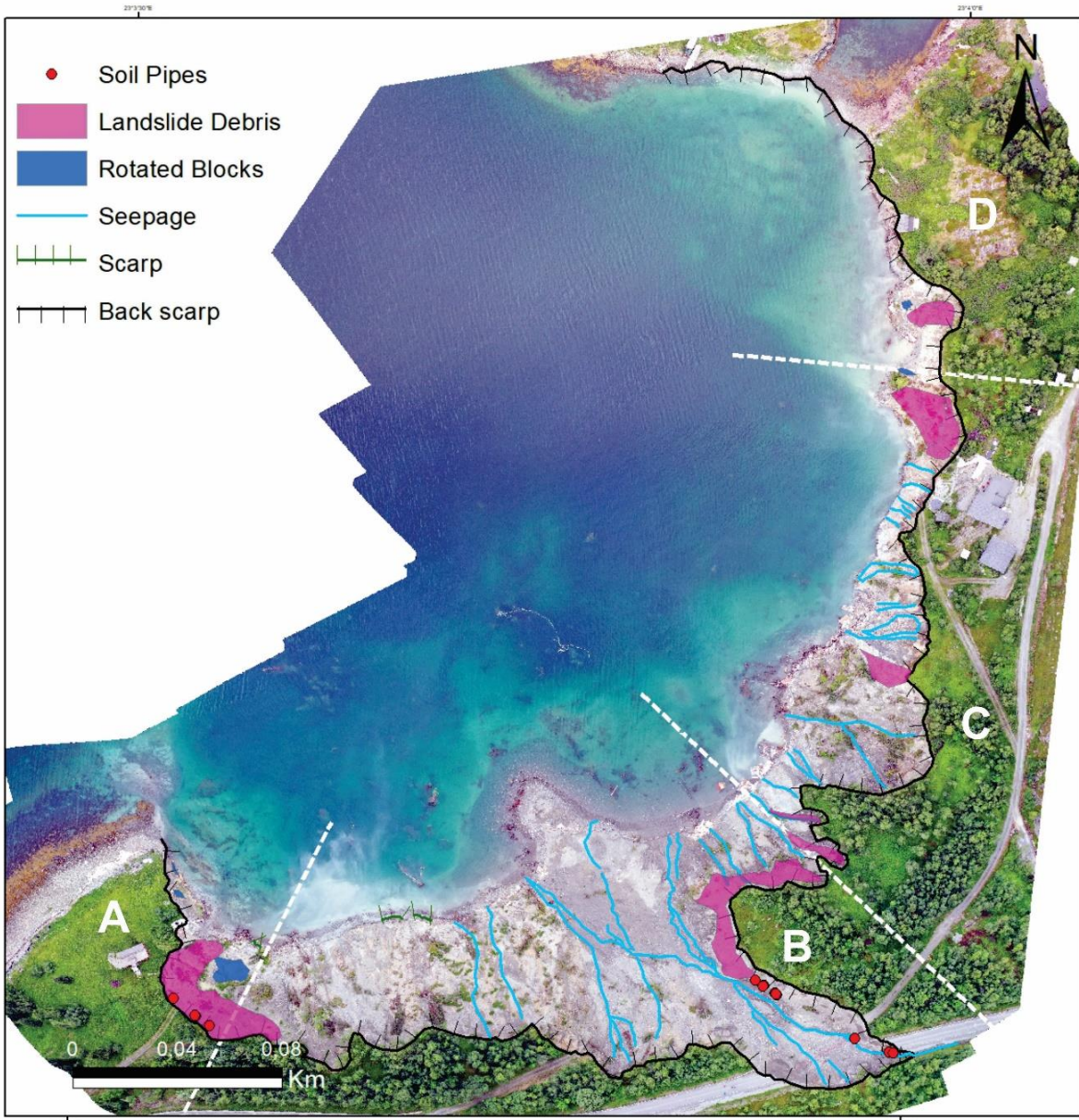
Figure 38 Perspective overview of the landslide area, showing sections divided by the stippled lines and geomorphological features. The UAV mosaic was taken on July 28th, 2020, 54 days after the event. Landslide debris can be seen floating in the water.

4.1.1 Landslide topography

The difference in topography from before and after the landslide event in 2020 can be seen in Prior to the 2020 landslide event, the area on land affected by the landslide had water channels that fed into the sea and down into a 50 m wide and 5-6 meter deep subsea channel further into the fjord. These channels are shaped by the surrounding bedrock, which protrudes several places on the seafloor on either side of the channel. Traces of a back scarp from the historic landslide event can be seen on land in the before topography (Pink line in Figure 39B).

In the post-landslide topography, a steep slope is formed in the back of the landslide area and below is an uneven terrain with landslide deposits on the beach, which gradually slopes into the sea (Figure 39C & D). The shoreline (0 m elevation marker from the ETRS 1989 datum) has become more irregular and has progressed relatively higher into the landslide area in the northwest. Large masses from the seafloor below the landslide back scarp are gone and two channels from the landslide area merge into the subsea channel seen in the pre-topography. This subsea channel has now become longer and 5-10 m deeper. In the south part of the landslide area, a steep back wall is followed by a weakly dipping surface at about eight m.b.s.l. A similar surface at the same depth can be seen further east (Arrows in Figure 39D).

Pre-landslide
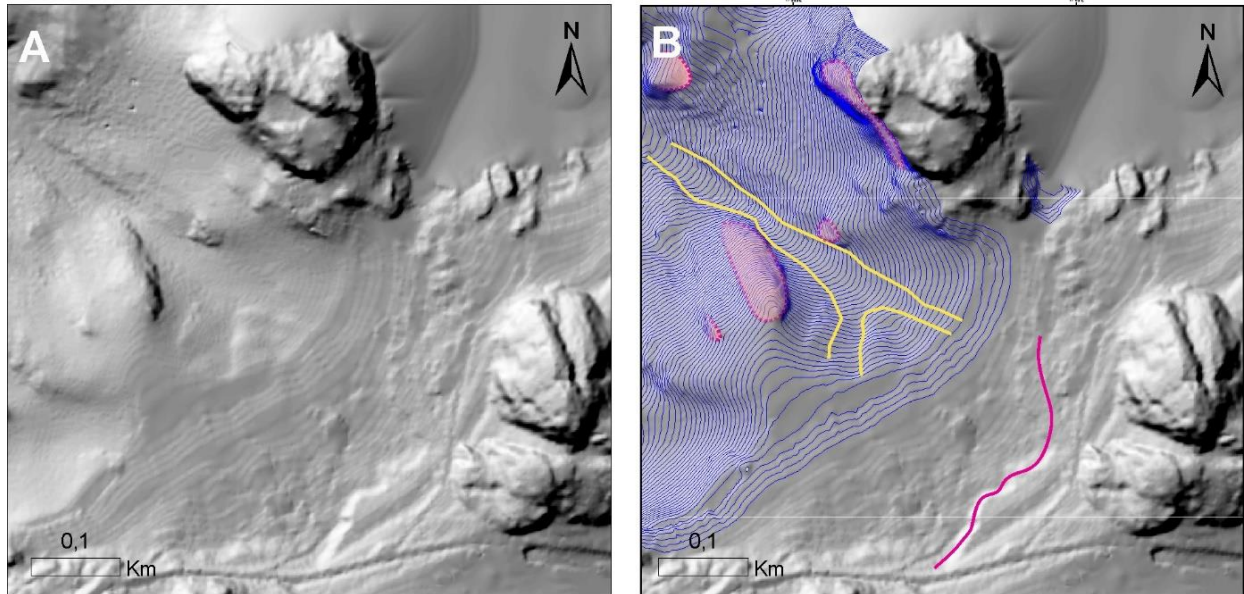
Post-landslide
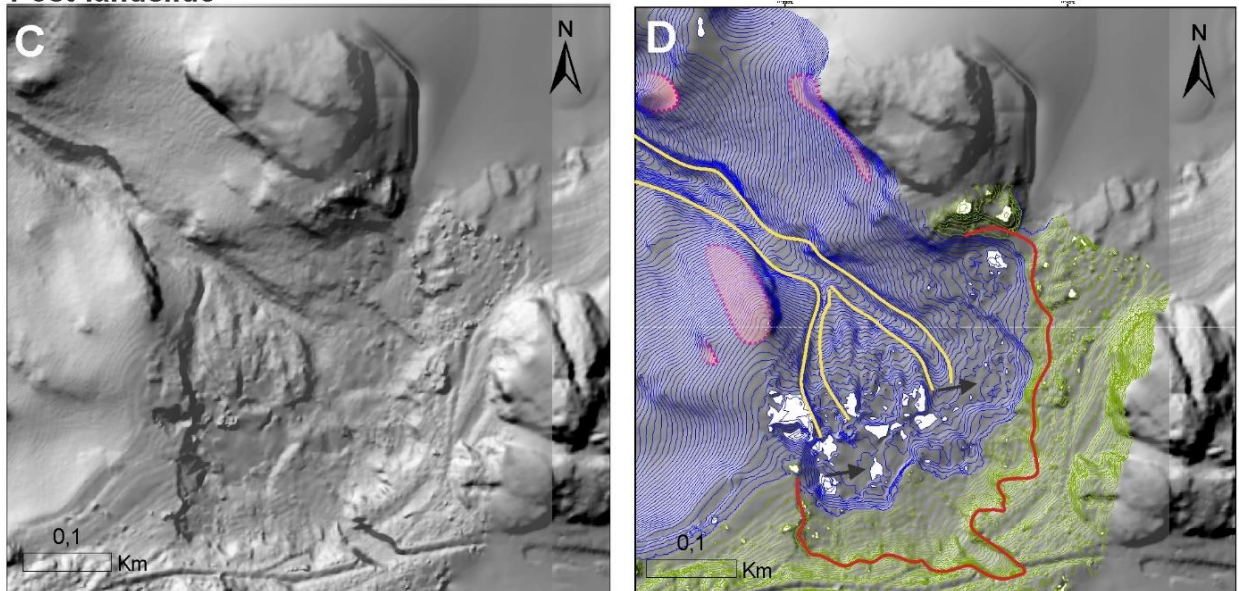
Figure 39 A) Hillshaded DEM-files of the study area before the landslide. B) Hillhade with Bathymetry contour (from 0 m asl and below). C) Hillshaded DEM-files of the study area after the landslide. D) Hillhade with Bathymetry contour (from 0 m asl and below) and terrain contour of the study area after the landslide. The arrows point at potential sliding surfaces at 8 m bsl.

4.1.2 Description of materials

Here we describe the common materials encountered in the site area. Material descriptions are based on field mapping of the road area, back scarp and beach (after New Zealand Geotechnical Society, 2005). Where it was not safe to access certain landslide areas, the occurrence of materials has been estimated visually. Materials are presented in stratigraphic order from the bottom-up, although many layers are repeating in the stratigraphic sequence and therefore, the order varies across the site.

Material 1: Silty CLAY; grey. Soft, very wet, high plasticity, extra sensitive/quick (Figure 40A). Interpreted as marine deposits.

Material 2: Silty CLAY with minor sand; light grey/beige; bedded. Wet, soft, high plasticity, extra sensitive (Figure 40A). Interpreted as marine deposits.

Material 3: Sandy silty GRAVEL, dark grey.Tightly packed; moist; well-graded; subrounded to subangular (Figure 40B). Interpreted as glaciofluvial deposits.

Material 4:: Sandy fine to coarse GRAVEL; grey. Loosely packed; dry; well graded; subangular to subrounded, fine to coarse sand (Figure 40B). Intepreted as glaciofluvial deposits.

Material 5: Gravely SAND; Greyish brown; bedded loosely packed; moist (Figure 40C). Intepreted as glaciofluvial deposits.

Material 6: Sandy fine to coarse GRAVEL with minor pebbles; brownish/beige; bedded; loosely packed, dry to moist; well graded; thick; rounded to subrounded; sand, fine to coarse (Figure 40D). Intepreted as glaciofluvial deposits.

Material 7: CLAY; bluish-grey; bedded. Very soft, moist, high plasticity, moderately sensitive (Figure 40E). Interpreted as marine deposits.

Material 8: Gravely fine SAND with silt; yellowish brown; massive, medium dense; dry to moist; low plasticity; contains shell fragments (Figure 40E). Intepreted as beach deposits.
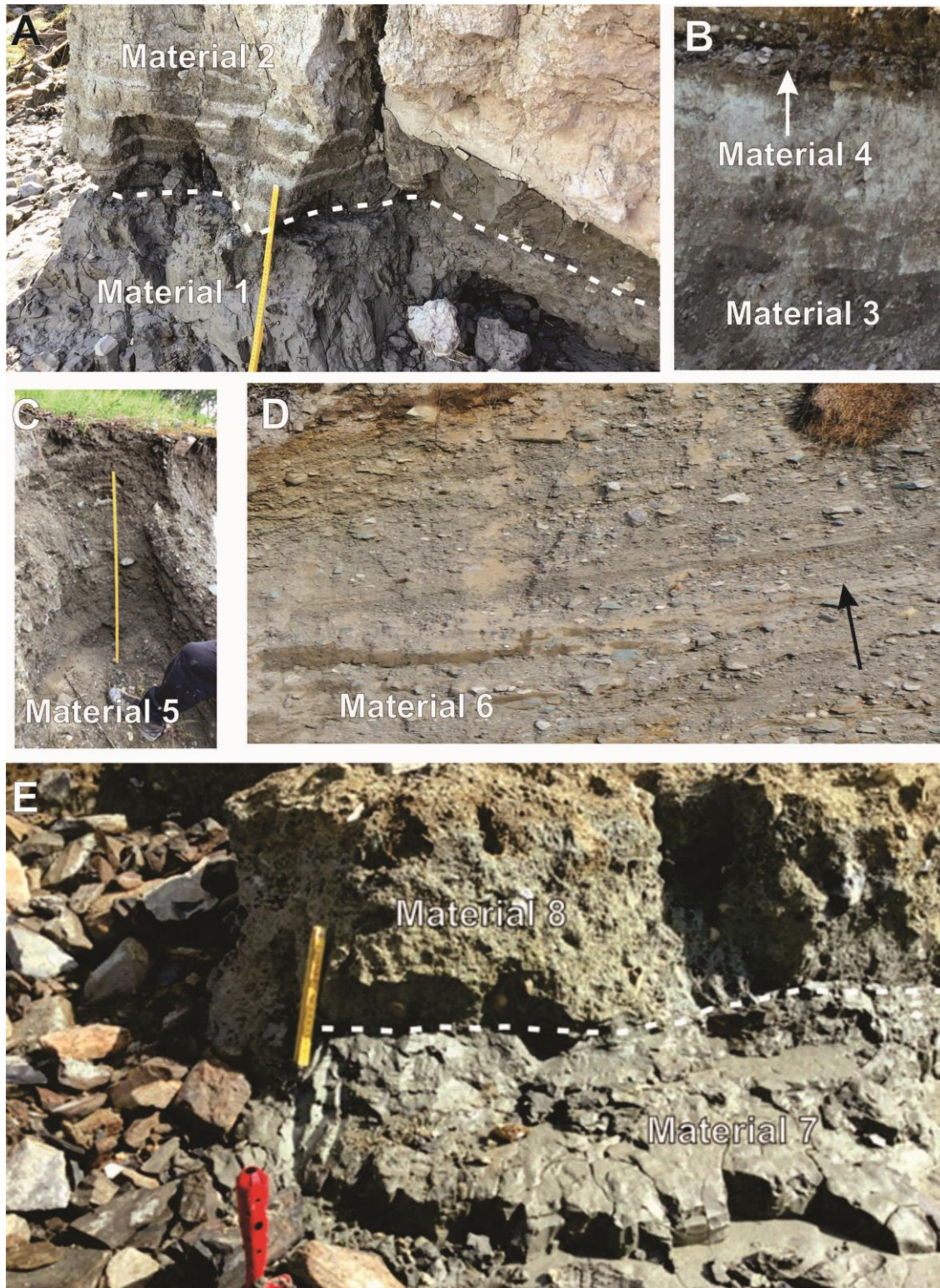
Figure 40 The different materials in the landslide area. A) Material 1, silty CLAY and 2, silty CLAY with sand B) Material 3, sandy silty GRAVEL and 4, sandy fine to coarse GRAVEL C) Material 5, gravelly SAND D) Material 6, sandy fine to coarse GRAVEL E) Material 7, CLAY and 8, gravelly fine SAND with silt.

4.1.3 Detailed section and outcrop descriptions

Here the different sections in the landslide area will be described closely. Fourteen different outcrops along the back scarp and floor of the landslide will be described based on fieldwork observations. Figure 41 shows the study area in front of the former E6-road and Storhaugen, with the divided sections and locations of the different outcrops.
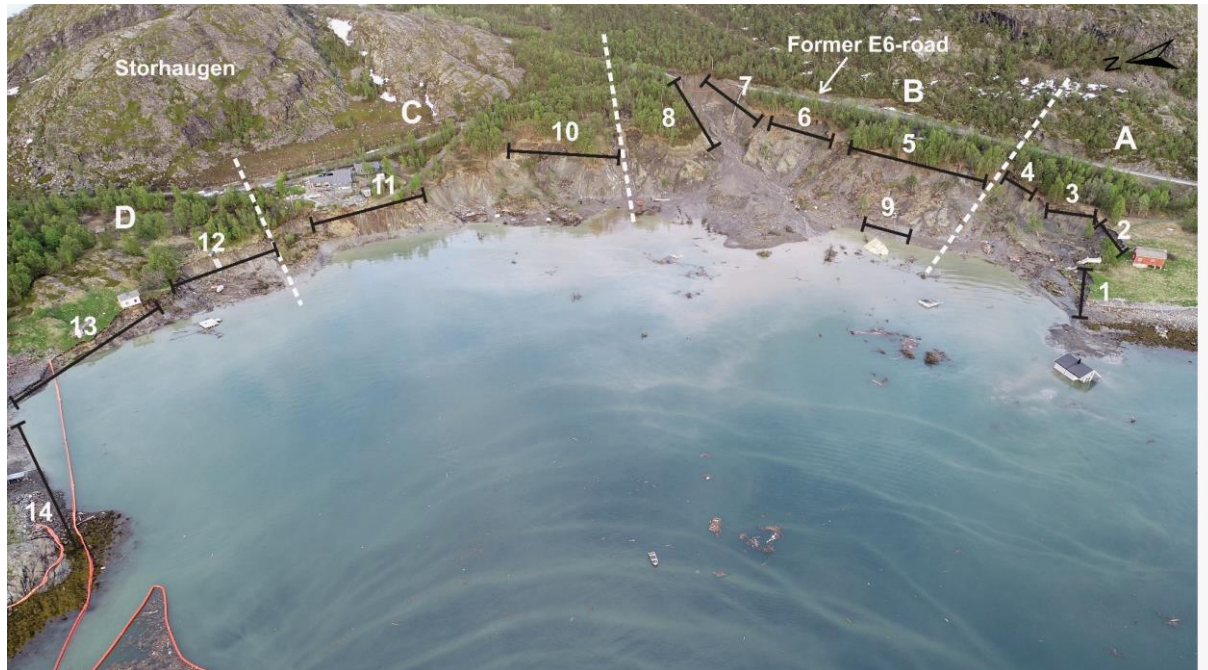
Figure 41 Overview of the study area from June 7th, 2020 with sections A,B,C and D and locations of outcrops 1-14 (Photo courtesy of Anders Bjordal, NVE).

Section A

Section A lies in the southwestern part of the landslide area and extends from the westernmost edge of the landslide scarp to the boundary of section B. This section is around 100 m wide from the west towards the east. The back scarp height is up to 11 m asl and has a 40° slope towards the northeast. The beach area consists of blocks of landslide debris up to 10 m long and 7 m wide. Among the landslide debris is vegetation and trees and remains of the house at 470 Kråknes Road that was transported by the landslide (Figure 42). The beach area has a gradual slope of around 10° into the sea. During low tides, a fine-grained, smooth

surface is well exposed at sea level. This section of the landslide area slid out towards the northeast on June 3rd, 2020 .
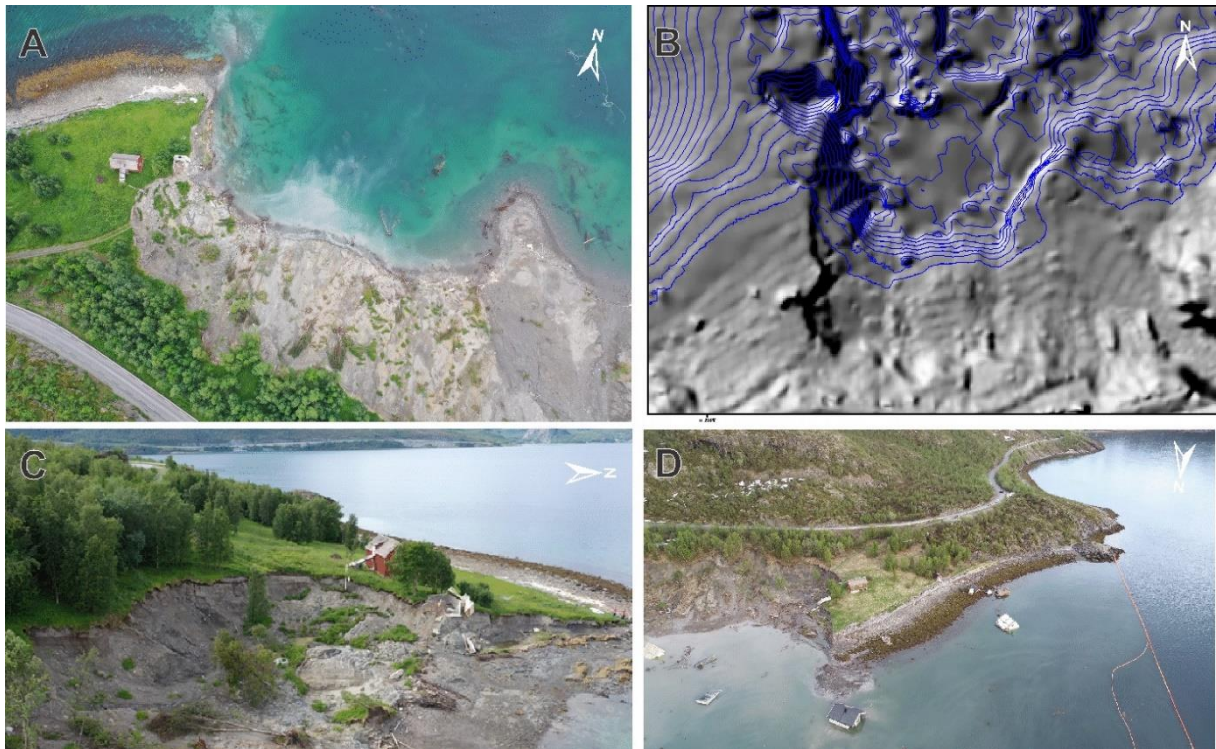
Figure 42 A) Orthographic overview of the section B) Hillshade based on 1 m DEM (top right) with 1 m contours from ba-thymetry,asl. C) Drone images from June 7th, 2020 of section A (Photo courtesy of Anders Bjordal, NVE).

Outcrop 1
In the eastern part of section A, materials 1 and 2 are exposed in the back scarp (Figure 42A & B). From sea level a 20-40 cm thick layer of material 1 is exposed, with a 50-100 cm thick bedding of material 2 above. Topsoil and vegetation mantle the scarp. Nearby the remains of the house at 470 Kråknes Road can be seen above the scarp (Figure 43

A). Some vegetation, landslide debris and rounded cobbles (likely glaciogenic) are deposited below the scarp. During low tides, bedding surfaces of clay (Material 1) are exposed along the shoreline due to landslide debris being washed away by waves. The surface has a gentle dip towards the north into the sea (Figure 43C).

Figure 43 A) Outcrop 1 in section A with bedding of Material 2 and 1. B) Bedding of Material 2. Inset: Matereial 1 when remolded between fingers. C) Material 1 surface exposed during low tides.

More of material 1 and 2 beddings are exposed in the back scarp further east in the outcrop and the height of the back scarp increases up to 5-6 m asl. The beds in this outcrop has a dip from 8-16° in the southeast direction dips in the southeast-. Rounded to sub-angular glacio-genic cobbles, boulders, trees, vegetation, and house remains are scattered across the beach in the release area. Some almost intact blocks of clay (Material 1 and/or 2) can be seen within the debris (Figure 43C).

Outcrop 2

Outcrop 2 is locates east of outcrop 1 (Figure 44A). Here the back scarp and materials are in-terpreted from a distance and through pictures. At the bottom of the scarp is 2-3 m of a dark colored layer of material 3. Above material 3 is a series of 0.5 to 1 m thick layers of clay, silt, and sand, interpreted to be the same as or similar to material 2. This layer is dry compared to the moister and darker colored material below. At the very top of the back scarp is a 20-30 cm thick layer of material 4 and topsoil (Figure 44B).

Figure 44 A) Gravel, Material 2 and 3 in the back-scarp of Outcrop 2. B) Close-up of the dashed square in A.

Outcrop 3

The soil layers observed in Outcrop 2 continues north in the section and have well-exposed bedding which can be traced from north to south (Figure 45A). In this part of the back scarp there is a clear boundary between material 2 in the top part of the back scarp and the darker colored material 3 in the bottom. Holes in the back-scarp are interpreted as soil pipe struc-tures that can be formed by fluvial erosion when there is a concentrated seepage with a

steep hydraulic gradient in a low-strength soil (Pierson, 1983). The pipe structures appear in the boundary between materials 2 and 3. Little or no water streams were seeping from these pipes during the fieldwork, but traces of previous streams could be seen below the pipe structures. More debris with rounded to sub-rounded cobbles and trees are seen on the beach below the back scarp (Figure 45B).

Figure 45 A)Back scarp with exposed bedding (white-dashed lines) and soil pipe structures. Vegatation and debris deposited below scarp. B) Landslide debris.

Outcrop 4

Outcrop 4 is located on the border to section B. Landslide deposits of gravel, angular boulders and vegetation are deposited beneath the well-exposed back scarp. The back scarp mainly consists of bedrock covered with thin layers of fine-grained sediments (Figure 46). The bedrock surface has an average dip of 24° with a W-NNW dip-direction. Similar bedrock measurements can be found in foliation east of this outcrop, in the bedrock exposed above the landslide area and the Kråknes road.

Figure 46 Outcrop 4 with areas of exposed bedrock marked within the red circles.

Section B

Section B (Figure 47) is north of section A with a back scarp that stretches 230 m from the southwest towards the boundary of section C in the northeast. The landslide area in this section stretches from the shoreline and all the way up to the former E6-road at 38 m asl. The majority of this section slid out on June 4th when the landslide event started, but the upper part of the section, which took parts of the former E6-road, slid out on June 5th and June 6th, 2020.
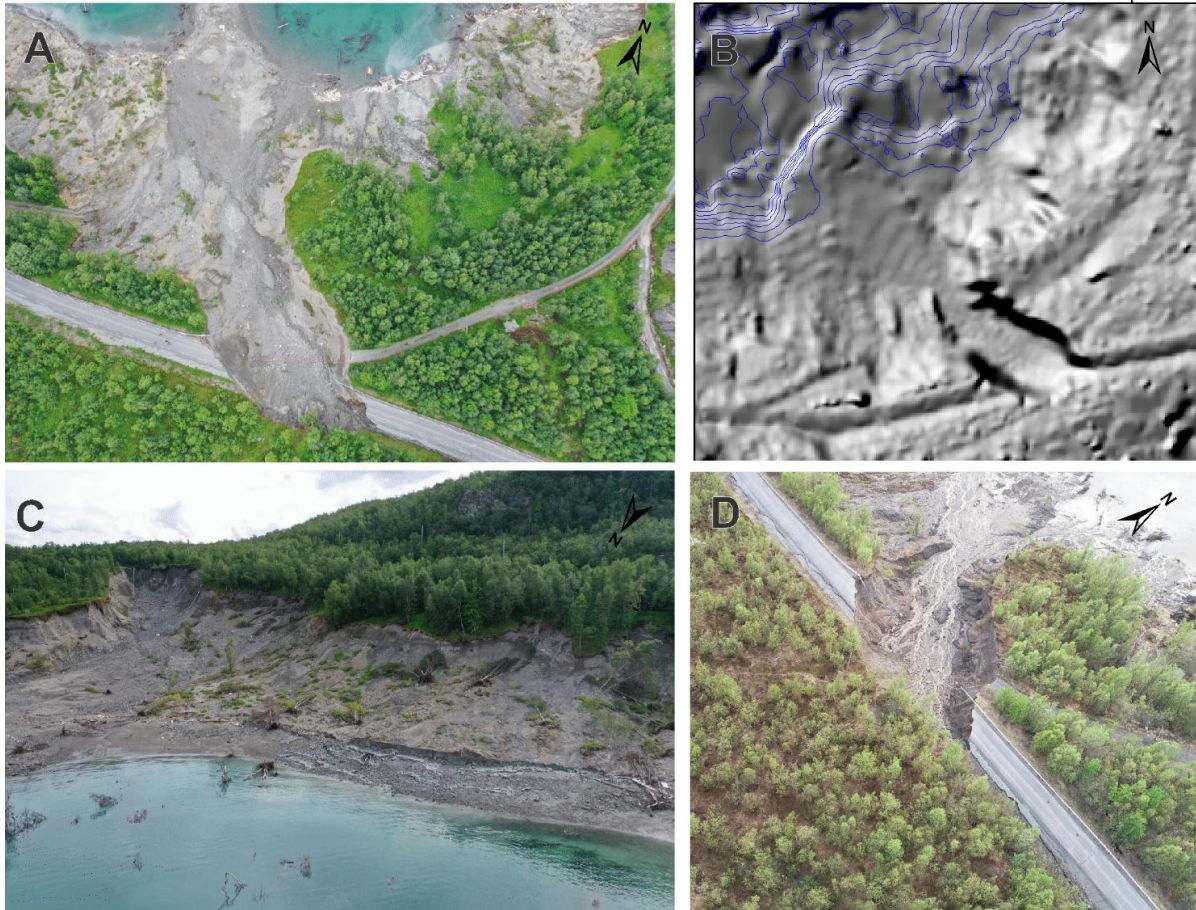
Figure 47 A) Orthographic overview B) Hillshade based on 1 m DEM with 1 m blue bathymetry contours, C) Drone photos from July 27th, 2020 D) Drone photo from June 7th, 2020 (Photo courtesy of Anders Bjørdal, NVE).

Outcrop 5

Outcrop 5 is located in the southwest part of section B and stretches 100 m from the border of section A towards the northeast and follows the 2-3 m heigh back scarp. South in the outcrop are northwest dipping beddings of material 2 with a layer of material 5 and topsoil on top (Figure 48A). This stratigraphy can be traced further north in the section but with an angular disconformity between materials 2 and 5 (Figure 48B). The disconformity disappears and is not seen again through the outcrop. Beddings of materials 2 and 5 continue further north and become thicker compared to the bedding in the southern part of the outcrop. Within material 5 are darker colored and moist areas (Figure 48C) and the presence of pebbles. At the foot of the back scarp is a gradually dipping surface towards the beach with landslide debris and vegetation.

Figure 48 A) Outcrop 5 with beddings of material 2 and 5. B) Beddings of material 2 and 5 with an angular disconformity. C)The arrow points at a moist area within material 5 in outcrop 5.

Outcrop 6

Outcrop 6 is a small outcrop seen through a close-up of the scarp from drone photos (Figure 49). Here the scarp mainly consists of a thick deposit of material 6 with beds dipping northwest. Within material 6 there are small cobble-sized rocks oriented with their oblong side in the dipping direction and seem to overlap each other in a consistent fashion. This orientation may resemble imbrication from a fluvial environment. By the tractor road in Figure 46, a soil sample was collected and classified as material 5. Based on these observations with the finer-grained material below coarser-grained bedding and the presence of imbrication, the deposits are likely to have been deposited in a glaciofluvial delta. The orientations of the beds also fit well the direction of the ice during YD (Figure 10).

Figure 49 Outcrop 6 with thick deposits of material 6 and imbrication.Close-up of material 5 by the tractor road.

Outcrop 7

Outcrop 7 consists of the back scarp in the part of the section where the landslide has worked its way back to the Kråknes Road at about 40 m asl. The back scarp is up to 10 m high and has a 50-60° dip towards the north. The outcrop mainly consists of beddings of material 6 and have several darker colored and moist spots where there is seeping water and

sediments into the landslide area (Figure 50A). Below the scarp are deposits of landslide debris and small braided water streams flow from the back of the landslide scarp towards the sea (Figure 50B).

Figure 50 A) Landslide pit and back-scarp up to 40 m asl. Beddings of material 6. The arrow shows water seepage from the back-scarp. B) Braided water streams below the back scarp.

4.1.3.1 Outcrop 8

Outcrop 8 is facing the southwest and stretches 80 m from 20 m asl in the northwest to 38 m asl in the southeast. It consists of the 8-10 m heigh back scarp with beddings of material 6. The beddings have a northwest dipping trend marked with white dashed lines (Figure 51B). In the northwest part of the outcrop, there are exposed bedding of fine-grained grey material, possibly clay and silt (Figure 51B). Within the outcrop are several soil pipe structures at the bottom of the scarp with small streams of water and sediments coming out of them. Several of these soil pipes seem to have been previously connected (Figure 51A).

Figure 51 A) Back scarp in outcrop 8. Arrows point at soil pipes within the back scarp. B)Beddings of material 6. Arrow points at beddings of clay/silt.

Further southeast in the outcrop, there are darker and moist areas within the beddings, and more soil pipe structures can be seen (Figure 52A). At the southeast end of the outcrop, parts of the former E6-road have been taken by the landslide (Figure 52B). In the back scarp right beneath the road, more soil pipes can be seen (Figure 52C). In late July, there was seeping of water and sediments between the beds in this part of the outcrop and a small water stream was seeping into the landslide area from the ditch above the outcrop.
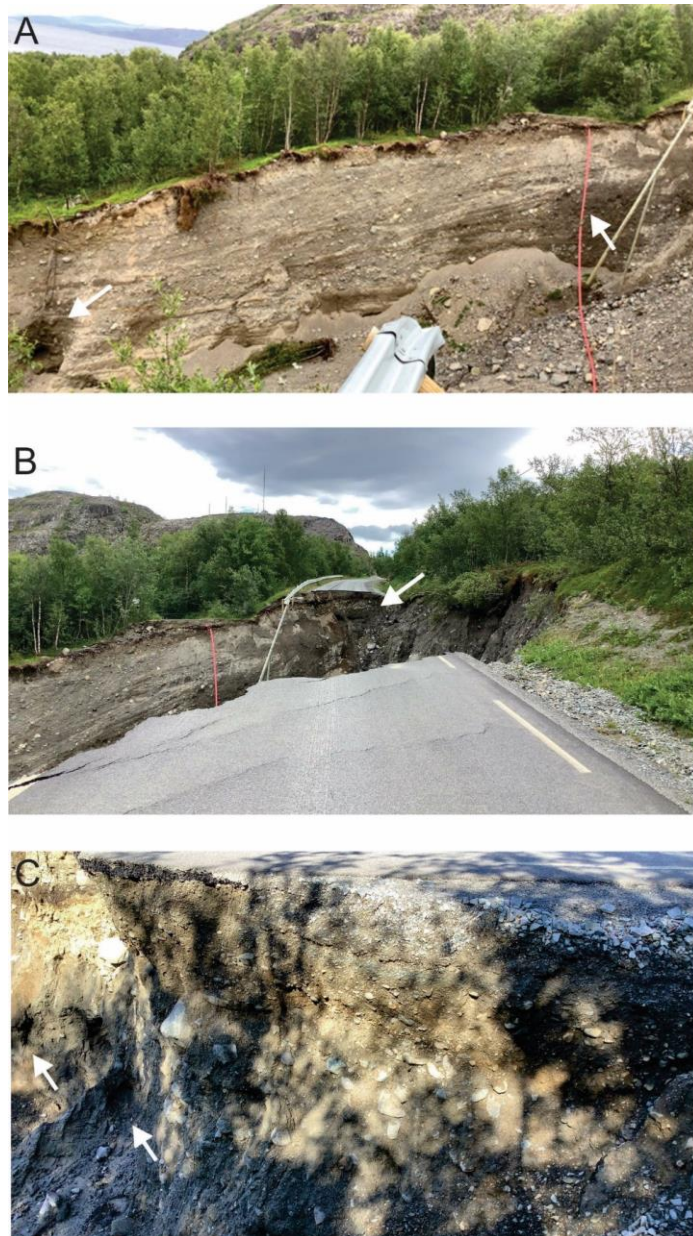
Figure 52 A) Seepage between beddings in outcrop 8. B) Back scarp beneath the former E6-road. The arrow shows moist gravel. C) Close up of moist gravel beneath the road. Arrows point at pipe-like structures.

Between outcrop 7 and 8 is a fine-grained surface from about 30 m asl towards the sea in the northwest with a gradual slope of 10-15° (Figure 53A). On this surface are small braided channels of water streams from the back of the landslide area into the fjord. Some dry stream channels can also be seen (Figure 53B). Talus, landslide debris and vegetation have been deposited on the beach between the back scarp and the sea, and vegetation can be seen floating around in the fjord (Figure 53A).
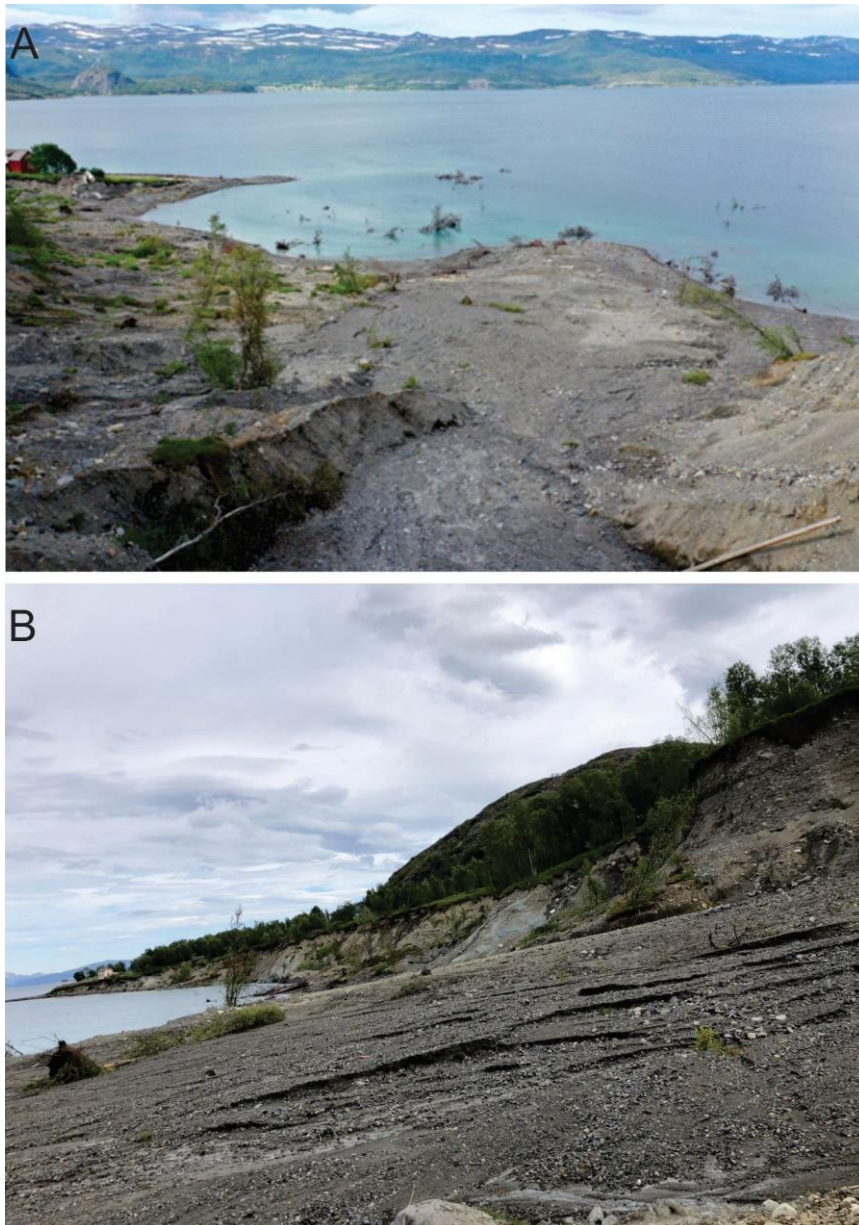
Figure 53 A) View of landslide area towards the west. B) Stream channels in clay covered by thin layers of silt and sand.

Outcrop 9

Outcrop 9 is exposed during low tides towards the northwest. It stretches 5-7m from the east towards the west and consists of a 1-1.5 m heigh in-situ scarp (Figure 54). The scarp consists of material 7 with beach deposits (likely material 8) on top and has stair-like morphology. The bedding has a dip from 6-9° in NW-NNW dip-direction and has cracks from being exposed to the sun.

Figure 54 Outcrop 9 of the scarp with clay/silt beddings covered with beach deposits that are exposed during low tides.

Section C

Sections C is located north of section B and stretches around 200 m from north to south. This is the section in which the landslide started on June 3rd, 2020. The back-scarp in this section has a height up to 8 m from sea level and has a slope ranging from 30-50° (Figure

55). Storhaugen, east of the section, consists of very fractured bedrock that also can be seen within the landslide back scarp. Right above the back scarp is a blue house located safely on top of bedrock, where a resident watched the landslide as it occurred.
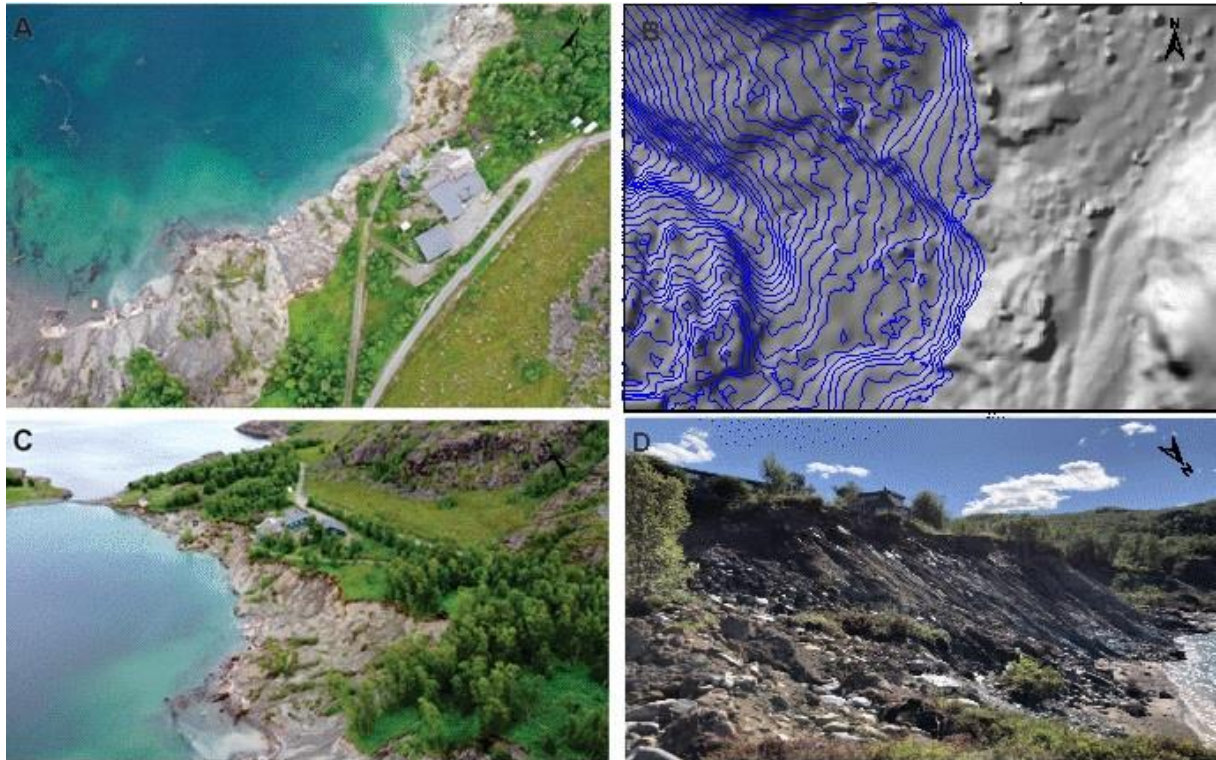
Figure 55 Section C. A) Perspective overview of sections C from July 27th,2020. B) Hillsahde from 1 m DEM-files with blue countours of bathymetry. C) Drone photo from July 27th, 2020.D) Picture from fieldwork on July 27th, 2020.

Outcrop 10

Outcrop 10 is located in the south part of section C at the border of section B. It includes about 40 m of the back scarp with a dip of about 40° towards the northwest into the sea. The back scarp mainly consists of bedrock covered with thin layers of fine-grained sediments and debris at the bottom. Above the bedrock is a 30-50 cm thick layer of or similar to material 2 with 50-60 cm thick layers of sand and gravel (possibly material 5 or 6) on top. In some parts of the back scarp are thin layers of clay/silt that seem to cover the bedrock (Figure 56B). Several places in the scarp there are moist areas within the gravel or in the boundary between the fine-grained and coarser-grained soils. In several places there is seepage of water and sediments between the bedrock and soil layers (Figure 56A). A stream of water running down the back scarp is also present in this area (Figure 56A).
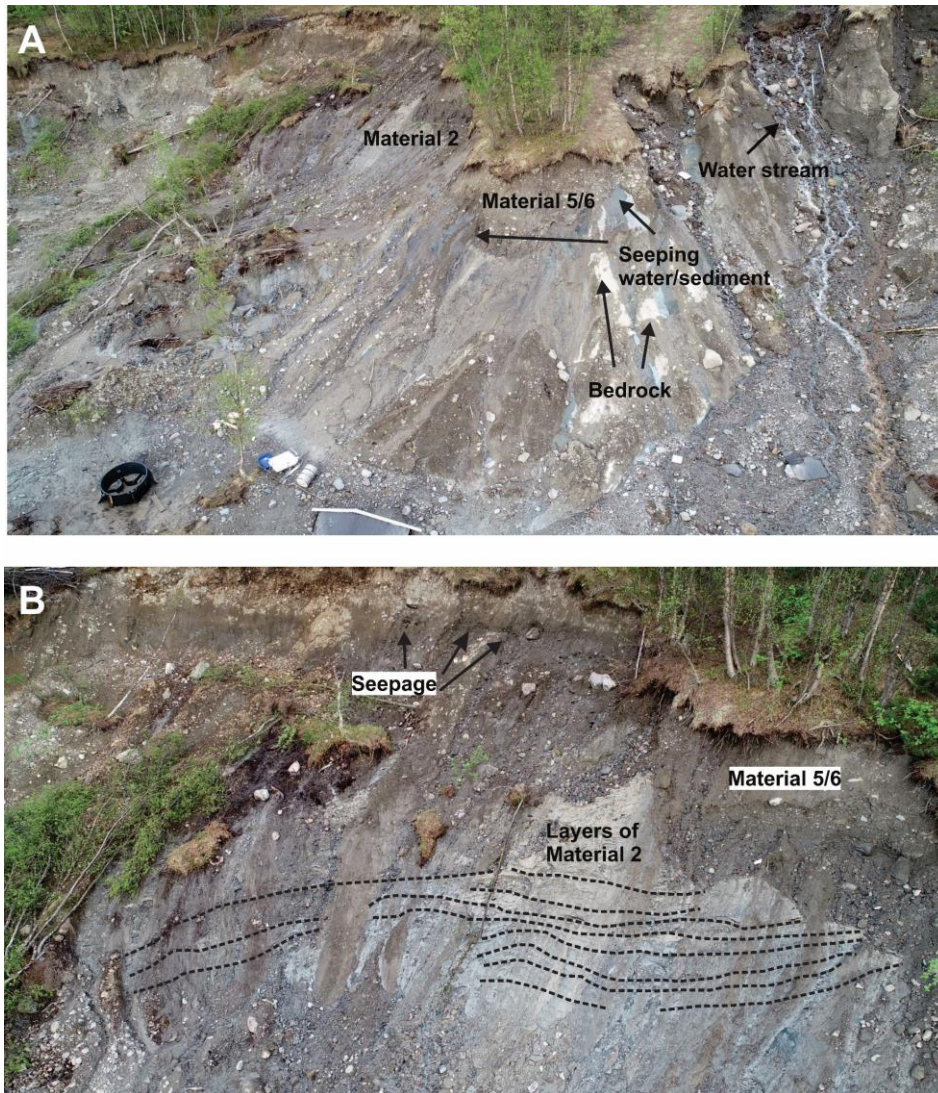
Figure 56 A) Outcrop with sand/gravel, layered clay/silt and rock. B) Close-up of the soils in A with layers of material 2 The arrows are pointing out areas where there is/have been seeping of water and sediment (Picture courtesy of Anders Bjordal, NVE).

4.1.3.2 Outcrop 11

Outcrop 11 is the 10 m high back scarp at the foot of the blue house, with a 40-45° slope angle into the sea that stretches 60 m from south to north (Figure 57). The bottom 7-8 m of the back scarp consists of bedrock covered with thin layers of sand, silt and clay. The bedrock is well exposed at the very bottom of the scarp with thin layers of clay/silt due to being washed by the waves. Above the bedrock is a 1-2 m thick layer of sand/gravel (possibly material 5 or 6). In the top of the scarp, there is also the presence of fill mass from the tractor

road. Between the bedrock and the soil layer on top, there is seepage of water fine-grained sediments that can be seen throughout the whole outcrop. Talus from the upper layer covers the bedrock where the slope allows it.
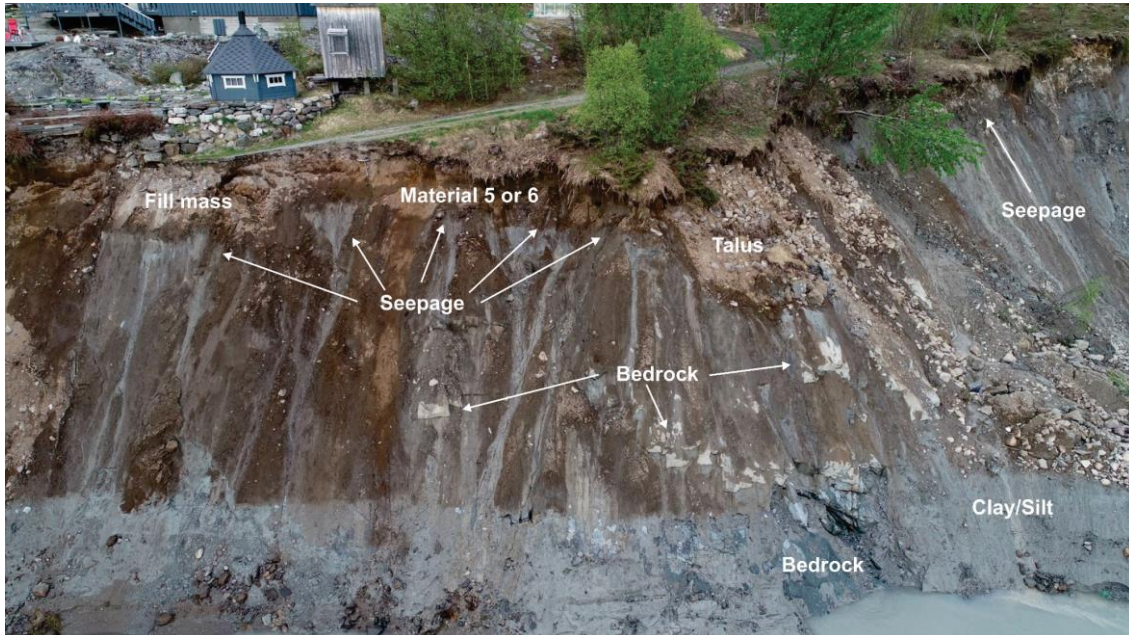
Figure 57 Outcrop 11 with the back scarp beneath the blue house. Water and sediments are seeping out between the bedrock and the soil. The yellow arrows show rock exposed in the scarp (Photo courtesy of Anders Bjordal, NVE).

Behind outcrop 11 and the blue house, there is a fractured bedrock with an average foliation striking NNW-SSE with a 15° dip (Figure 58). This foliation is cut by E-W striking faults (See chapter 4.2).

Figure 58 Fractured bedrock at Storhaugen, east of section C.

Section D

Section D is the northern part of the study area and follows the scarp for 170 m from the border of section C in the southeast towards the northwest. The scarp height in this area varies from 1 to 10 m asl and faces the south and the southwest (Figure 59). Parts of the landslide in this area occurred underwater, and therefore, the back scarp is not well exposed in most outcrops. This section of the study area slid out after section C on June 3rd, 2020 and destroyed parts of the dock located in the section.
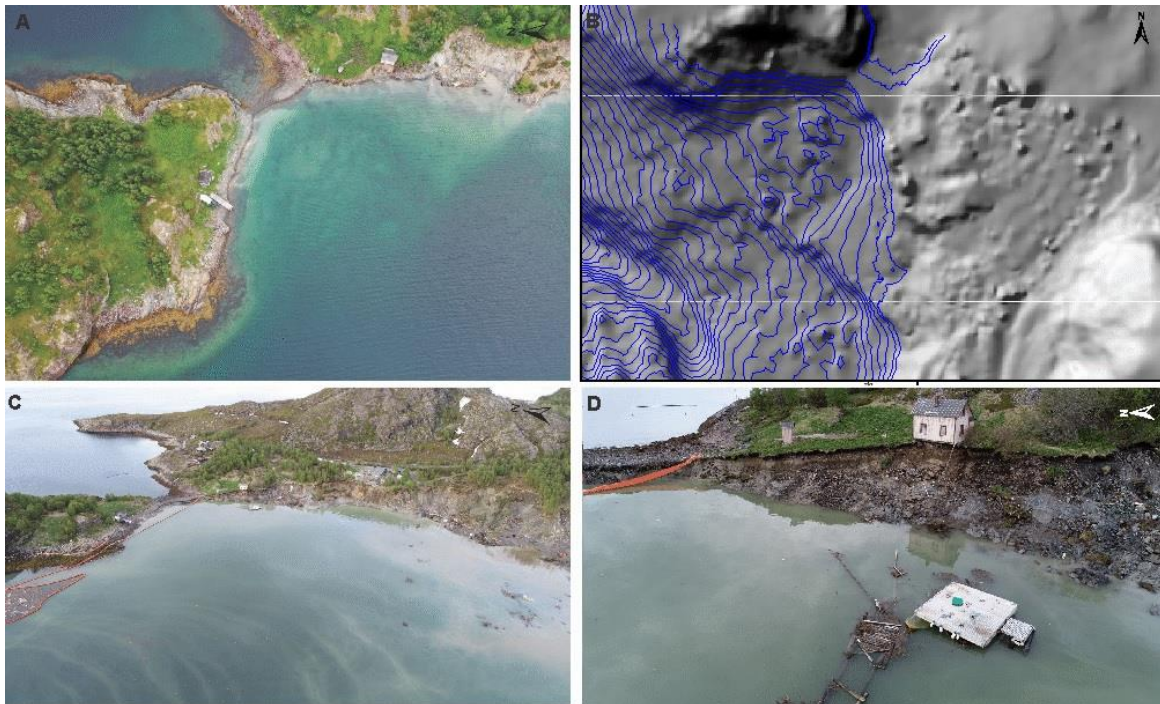
Figure 59 Section D A) Orthographic overview of the section. B) Hillshades based on 1 m DEM with 1 m blue contour of bathymetry. B) Drone image from June 7th, 2020 (Photo courtesy of Anders Bjordal, NVE). D) Close up of scarp below shed in the section from June 7th, 2020 (Photo courtesy of Anders Bjordal, NVE).

Outcrop 12

Outcrop 12 is on the border of section C and stretches about 70 m from the southeast towards the northwest. It includes a steep back scarp dipping 40-50° towards west -southwest and an almost horizontal to gradually dipping surface of clay below the back scarp that is exposed during low tides. The clay surface is considered to consist of material 7 and has several striations striking towards NW, and small rounded to sub-rounded rocks from 1-10 cm

of length can be seen within the material (Figure 60A). Most of the rocks stuck on the surface are deposited with their long side in the same orientation as the striations. North of this surface is a big mass of clay (material 7) with possible tension cracks (Figure 60B).

The back-scarp mainly consists of material 7, which is very dry and has desiccation cracks (Figure 61A & B). The back scarp is covered by landslide debris and within the debris are exposures of bedrock (Figure 61A). The slope of the scarp seems to follows the surface of the bedrock in the areas in which bedrock is exposed (Figure 61B). At the foot of the scarp northwest in the outcrop is a very fractured bedrock surface exposed with an approximate dip of 30°in the northwest direction. Some of the fractures are interpreted as glacial striations stretching from the southeast to the northwest (Figure 61C). Throughout the outcrop are large amounts of debris of angular and sub-rounded cobbles and boulders deposited below the back scarp.

Figure 60 A) Clay surface with striations below scarp in outcrop 12. The arrows show rocks with their long side in the same orientation as the striations. B) A mass of clay with tension cracks.

Figure 61 Outcrop 12 A) Yellow arrows show bedrock exposed in back-scarp. B) Close-up of bedrock in the scarp and desiccation cracks in material 7. C) Outcrop with fractured bedrock and possibly glacial striations. Pink arrows point at cracks.

Outcrop 13

Outcrop 13 is located north of outcrop 12 and stretches 20 m from the southeast towards the northwest. It consists of a 1-2 m heigh back scarp facing towards the west with a 50° slope angle (Figure 62A). The back scarp is located at the foot of a little pink shed which is in danger of failing. At the bottom of the scarp is a 1-1.2 m thick layer of material 8 (beach deposits) covered by a 50-70 cm thick layer of sand (Possibly material 5), gravel and top soil. Below the back scarp is a gradually dipping uneven surface of material 7 which is connected to material 8 with a clear boundary (Figure 62B & C).
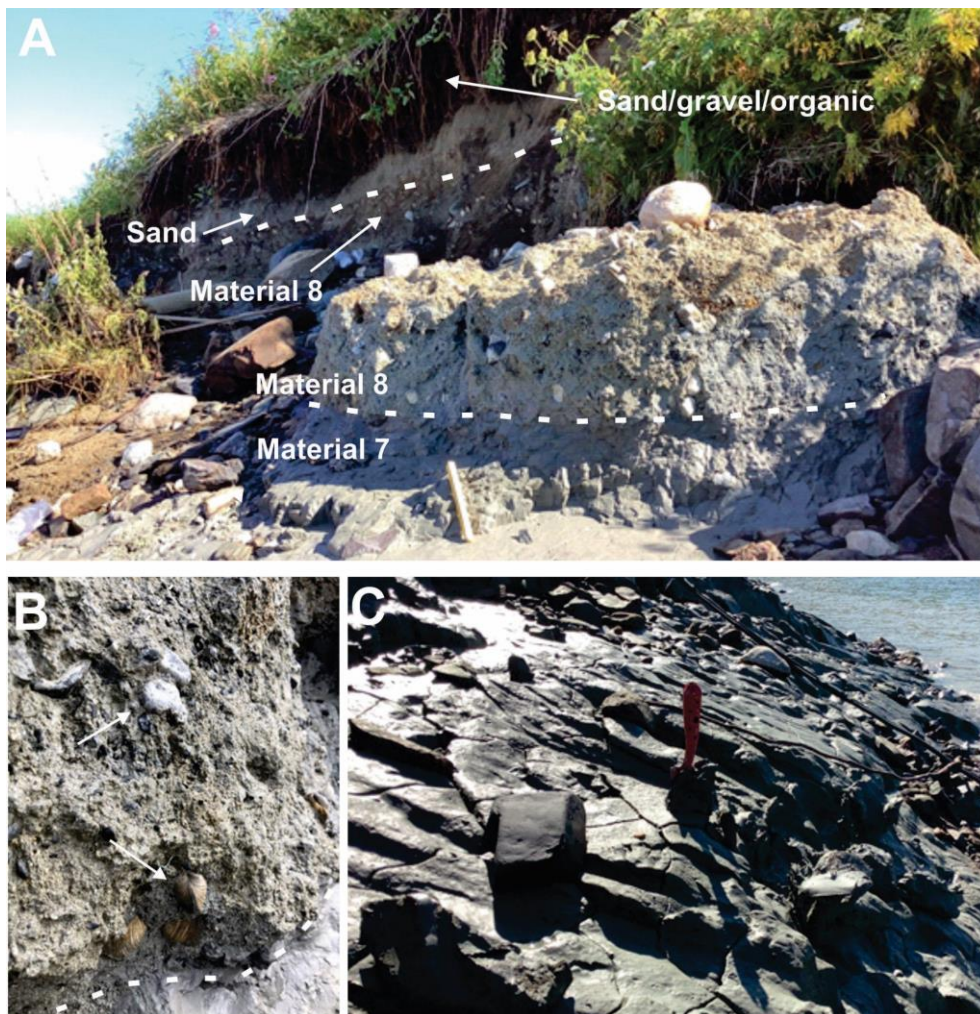
Figure 62 A) Back scarp in outcrop 13. B) Close up of material 8 with arrows pointing at shells and the stippled line is the boundary to material 7 below. C) Uneven surface of material 7.

Outcrop 14

Outcrop 14 is in the most northern part of the study area on a little peninsula and stretches 30-40 m from southeast to northwest. The scarp in this outcrop is facing south and is barely exposed even during low tide. This part of the landslide slid out mainly underwater and destroyed parts of the dock (Figure 63). The outcrop mainly consists of bedrock, which is covered by vegetation and subangular to subrounded cobbles and boulders. Underneath and in between the cobbles and boulders are deposits of silt or a material similar to material 8 (Figure 64A). A thin layer of material 7 with drought cracks covers the bedrock located close to the dock (Figure 64B). The top of the barely exposed back scarp consists of materials 7 and 8 with cobbles and boulders on top (Figure 65).

Figure 63 Dock and scarp along the shoreline in the northern part of the landslide area. The dock was destroyed because of the landslide. The picture is taken during high tide about 12 days after the landslide occurred.

Figure 64 Outcrop 14 A) Material 7 and 9 between cobbles and boulders. B) Material 7 covering bedrock.

Figure 65 Top of the back scarp in outcrop 14 that can barely be seen above water during low tides.

4.1.4 Orientation data

Orientation measurements of joint surfaces and foliation of the rockmass were taken from Storhaugen east of the landslide scarp, within the landslide area, and next to the former E6-road are presented here. Forty measurements were taken in total. They have an average dip direction towards the northwest with an average dip of 15° (Figure 66). Bedding and surfaces of fine-grained materials, mainly from the back scarp in section A and the scarp in section B, have also been measured. Due to the difficulty and risk of being in the landslide area, only 14 different measurements of these beddings and surfaces were made. These beddings tend to dip towards the west-northwest with an average dip of 9 ° (Figure 67).

Symbol	Feature
◇	Pole Vectors

Color	Density Concentrations		
	0.00	-	2.60
	2.60	-	5.20
	5.20	-	7.80
	7.80	-	10.40
	10.40	-	13.00
	13.00	-	15.60
	15.60	-	18.20
	18.20	-	20.80
	20.80	-	23.40
	23.40	-	26.00

Contour Data	Pole Vectors
Maximum Density	25.93%
Contour Distribution	Fisher
Counting Circle Size	1.0%

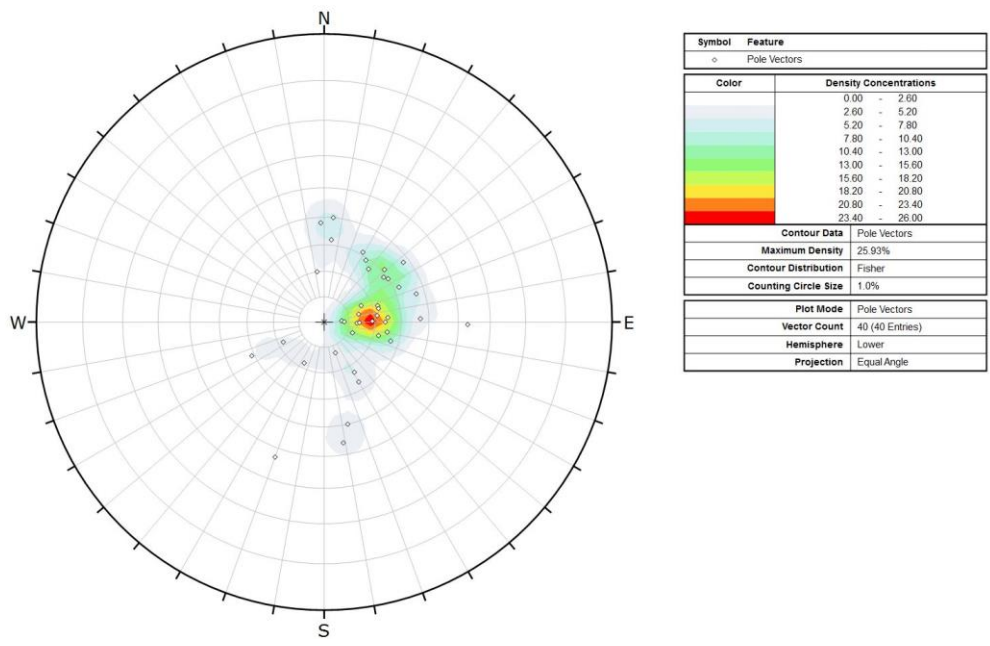| Plot Mode	Pole Vectors
Vector Count	40 (40 Entries)
Hemisphere	Lower
Projection	Equal Angle

Figure 66 Dip and dip directions of foliation and surfaces in becrock within and around the landslide area displayed in a stereonet. Projected with pole vectors in the lower hempisphere and with equal angle projection.

Symbol	Feature
◇	Pole Vectors

Color	Density Concentrations		
	0.00	-	5.60
	5.60	-	11.20
	11.20	-	16.80
	16.80	-	22.40
	22.40	-	28.00
	28.00	-	33.60
	33.60	-	39.20
	39.20	-	44.80
	44.80	-	50.40
	50.40	-	56.00

Contour Data	Pole Vectors
Maximum Density	55.96%
Contour Distribution	Fisher
Counting Circle Size	1.0%

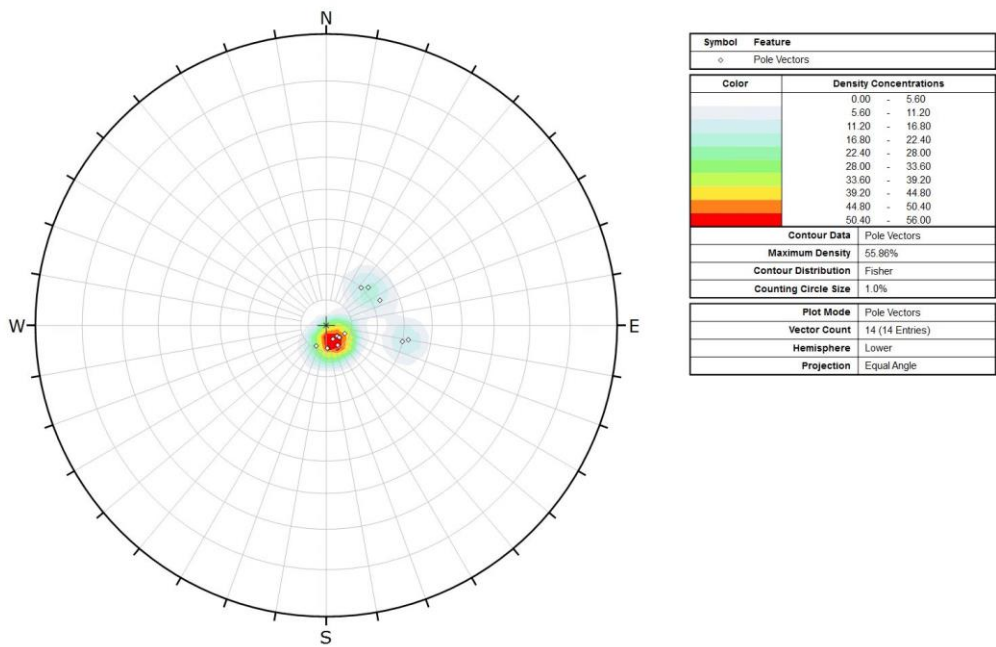| Plot Mode	Pole Vectors
Vector Count	14 (14 Entries)
Hemisphere	Lower
Projection	Equal Angle

Figure 67 Dip and dip direction of fine-grained soil beddings from within the landslide area displayed in a stereonet. Projected with pole vectors in the lower hemisphere with equal angle projection.

4.2 Cross-sections

Here the topography and cross-sections of the landslide area before and after the landslide are presented. The cross-sections are made based on core samples collected by Multiconsult (Appendix A) and the field observations in chapter 4.1 to best illustrate the stratigraphy and morphology in the study area.

Ten different cross-sections have been made in the study area. The sections are from five different locations and for each location, a cross-section from both before and after the landslide is illustrated. Figure 68 shows an overview of the location of the different cross-sections and the different boreholes and outcrops they are based on.
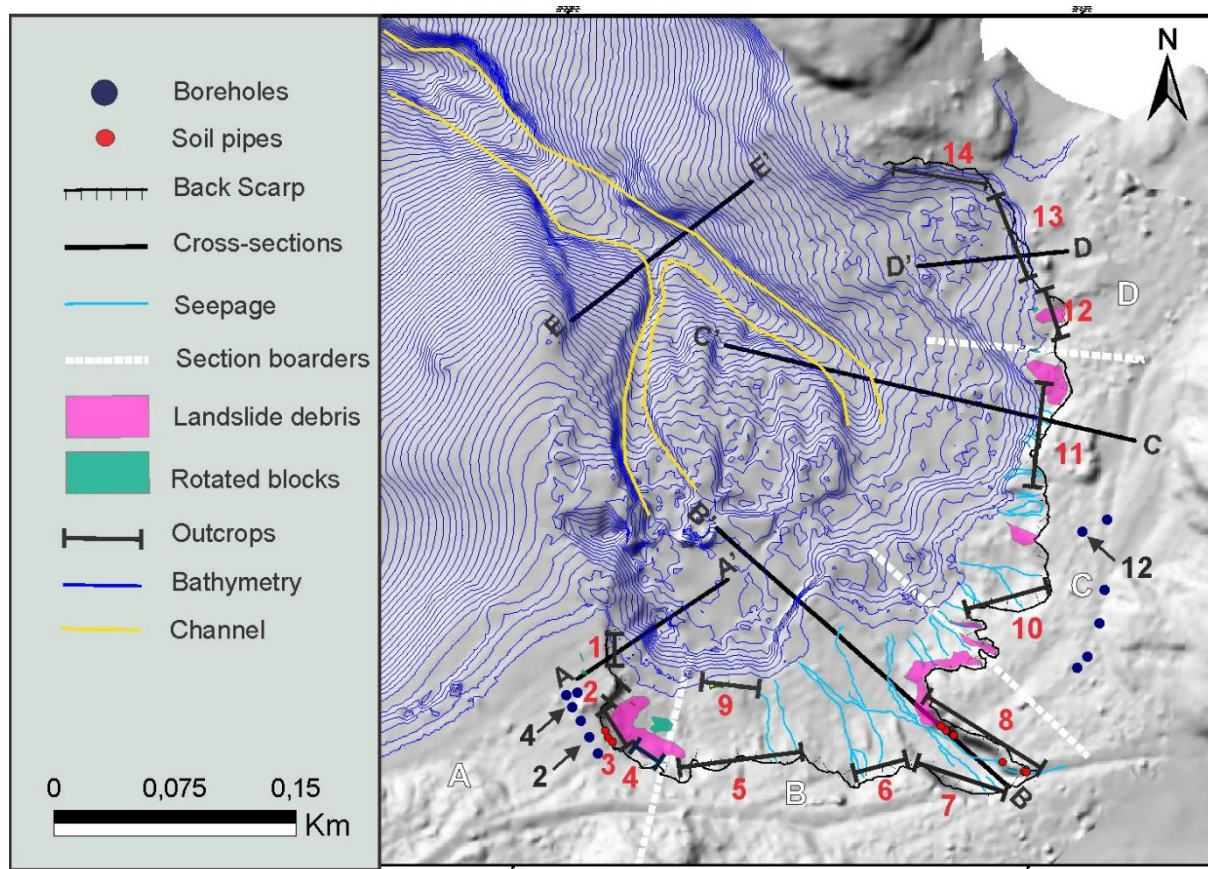

Figure 68 Location of cross-sections in the study area, with the different outcrops numbered in red from 1-14. The black numbers show the boreholes where core samples 2,4 and 12 are collected.

Cross-section A-A'

In section A, a cross-section stretching 115 m from SW-NE has been illustrated (Figure 69). The layers in the cross-section are based on field observations and core sample number 4 collected by Multiconsult AS (See Appendix A). The section mainly consists of clay with layers of sand and silt and some gravel. The sediment has low sensitivity (S_t=7-17) in the uppermost layers until they become more sensitive at about 12 m depth (S_t=29). At about 13-14 m depth, there is a layer of highly sensitive clay which is classified as quick (S_t=49). Based on literature (See chapter 2.1.2), it is interpreted that the layer of quick clay is not continuous but in small pockets within the marine deposits. The cross-section goes from being relatively horizontal before the landslide occurred to have a 10-30 ° slope angle after. The post landslide cross-section has a "stair-like" morphology between the 20 and 60-meter mark before the slope flattens out at about 10 m below sea level. Where the slope flattens out, there is hummocky material interpreted as landslide debris from the release area above. This weakly dipping surface can also be seen in the post topography in Figure 39D.

Cross-section B-B'

Cross-section B-B' is located in section B and stretches from the former E6-road and 250 m into the fjord from southeast to northwest. The profile section from before the landslide event shows a 1:6 gradual slope from about 45 m asl to sea level. The profile sections Figure 70) from both before and after the landslide event is interpreted to have bedrock covered with glacial deposits from the last glacial maximum based on the geotechnical reports and the glacial history in the area. The thick layers of gravel and the underlying layers of clay/silt observed in the field (Material 7 and Material 6) are interpreted as marine and glaciofluvial deposits based on soil classification and grain orientations observed during fieldwork (See chapter 4.1.2). The geotechnical data close to this section (Core sample 12) suggest that there are layers of sand and some gravel grains within the clay deposits which are illustrated within the marine deposits in the cross-sections. The profile from post landslide event shows a "stair-like" morphology with a back scarp and sub-scarp dipping at around 30 °, followed

78

by shallow surfaces with a 5-7 ° gradual slope. From 100-170 m distance in the profile section, marine deposits with a thin cover of beach deposits are exposed with a gradual slope into the fjord as observed in the field. Beneath sea level, some of the landslide masses have been deposited, but the majority of the landslide mass must have a longer run-out distance.

Cross-section C-C'

Cross-section C-C' from section C (Figure 71) has similar deposits as seen in cross-section B-B' with bedrock covered with till, marine deposits and glaciofluvial deposits. The cross-section stretches 250 m from the southeast towards the northwest. The illustrated layers are based on the closest located core sample (12) and the observations in the back scarp from a distance during fieldwork and drone photos (See chapter 4.1.3). Bedrock is well exposed in the southeast, providing a foundation for a house at the top of the scarp. The bedrock has a steep slope towards the northwest as it is exposed in the back scarp around sea level after the landslide event. The presence of till has not been observed but is interpreted to be deposited on top of the bedrock based on the up to 4 m thick layers with high probing resistance above the bedrock during geotechnical investigations. Clay/silt (Possibly material 2 or 7) that covers the bedrock in the back scarp is interpreted as marine deposits with smaller layers of sand and gravel grains in between. The marine deposits are covered with coarser-grained layers, which can be seen traced through section C to section B, and are interpreted to be the same glaciofluvial deposits seen in section B (Material 6).

The morphology in cross-section C-C' from before the landslide event has a weakly dipping slope around 10° towards the northwest. After the landslide occurred, a "stair-like" morphology was created. The morphology between the 70-170 meter marks in the post landslide section could be deposited from landslide masses further upslope, or it could be a potential sliding surface or a combination of both.
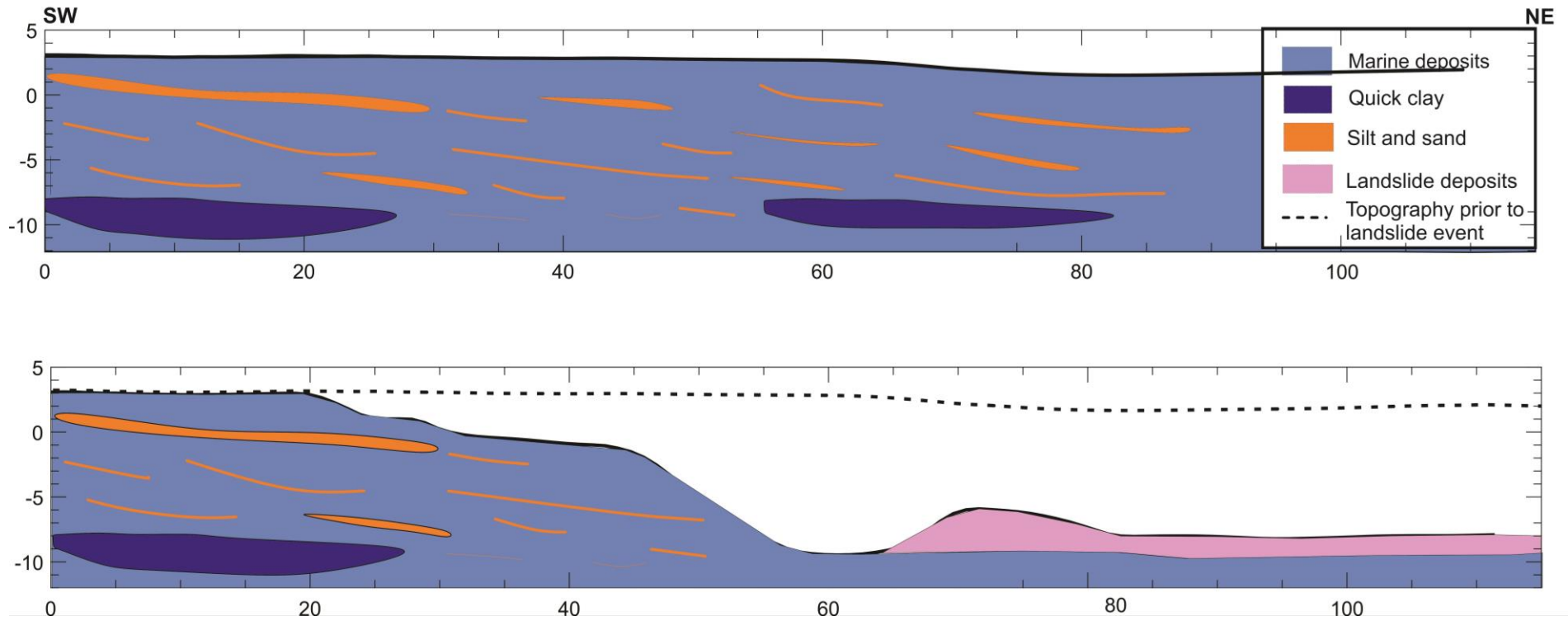
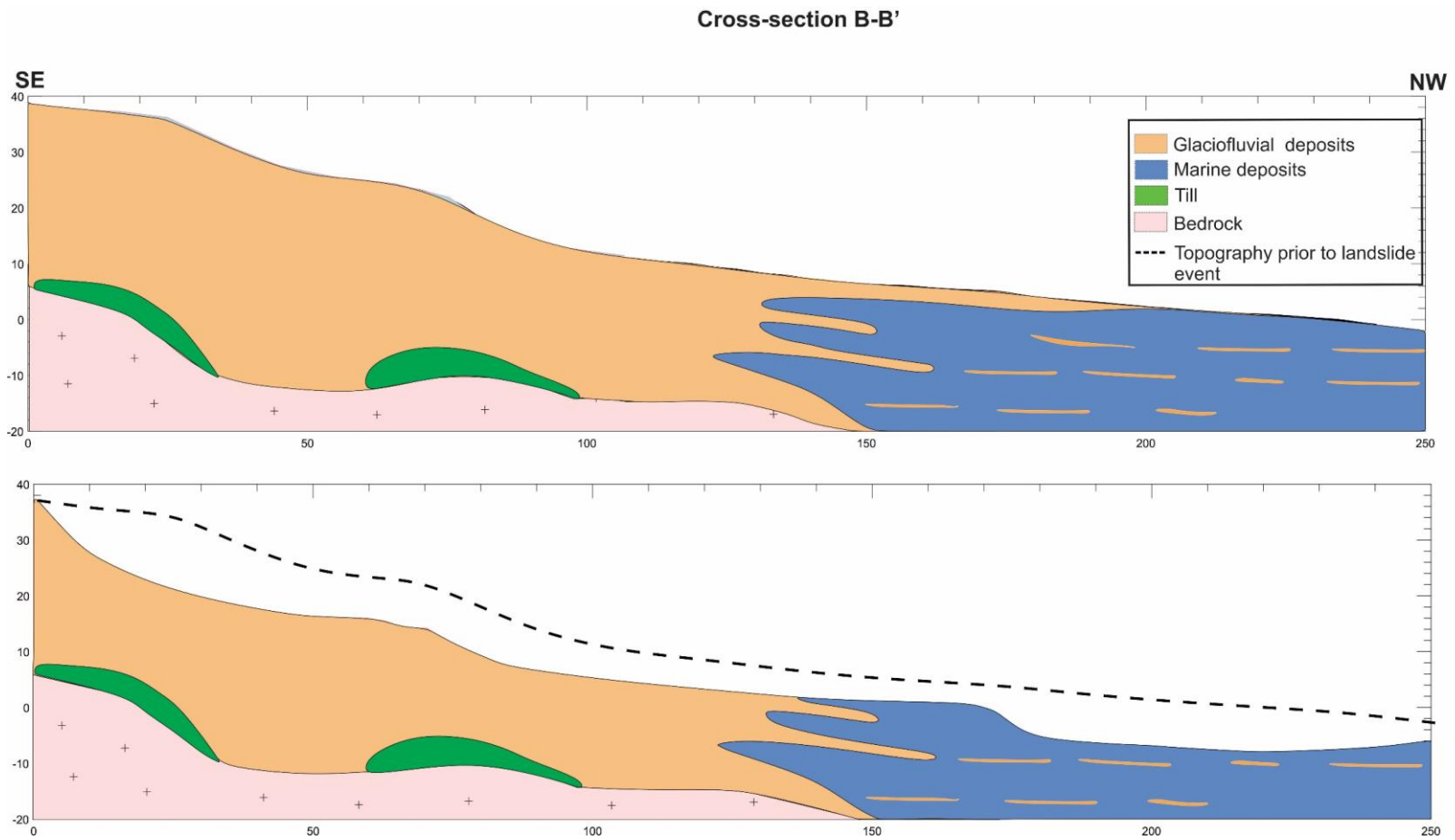*Figure 69 Cross-sections A-A' from before (upper) and after (lower) the landslide..*

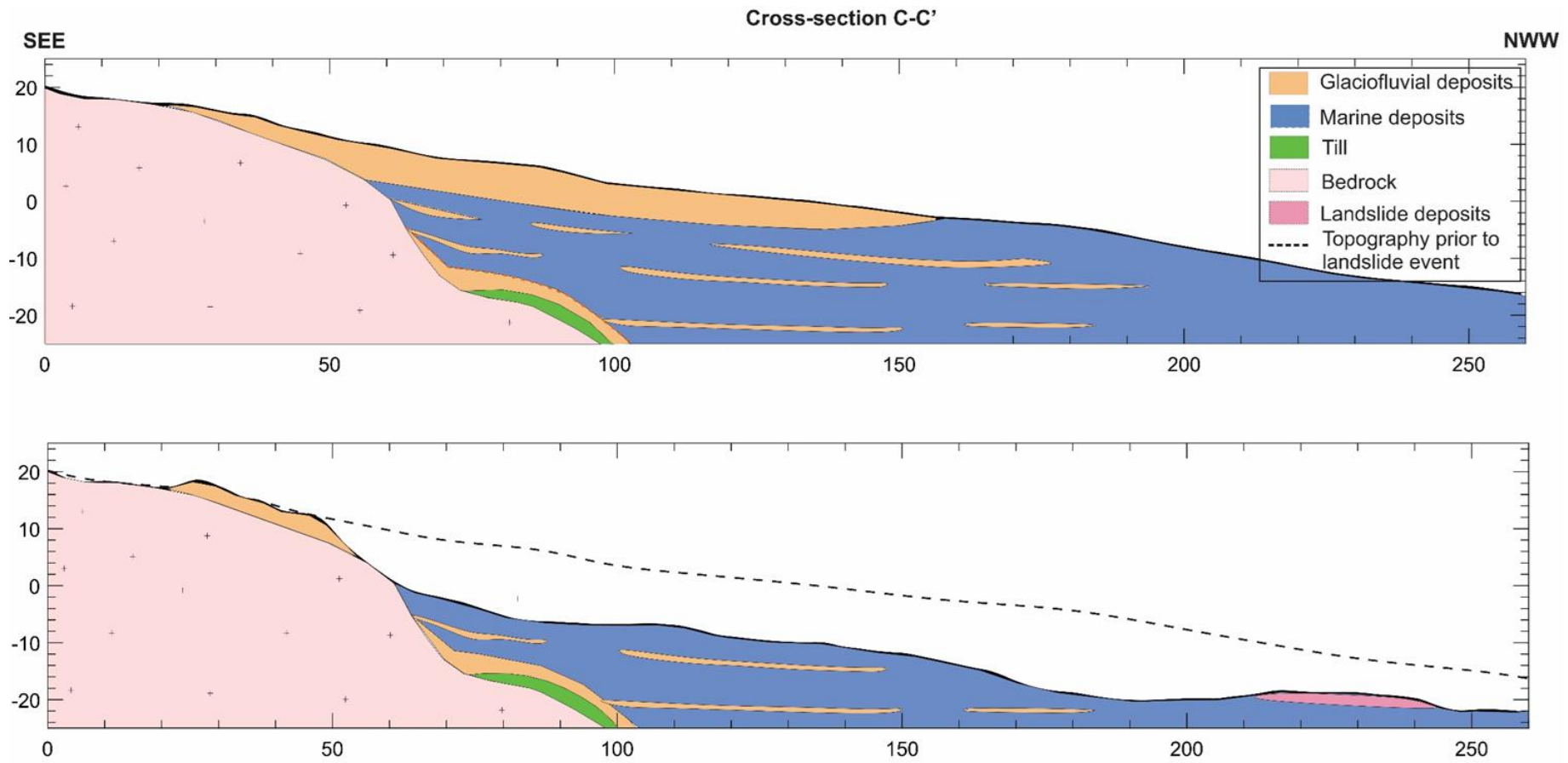*Figure 70 Cross-sections B-B' before (upper) and after (lower) the landslide occurred.*

Figure 71 Cross-section C-C' before (upper) and after (lower) the landslide.

Cross-section D-D'

Cross-section D-D' is from the northern part of the study area in section D (Figure 72). The cross-section stretches about 100 m from the northeast east towards the southwest west and mainly consists of bedrock, marine deposits, beach deposits and possibly glaciofluvial deposits and till. Before the landslide occurred, there was a weakly dipping slope throughout the cross-section. After the landslide, the morphology is steeper but still gradual towards the sea with a surface at 8 m bsl that seems similar to possible sliding surfaces seen in the post-landslide topography in sections A and C (Figure 39D). The bedrock is considered to be uneven and steep. Even though the bedrock is not exposed in the back scarp in this cross-section, it can be seen in several places within the back scarp further south in section D (Outcrop 12). Based on field observations the gravel and sand deposits are classified as beach deposits because it is unsorted and consists of shells and shell fragments (see chapter 4.1.4). The beach deposits are deposited on top of clay and silt interpreted as marine deposits.

Cross-section E-E'

Cross-section E is of the seafloor right outside of Kråknes (Figure 73) and stretches 140 m from the northeast to the southwest. Because this cross-section is located underwater and there are no seismic data accessible for this study, the cross-section is mainly based on the provided DEM-files and surrounding deposits. The cross-section crosses the subsea channel seen in the topography map (Figure 39B & D) and based on the protruding bedrock on each side of the channel, it is interpreted as the section mainly consists of bedrock which shapes the morphology. The bottom of the channel is interpreted to be filled with fine-grained deposits (Material 7). Before the landslide, the bottom of the channel was at about 30 m bsl and due to the erosion from the landslide mass, the depth increased by 5-6 m.
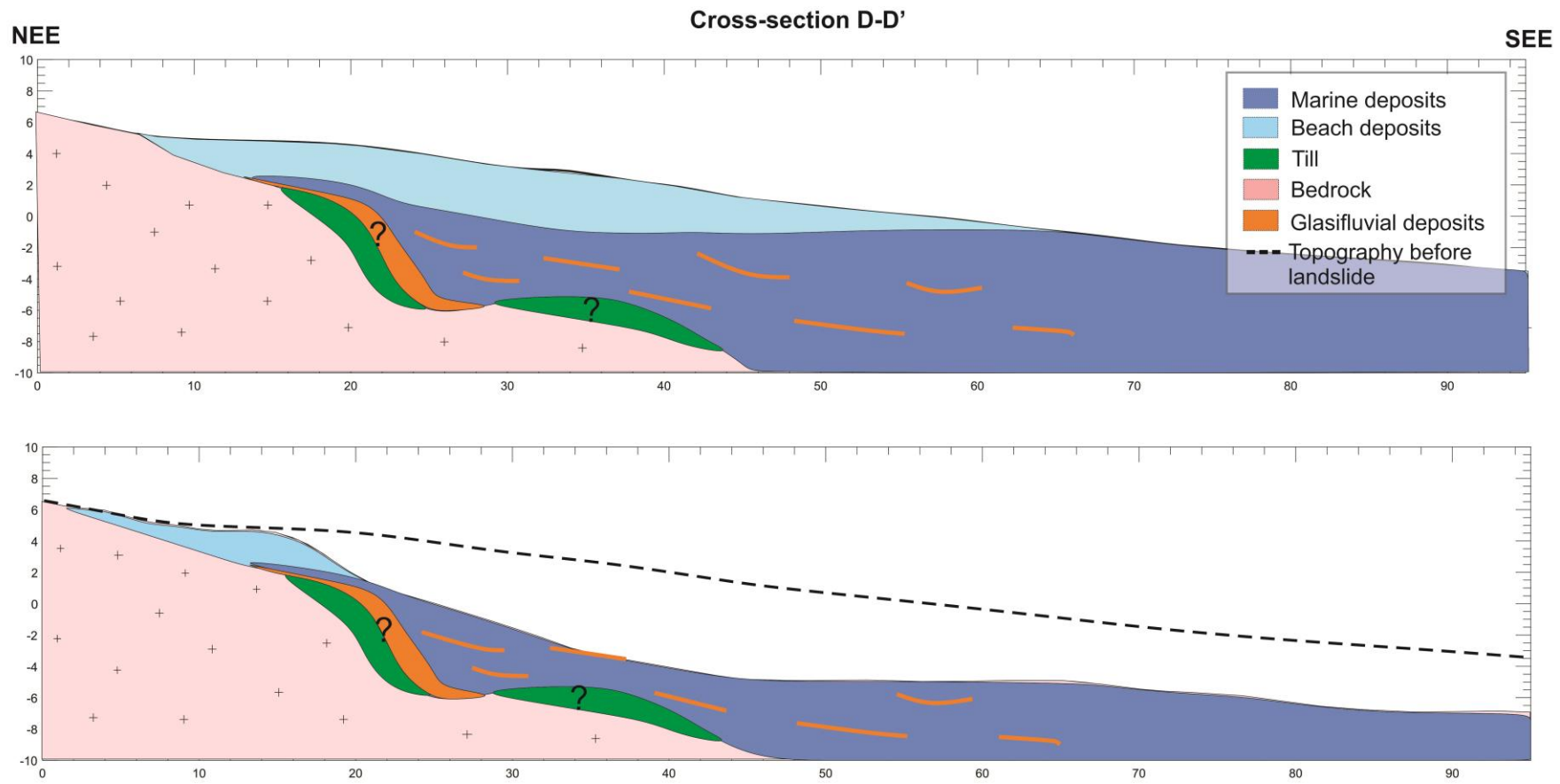
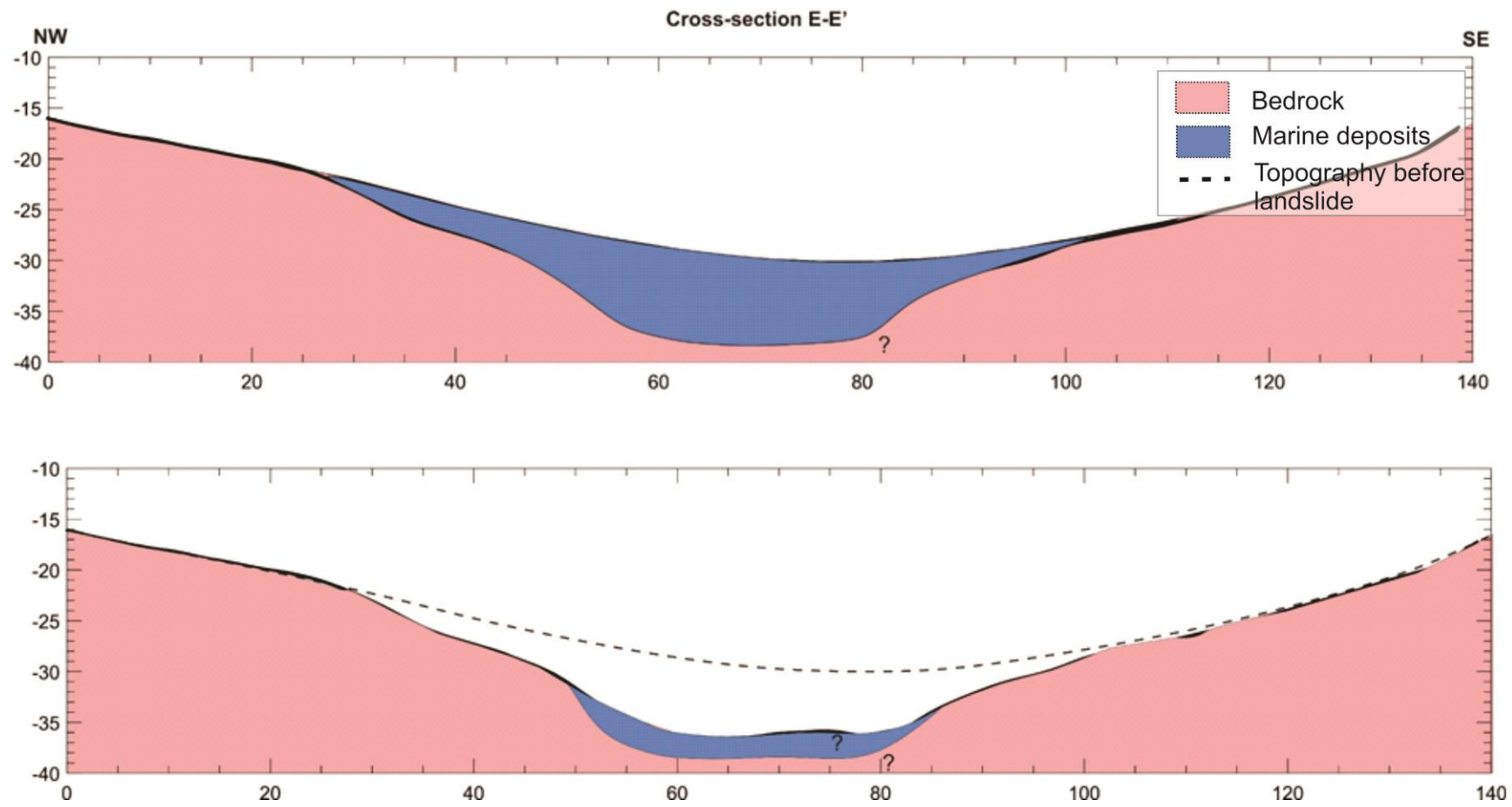*Figure 72 Cross-section D-D' before (upper) and after (lower) the landslide.*

Figure 73 Cross-section E-E' before (upper) and after (lower) the landslide.

4.3 Sequence of events

An eyewitness has described the landslide's sequence of events based on what he saw on the day the major landslide event started. Figure 74 illustrates the sequence of events based on the eyewitness who witnessed it all from his house, safely located on bedrock (The red circle in Figure 74). The landslide area is divided into 12 different blocks, which are numbered in the order the masses slid out. The eyewitness was working outside of his house when the electricity disappeared as power cords are pulled out of the house towards the sea. He then witnessed his childhood home (block 1) sink into the sea and his dog and the doghouse (block 2) followed 10-15 seconds after (Gylland et al., 2021). Blocks 1-7 slid out consecutively from around 3.15 pm on June 3th 2020, while blocks 8 and 9 followed shortly after. At 4.20 pm the same day, block 10 slid out. A few days later on June 5th, parts of the former E6-road were destroyed as block 11 slid out, according to NVE. On June 6th, block 12 is the last slide to be initiated.

It is not certain that block 1 in Figure 74 is in fact the initiating landslide, as it is possible the landslide event was initiated below sea level or other places which the eyewitness would not be able to see. However, the eyewitness did not observe any bubbles or strange activity in the sea prior to the landslide.

After blocks 1-9 (Figure 74) had failed, the coast guard came to Kråknes by boat to inspect the area on June 3rd. As a small boat came up close to the landslide area, the crew explained that the water below them suddenly started to disappear and that the boat "fell" down. Shortly after, the sea level started to rise again and the crew later witnessed the failure of block 10. This episode could have been caused by an underwater landslide, where the seafloor failed and caused a sudden drop in sea level.

Figure 74 Map of the sequence of the landslide event. The numbers indicate in what order the area slid out. The red circle is the location of the eyewitness on who this reconstruction map is based on. Arrows show sliding direction (Based on the information provided by Anders Bjordal from NVE during fieldwork).

4.4 Previous landslide activity

Terrian maps from before the landslide event occurred may indicate that there has been historic landslide activity in the greater area of the 2020 landslide (Figure 75). A scarp with a high slope angle (50-70°) towards the northwest is located in section B. How and when this potentially occurred is unknown, but the lack of shorelines in the old landslide area, may suggest that it occurred less than 1000 years ago when the sea level was not much higher than today. This is based on the fact that if the historic landslide were to be older than this, the uneven shoreline would have been flattened out by wave activity as the sea level decreased (Gylland et al., 2021).
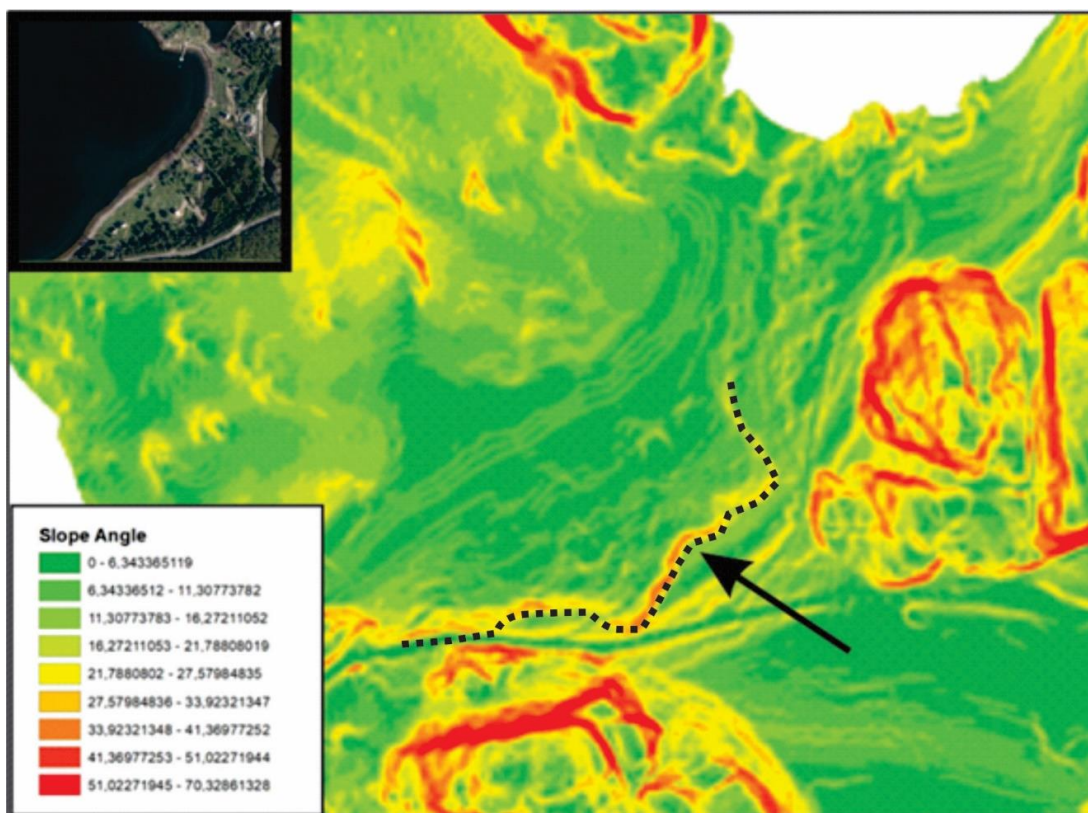
Figure 75 Arrow points at the scarp of a historic landslide event at Kråknes. The colors show the slope angles within the landslide area before the 2020 landslide event.

Prior to the main landslide event, a small landslide was reported to NVE on May 29[th,] 2020, by the owner of one of the cabins at Kråknes (). The small landslide did not affect any of the buildings but destroyed the water supply to one of the private-owned cabins and led to water leakage. Around the same time, it was also reported that there were significant amounts

of meltwater in the terrain surrounding Kråknes, and locals pointed out that there was a lot of clay in the area.

Figure 76 Small landslide event in the study area from May 29th. Photo courtesy of Marit Ekerhovd (Regobs.no, 2020)

On June 2nd, 2020, a new fracture in the access road to Kråknes Road 450 was developed and was reported to NVE (Figure 77). The fracture was 30-40 m long and had a movement downward and out towards the sea. The fracture was then filled with sand from excavations done at Kråknes Road 465 (see chapter 4.7.2 for more about the excavation).

Figure 77 Fracture in the access road to Kråknes Road 450. The fracture is filled with sand. Photo courtesy of Egil Bakkeby (Gylland et al., 2021).

4.5 Hydrometeorology

Some of the hydrometrical conditions in and around the study area in the days close to the landslide occurred are briefly described below. It is to be noted that the presented data of snowmelt and precipitation is recorded at Sopnesbukt in Landfjordbotn, about 50 km west of Kråknes. The given values could therefore vary somewhat from Kråknes. The groundwater measurements for the Alta area, including Kråknes, are based on data from NVE's groundwater stations located 70 km and 40 km away from Kråknes in Lakselv and Kvaenangen (Figure 78).

Figure 78 Map of weather stations and groundwater stations that the hydrometrical data is from (red circles). The study area is within the yellow circle.

4.5.1 Snow depth and precipitation

In the winter season in 2020, the percentage of snow or water equivalent in the surrounding area of Kråknes was 90-300% of the normal value (Geodata AS, 2020). The normal value is the median value in the time period from 1991 – 2020. In Figure 79, the amount of snow from January to June 2020 is illustrated based on the median value. On May 1st the data shows that the amount of snow at Kråknes was up to 300% of the median value. However, data from the metrological institute shows that the maximum snow depth was around 170 cm in February and March 2020, before the snow depth started to decrease in April and May (Metroligisk Institutt, 2020). From May 1st to June 1st the snow depth dropped from a total of 130 cm to only 10 cm, implying a large and rapid snowmelt event (Figure 79). Similar

amounts of snow have not been recorded in the month of May in this area since 1996
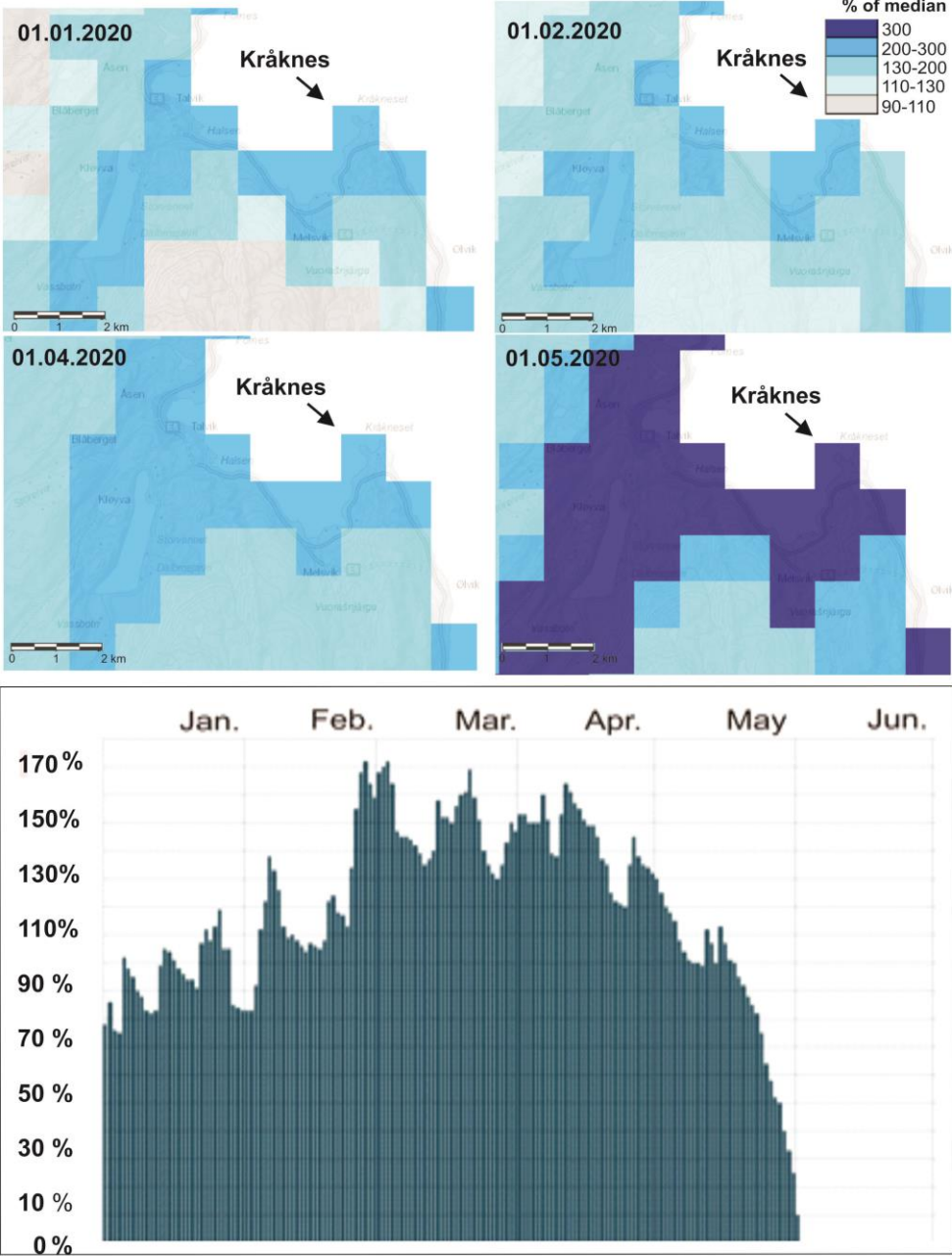(Geodata AS, 2020).

Figure 79 Illustration of the percentage of snow surrounding the study area January-May 2020 (Geodata AS, 2020). Graph of the snow depth in cm (Metroligisk Institutt, 2020).

In the days prior to the landslide event, hydrometric data from Geodata AS (2020) show that there was an increase in snowmelt in the area surrounding Kråknes. On May 24[th,] the temperature increased, and 28 mm of rain and meltwater was recorded in the area. The day the landslide event starter on June 3[rd,] only 5 mm of rain and meltwater were recorded (Figure 80). In this time period, there were insignificant amounts of rainfall in the area; therefore, the supplied water is considered to be meltwater.
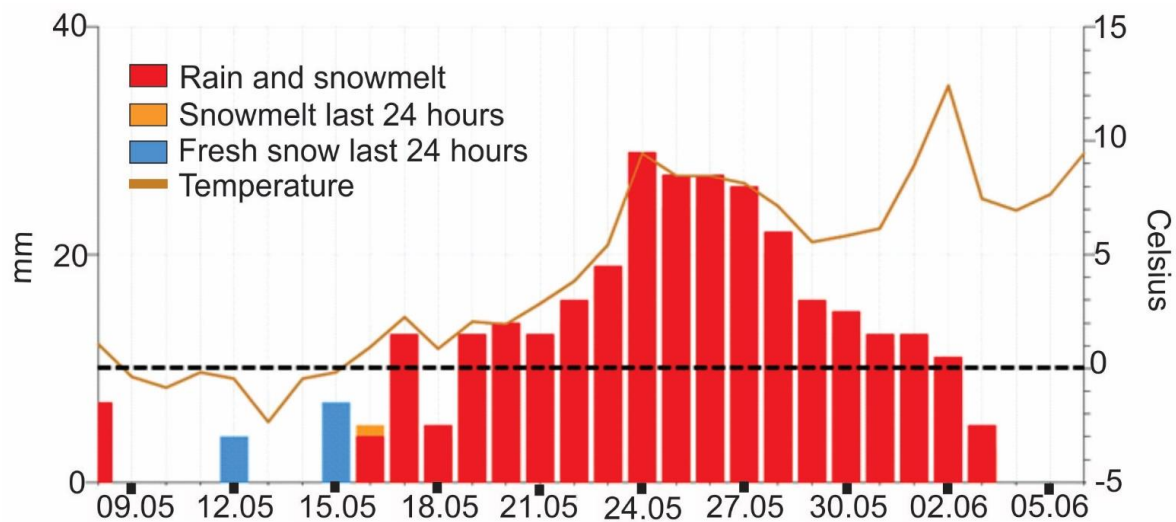
Figure 80 Graph showing the temperature and the amounts of rain and snowmelt from May 9th- June 5th, 2020 (Geodata AS, 2020).

4.5.2 Saturation of soil

Simulated data of the percentage of water saturation in the soil from senorge.no show that the soil in the Alta area was 100% saturated on the day the landslide event started (Figure 81A). Historical data from 1957 until 2020 show that the water saturation has only been this high on four occasions during this time period (Figure 81B). In 1996, 2013, 2014 and 2017 the water saturation was close to 100% or more compared to reference years between 1981-2010. These values were all related to snowmelt during springtime (Gylland et al., 2021).
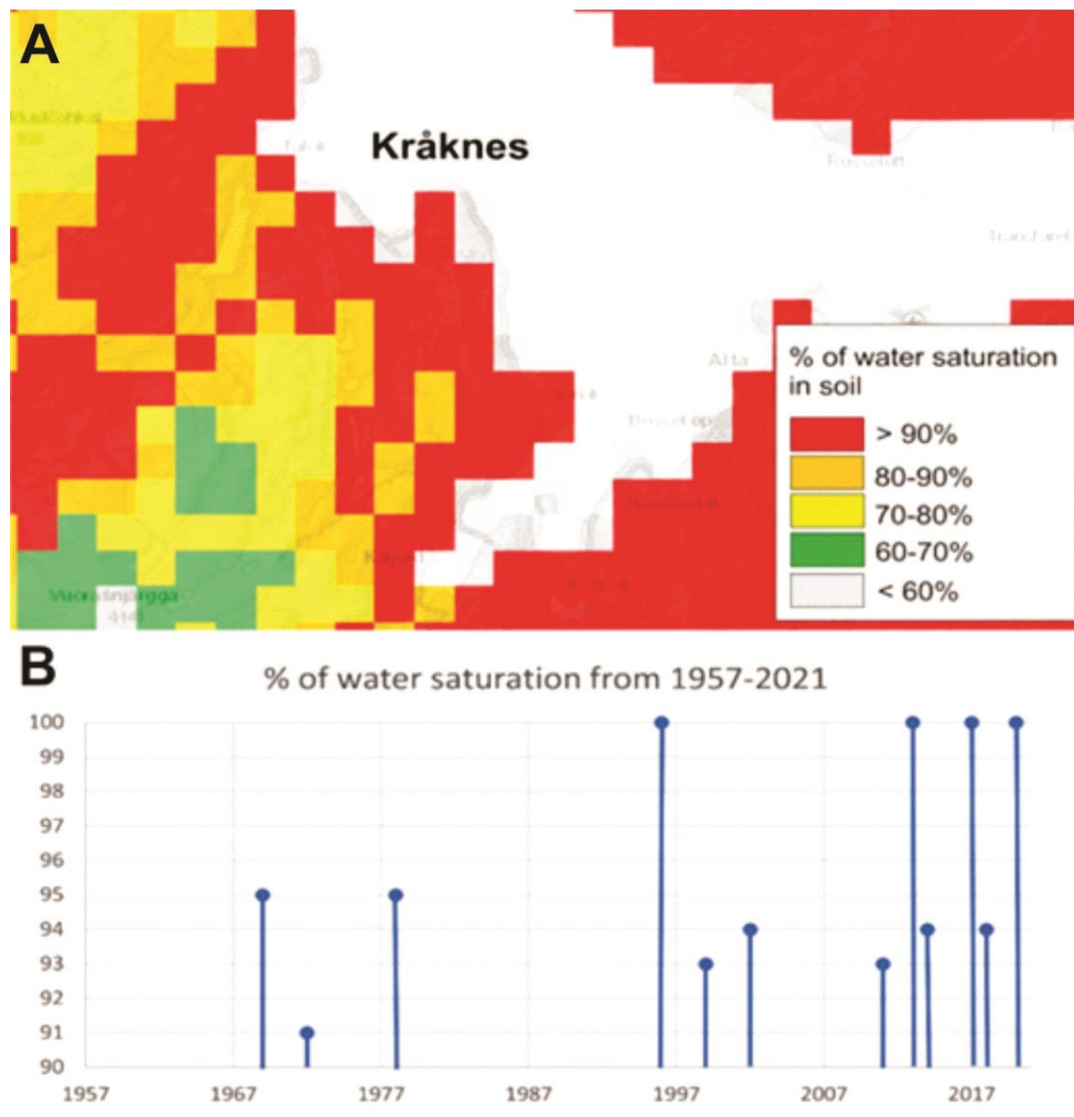
Figure 81 A) The percentage of water saturation in the soil at 8 am, June 3rd, 2020 (Geodata AS, 2020) and historical years with more than 90% water saturation (Geodata AS, 2020; Gylland et al., 2021).

4.6 Water observations

Kråkvikdalen (Figure 82), the valley above the road framing the upslope side of the landslide, acts as a bowl for the Kråknes watershed. Surface water drains from the surrounding mountains into the bowl, where in subsequently drains to the beach. The water travels through a system of unlined ditches and culverts around the main road, as well as through the ground in the thick beach deposit gravels overlying the Kråknes clay.

Figure 82 Map of water presence at and around Kråknes showing water streams, wells and significantly wet areas in the days prior to the landslide. The bog and disappearing water streams were observed during field work.Ortho-photo from 2018.

Before the landslide, Kråknes was characterized by streams and manholes that collected water from the slope above the Kråknesroad. Wells was put on several of the manholes and the inhabitants explained that the wells would fill up shortly after they were emptied (Figure 82).

In the days prior to the landslide event, there were large amounts of water observed in the area around Kråknes. Kråkvikdalen (Figure 82) was described as "*floating in water*" and the ground was vibrating in the days prior to the landslide. Locals that normally hiked in the area explained that it was not possible to access the area due to the large amounts of water on

the ground (red circle in Figure 82). The high amount of water from Kråkvikdalen flooded the area between the tractor road and the cabin properties (red circle). New culverts were put in above the tractor road a few days before the landslide event to prevent the water from flooding the area (Figure 83). Significant amounts of water built up in the ditch system parallel to the main road, eroding tunnel gullies in the ditch floor, and undercutting the shoulder of the road (Figure 84C). After the landslide even there were still small streams of water running from the ditch north of section B into the landslide area (Figure 85A). South of section B, the eroded channels were completely dry (Figure 85B & C).

Figure 83 Culverts added to increase drainage to the beach through the tractor road.

A few days after the landslide event, there was still a large amount of water present in the area above Kråknes Road and seepage of water could be seen on the tractor roads (Figure 84B). Small surface streams of water could be tracked from the bog in Kråkvikdalen in the direction of Kråknes, but the water suddenly disappears into the ground at about 350 m from Kråknes road and 68 m asl (Figure 82). There are little or no surface water between this point in Kråkvikdalen and the Kråknes Road during fieldwork, but water appears again from the soil above the road and seems to be the source of the smaller water streams that eroded the ditch systems parallel to the main road (Figure 84C)

Figure 84 A) Wet area in Kråknesdalen above the Kråknes Road on June 7th, 2020(Photo courtesy of Anders Bjordal, NVE). B) Moist tractor road on July 28th, 2020. C) Erosion from water streams in the ditch along Kråknes Road on July 28th, 2020.

Figure 85 Eroded channels in the ditch system along the Kråknesroad north of the section B. B) Dry channels in the ditch south of section B. C) Close-up of dry channels.

4.7 Human activity

4.7.1 Reconstruction of the E6-road

Before the E6-road was reconstructed between 2013-2016, the E6-road passed through Kråknes (Now called Kråknes Road) and was the main access road in and out of Alta City and northern Norway. During construction of the new E6-road, a deposal site for cut material was made in 2015 at Storhaugen east of Kråknes (Figure 86). According to SVV (Norwegian Public Roads Administration), the disposal material was deposited on bedrock and consisted of sand and silt. After the new E6-road was constructed, SVV made improvements on the former E6-road with new asphalt and railing. The ditch above the road was cleaned, but no new culverts were put in.
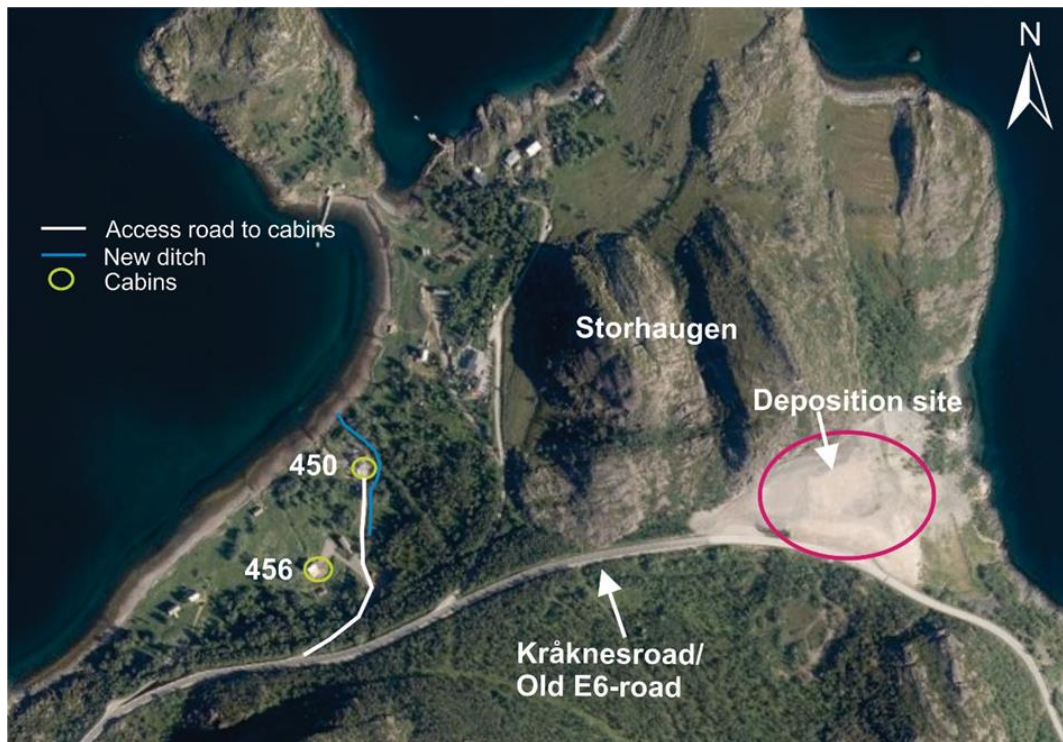
Figure 86 Locations of different human activities before the landslide event in 2020

4.7.2 Digging and filling at properties

In 2015 an older cabin in Kråknes Road 450 was torn down and a new cabin was put up (Figure 86). Because of the soft ground, a new filling had to be put in as a foundation. Excavated material from the cabin plot were placed as an embankment towards the sea with a septic tank installed within (Gylland et al., 2021). According to the owner of the cabin, 80 truckloads of fill material that came from the disposal site at Storhaugen were used to raise the level of the cabin plot. In a news article that came out in March 2021, Alta municipality claims that the cabin owner never applied to load the ground at the plot and that it would never have been approved due to the ground conditions at Kråknes (Cissè, 2021). The road leading to the cabin at Kråknes Road 450 was also improved using excavated material from the property at Kråknes Road 456 and a new ditch for water drainage around Kråknes Road 450 was made. At Kråknes Road 450 the cabin footprint of slightly more than 1000 m² was raised by 2 m, while 400 m² was removed from the terrain at Kråknes Road 456 (Gylland et al., 2021). Slope stability calculations at Kråknes have been done to compare the stability before and after the cabin in Kråknes Road 450 was upgraded. The stability analyses show that

the area was already unstable with a factor of safety equal to 1.07, and that the filling made it more unstable with a decreased factor of safety equal to 1.01. (Multiconsult Norge AS, 2021,and the thesis from a concurrent masters project ; Sandnes, 2021).

4.8 Numerical modeling

Two different scenarios have been simulated in DAN3D to try and recreate the Kråknes landslide event. In the first scenario, the landslide event was initiated below sea level (Run 1). In the second scenario, the landslide was initiated asl (Run 2). For both the simulations the same material param are used (See chapter 3.3.1). The initial and total volume of the two runs are calculated by using calculating functions in Surfer on the grid files provided to create the simulations in DAN3D. The movement of the landslide mass is represented by the contoured nodes at 5, 10, 15, 20 and 24 seconds from initiation and shows the thickness of the landslide mass in that given node (Figure 87 & 88). The red dotted line in Figure 87 and 88 shows the approximate outline of the simulated impact area of the slide.

For both scenarios, both the Bingham and Plastic rheology has been tested. For the Bingham rheology, the simulations stopped at 0 seconds in both scenarios, even when the sensitivity of different input param was tested. The presented modeling results have therefore been performed with the plastic rheology, where the viscosity is considered to be equal to zero.

4.8.1 Model results

Run 1 has its initiating landslide mass below sea level, outside of section C. The total initial volume is calculated to be 344 841m^3 and by the end of the landslide event, the total volume is m^3 671 687m^3. However, the total volume of the landslide mass is probably bigger than what can be calculated, as an unknown volume of the landslide mass may have been transported several km into the fjord. The run-out distance and thickness of the simulation for this scenario are seen in Figure 87 and show that the landslide mass came to a complete stop 24.8 seconds. The total simulated run-out distance is 411.4m and the average thickness of the landslide was initially 5.6 m and decreased to 1.09 m by the end of the landslide.

For run 2, the landslide is initiated asl and has an initiating volume of 148 770m^3 and a final volume of 168 102.87 m^3. The simulated run-out distance and thickness can be seen in Figure 88, where the landslide comes to a complete stop at 24.2 seconds. The average thickness of the landslide was initially 5.3 m and decreases to 0.5 m at the end of the landslide and the total simulated run-out distance is 275 m.

Based on the fact that DAN3D does not take into account the buoyancy effects for subaqueous slides, an attempt was made to change all the elevation values for the path topography and the source depth file to all be asl to avoid this problem since the Kråknes landslide is partly subaqueous. However, the attempt did not give in any satisfactory results and was therefore neglected, and no further work was done with these files.

Out of the two different simulations, the run-out in run 1 looks to be more realistic based on the shape of the landslide mass compared to the morphology in the post-landslide topography. The landslide mass does not spread out wide but stays narrow and follows the subsea channel. The total run-out distance in this simulation is 411.4 m, which is shorter than the empirical estimations for retrogressive landslides in channelized terrain suggests. The empirical calculation is three times the length of the release are (chapter 2.2.5), which is 3 x 160 m = 480m for the release area in run 1. For run 2, the total simulated run-out distance is 275 m. The empirical calculations with a 140m long release area give a run-out distance of 420 m in channelized terrain. However, the run-out in run 2 seems to spread out wide compared to the more channelized run-out in run 1. By using the calculation method for run-out in open terrain, the run-out distance is 140m x 1.5 = 210m.

The maximum velocity of the simulation in run 1 can be seen in Figure 89. The velocity gradually increases between 0 and 23 seconds from 0 to 46.3 m/s before reaching its peak of 58.2 m/s at 24.2. The maximum velocity for run 2 can be seen in Figure 90. The graph show a gradual increase in velocity between 0 and 15 s from 0 to 25 m/s, before it has an exponential increase between 15 to 24 s from 25 to 128 m/s.

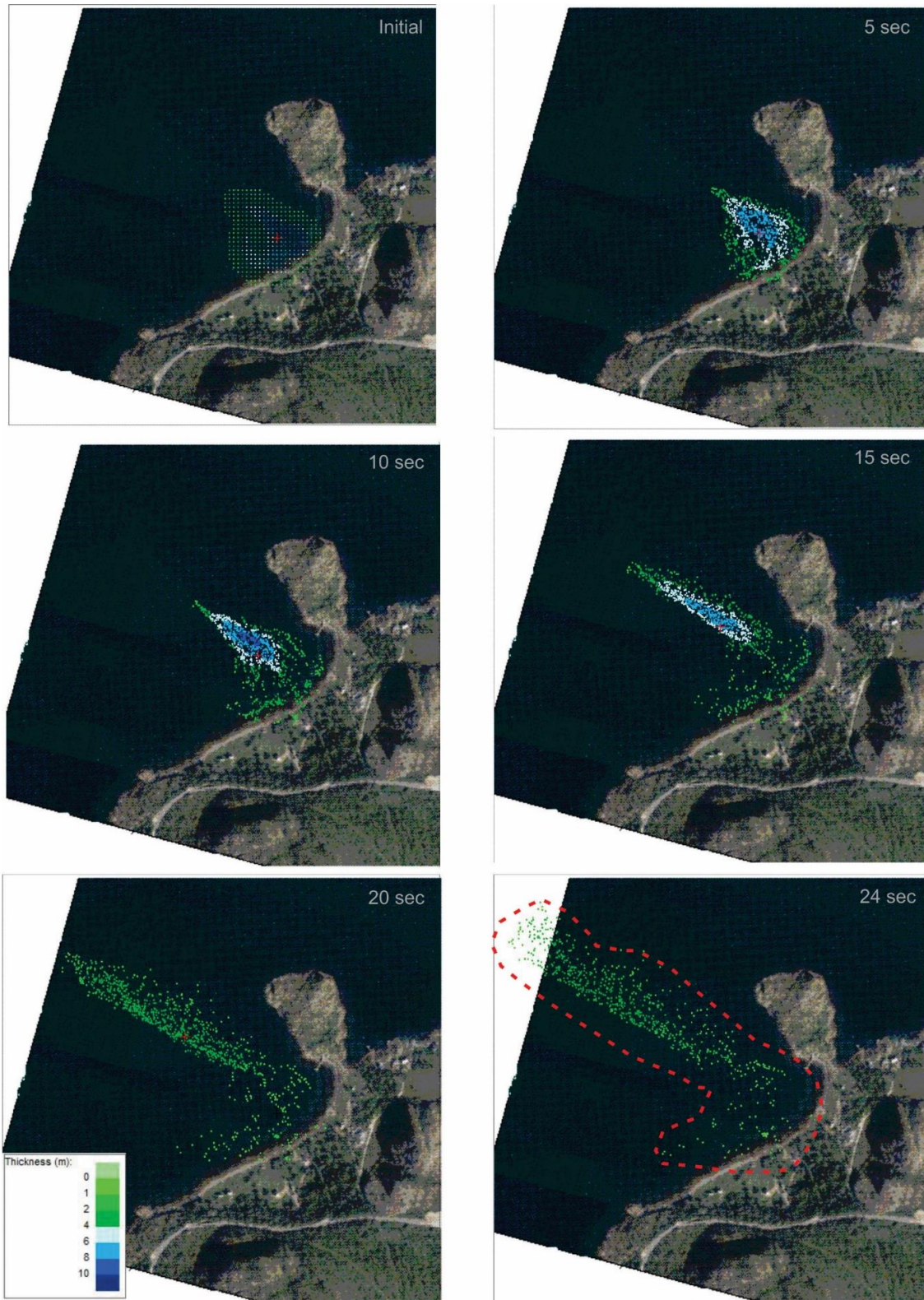*Figure 87 Run 1. Simulation if landslide was initiated below sea level. The red dotted line shows the impact area*
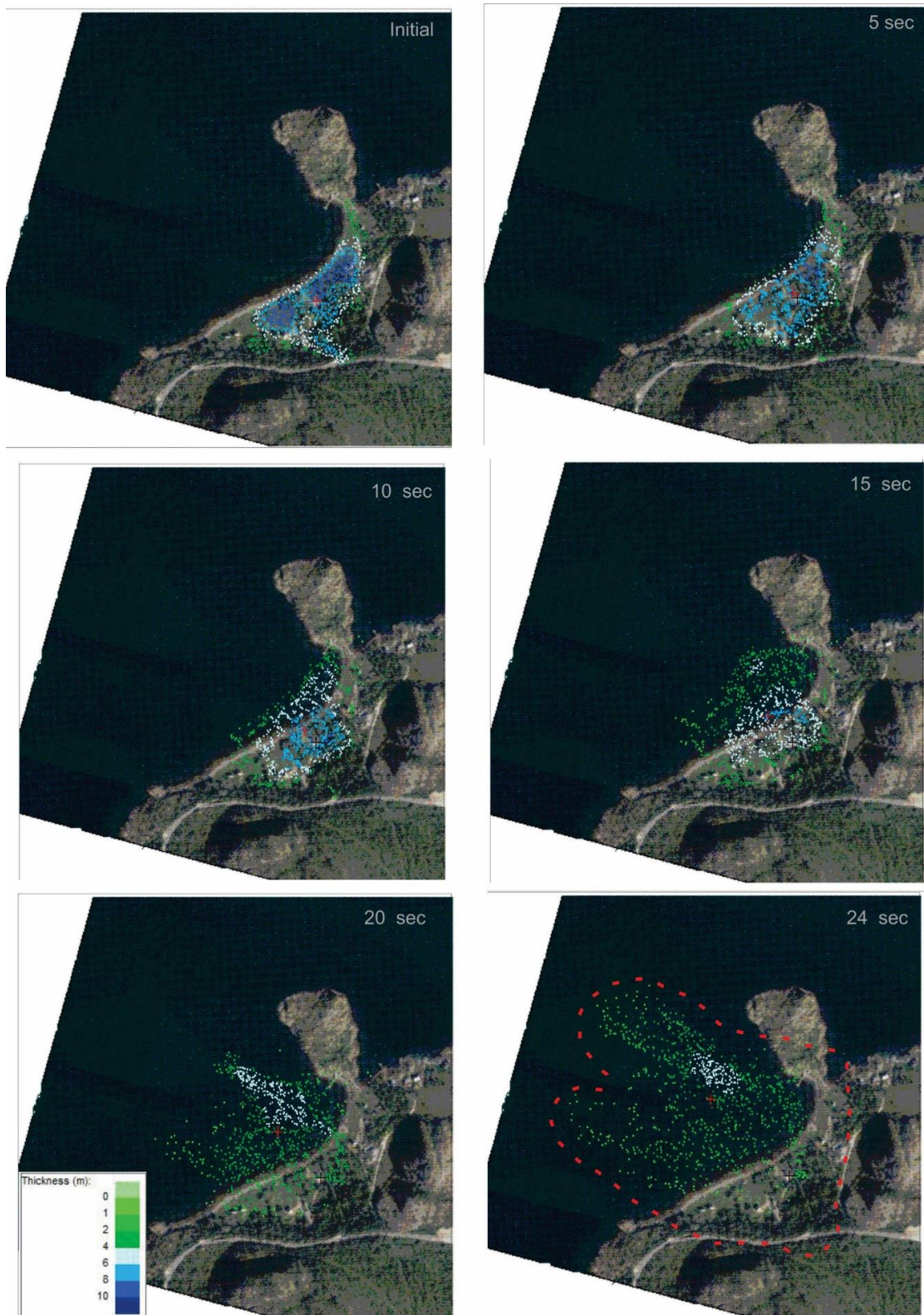
Figure 88 Run 2. Simulation of the landslide thickness and movement from DAN3D. The red dotted line shows the whole impact area.
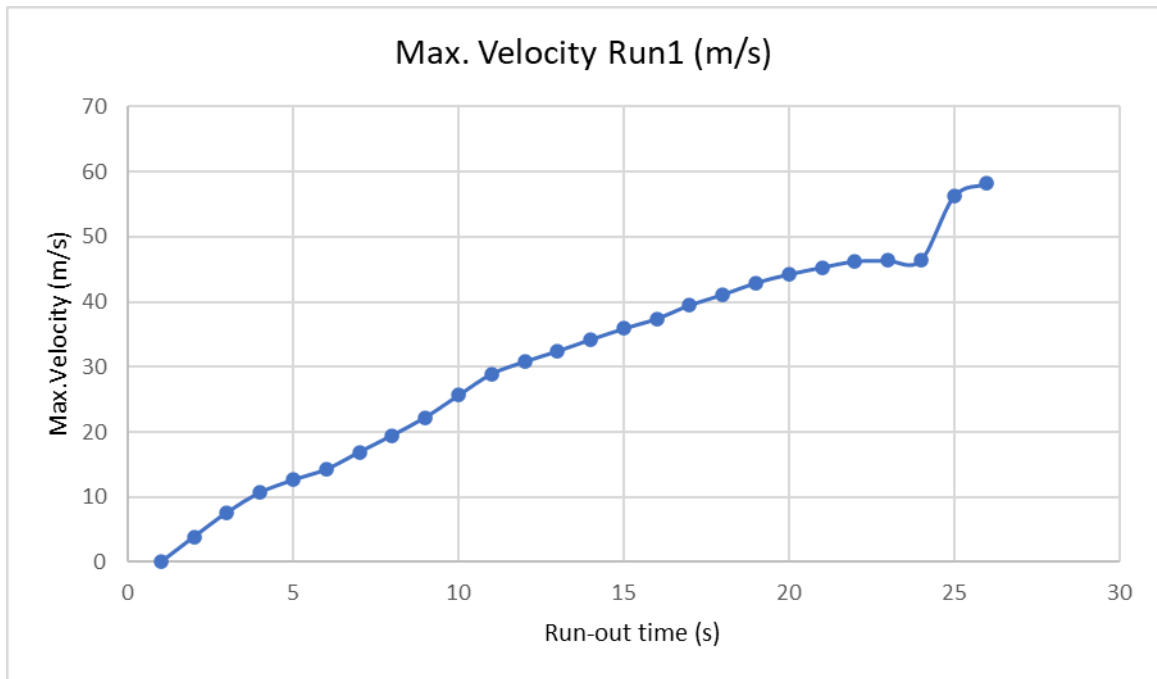
Figure 89 The maximum velocity of the landslide throughout the simulation time in run 1.
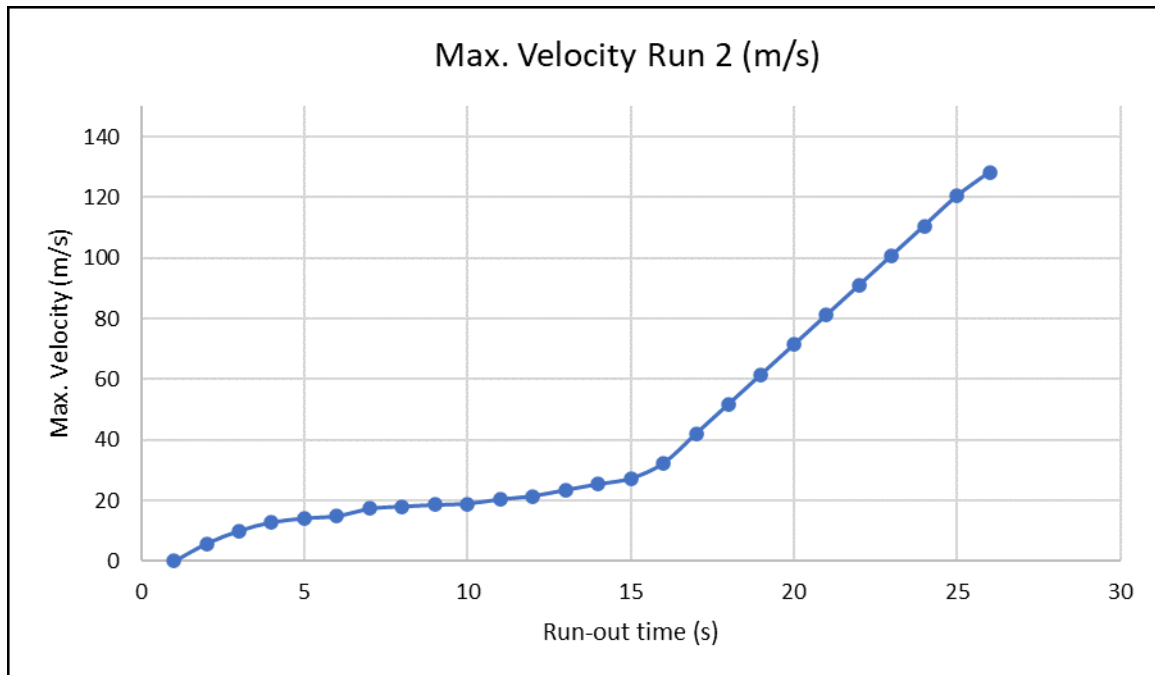

Figure 90 The maximum velocity of the landslide throughout the simulation time in run 2.

5 Discussion

Here the results of the study will be discussed to better understand what could have caused the landslide at Kråknes on June 3rd, 2020, and how the landslide event developed after initiation. Two scenarios will be proposed to fulfill the main goal of this thesis and reconstruct the landslide event.

5.1 Landscape development

The landslide area is a typical glacial landscape with glacial and glaciofluvial deposits in a fjord. The ice has formed what seems to be an ice-marginal delta (Section B) during deglaciation, with well-sorted and increased grain size from the bottom towards the top at Kråknes. The main stratigraphy in the area consists of these glaciofluvial deposits on top of marine deposits, till and bedrock. Beach deposits are also present in some parts of the study area.

The soil layers in the landslide area mainly dip towards the northwest, which is similar to the dipping trend in the bedrock. Some of the exposed bedrock within the landslide area have striation marks that stretch from the southeast towards the northwest (Figure 61C). The orientation of the striations and the soil layers fits well with the direction of movement the ice had during the last ice age, according to literature (Figure 10). The melting of the ice and the uplift of land have exposed the marine deposits and ML, and formedthe Tapas shoreline and other beach ridges, and erosion by wind and water have formed the valley (Kråkvikdalen) southeast of the study area. At some point through the last 1000 years, a historic landslide has occurred at Kråknes, leaving a steepscarp behind the beach at Flatstrand. In modern time human activity has modified the area by construction of buildings, roads and drainage systems. From June 3rd -6th, 2020, the Kråknes landslides occurs and leaves a 600 m wide a landslide area with steep back scarp and gently dipping beach area.

In the landslide area, striations are seen on a clay surface in the beach area during low tides with the same orientations as the glacial striations in the bedrock (Figure 60A). These are interpreted to have been created by the landslide masses that scoured the clay when they slid out. Their orientation suggest that parts of the landslide mass slid out on a surface with the

85

same orientations as the soil beddings exposed in the back scarp. In sections B, C and partially D, gently dipping clay/silt (Material 7) sliding surfaces with a northwest dip direction supports this,while the landslide masses in section A slid out towards the north. The possible sliding surface can also be seen within the bathymetry as gradual dipping surfaces at about 8 m bsl.

In Kråvikdalen the surface water drains towards Kråknes through permeable glaciofluvial deposits (material 6), and possibly fractured bedrock in the ground, and comes seeping out in the landslide back scarp between layers of glaciofluvial deposits and marine deposits, and between soil-layers and bedrock. Collected core samples show that there are layers of sand and silt within the marine deposits, and these layers are interpreted to stretch out into the fjord. Figure 91 illustrates the general stratigraphy in the study area and how the groundwater flow travels through the glaciofluvial layers from Kårkvikdalen towards Kråknes.
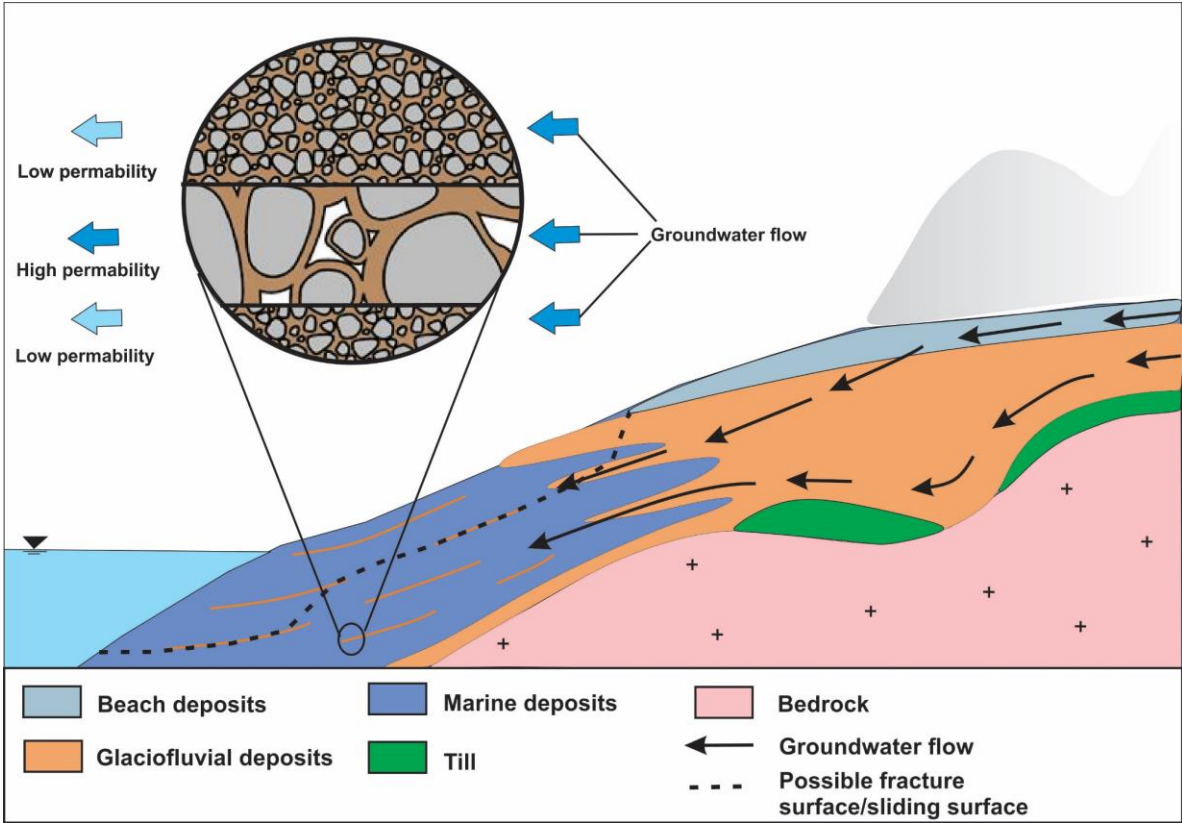

Figure 91 Illustration of the general stratigraphy at Kråknes with groundwater flow from Kråkvikdalen, through the glaciofluvial deposits at Kråknes and into the Altafjord. Inset is an illustration of the grain size of the marine and glaciofluvial deposits and their permeability.

5.2 Possible failure mechanisms

There are several possible failure mechanisms that could have caused the landslide event at Kråknes. Here a combination of predetermined and triggering factors will be discussed based on the collected data and field observations.

Topographic and quaternary conditions

The topographic conditions and quaternary deposits at Kråknes make it easy for water to in-filtrate the ground and saturate the slope towards the fjord, as discussed above. This is seen throughout the landslide scarp, where there is seepage of water and sediment between coarse-grained material (glaciofluvial deposits) and fine-grained material (marine deposits) and between coarser-grained material and the bedrock. The glaciofluvial deposits are per-meable due to the bigger particle sizes and pore space in between them, while the marine deposits are less permeable or impermeable due to being more compact with smaller grain sizes and less pore space. When a high amount of rain or meltwater is added to the coarser-grained soil, excess pore pressure is built up when the finer-grained layers below prevent the water from flowing into a lower-lying area because it needs more time to drain com-pared to the coarser-grained layers above. The hydrometrical data from the days before the landslide shows that there were high groundwater levels after large amounts of snowmelt in the area that could increase the pore pressure in the ground.

The interpreted stratigraphy in the area (Figure 91) with glaciofluvial deposits from Kråkvikdalen continuing into the landslide area and into the fjord within the marine deposits could give a geological scenario where the groundwater levels have increased in the higher-lying areas and caused an increase in pore pressure in the sediments deeper down and be-low sea level. This scenario may create weak layers and possibly hydraulic fracture (soil pip-ing) between layers of different textures and hydraulic properties. Several soil pipe struc-tures are seen in the landslide area in the contact zones between coarser and finer-grained layers. These soil pipes can rapidly transmit water and speed drainage from hillslopes, but if the soil pipes are blocked or are dead-end pipes, they can be filled with water when there

are high amounts of rain or meltwater. This can produce excess pore pressure in the surrounding sediments. If a slope is already close to failure because of other predetermined factors, it is possible the pore pressure from the soil pipes may cause slope failure (Pierson, 1983). Figure 91 illustrates a likely scenario at Kråknes, where a layer of the permeable glaciofluvial soil is trapped between two layers of less permeable marine deposits. The groundwater flows through the glaciofluvial deposits but is impeded in the marine deposits, which can cause excess pore pressure followed by a decrease in the sediments' shear strength and eventually create a weak layer that decreases the slope stability. A weak layer could also have been formed in stratified beds from turbidity currents/flows from the prehistoric landslide in the area. Rapid deposition of landslide mass in the catchment area of the fjord after the prehistoric landslide may have produced biogenic gas due to the burial of benthic ecosystems, which increases the compressibility and reduces the shear strength of the sediments (L'Heureux et al., 2012). Such weak layers can, under critical conditions, form the sliding surface of the failure. The initial topography at Kråknes with a moderate dipping fjord where beds are able to accumulate in the slope, in addition to a prehistoric landslide event, creates good conditions for such weak layers to be formed. However, to confirm the existent of such a layer at Kråknes, seismic data would be necessary in a combination with bathymetry and terrain data. Unfortunately, there are no seismic data available for this study.

The landscape development and topography in the area also creates good conditions for the groundwater to flow through the marine clay over time and create pockets of quick clay. Quick clay is found in the study area in core samples collected from section A. Even though quick clay has not been physically found in other places of the study area, it is likely there has been more quick clay in the beach zone which made the area highly sensitive to external influences.

Human activity
Human activity is one of the main triggering mechanisms for landslides along fjords, and may also have had a critical impact on the Kråknes landslide event. After the reconstruction of the E6-road from 2013-2016, no improvements were made to the drainage system around

Kråkes Road (former E6-road). Based on field observation on the presence of water in Kråvikdalen and at Kråknes, it is questioned if the drainage in the area is properly done during the reconstruction. However, this would need further investigation and does not necessarily have an impact on the 2020 landslide event.

Another human activity has been shown to have made critical changes to the slope stability in the area. The 80 truckloads of fill material (1000-1200m^3) that were added at Kråknes Road 450 in 2015 decreased the already unstable stability at Kråknes. The loading of the fill material causes an increase in the pore water pressure and shear stress in the sensitive clay because the loading happens more rapidly than the water can flow out of the soil. The concentrated shear deformation is therefore increased, and the peak strength of the soil is exceeded. If this does not cause an immediate failure, the shear strength of the material is permanently reduced, even though the pore water pressure decrease over time (Strain-softening) (Thakur et al., 2018). The reduction in shear strength spreads through the soil layer and can eventually create a shear band and potential sliding plane. Figure 92 illustrates a shear band that has been subjected to strain softening and the surrounding soil, which has not yet reached its peak shear stress. This process is considered a predetermined factor, and an initial trigger mechanism such as high amounts of meltwater can have caused the initial failure by increasing the pore water pressure and total stress within the shear band.

According to the hydrostatic data, the amount of meltwater and percentage of saturated soil in the spring of 2020 was the highest level since the loading of the fill material in 2015. The saturation of the soil was up to 100%, and locals explained there were high amounts of surface water in Kråkvikdalen in the days prior to the landslide. The meltwater is therefore considered the triggering mechanism of the initial slide, while the stratigraphy and loading during construction are the predetermined factors of instability.
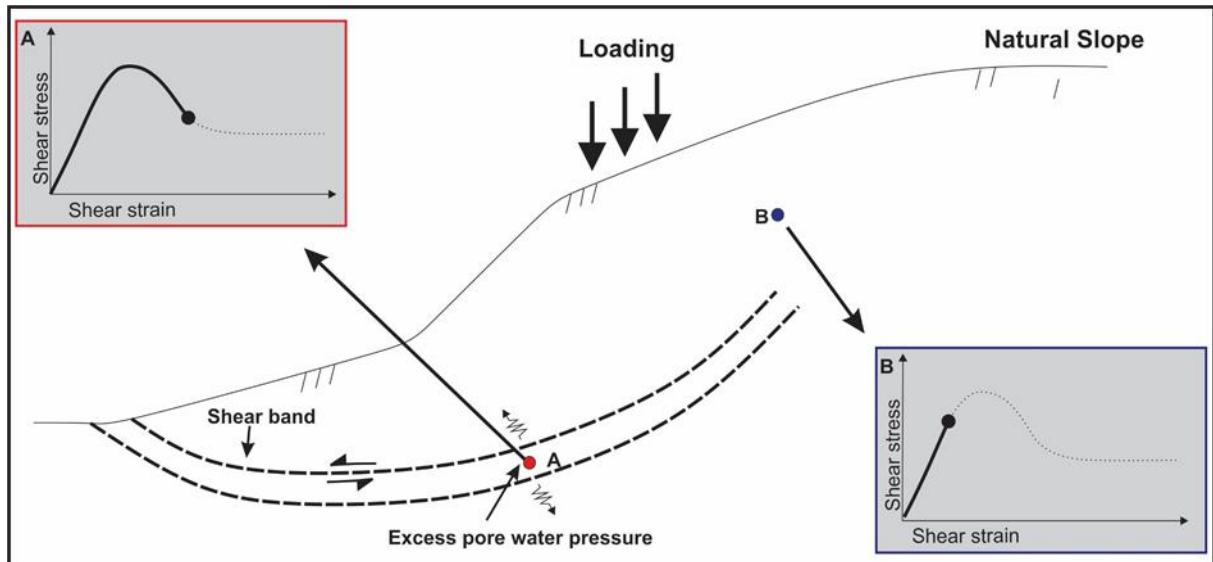
Figure 92 Loading of material on a natural slope where local excess pore water develop and a soil layer is subject to strain-softening (A) which creates a shear band and possible slidiing surface within the sensitive clay. The surrounding soil (B) has not yet reached it's peak shear stress and has a higher shear strength than the soil within the shear band (Inspired by Thakur et al., 2018) .

5.3 Modeling

Two scenarios of the landslide event were simulated in DAN3D. The first scenario, run 1, where the slide was initiated from below sea level, had the run-out that fit the landslide morphology the best. The run-out from below sea followed the narrow channelized topography that can be seen in the hillsahded DEM-files from both before and after the landslide event (Figure 39). The run-out distance also stretches through the whole channel and into the fjord, which correlates well with the eroded area from the bathymetric data. For the simulation that started above sea level, the run-out comes to a complete stop at about 275 m from the shoreline and does not follow the channelized topography as the first simulation did, but instead spreads out wider (Figure 87 & Figure 88). A simulation with both landslide masses from above and beneath sea level was also done, but the results were almost identical to the simulation in run 2.

The fact that the simulation is spread out more widely in run 2 could be because of the Plastic rheology which has a viscosity value equal to zero. Attempts were made to model the

landslide with the Bingham rheology, which according to literature, would be the best rheology to take into account the remolded shear strength of the material. These simulations did not give any good results as the model stopped at the initial simulation time for both scenarios. For the Bingham rheology, the viscosity was given by the equation proposed by Locat and Dembers (Eq. 8), which were based on studies on Candian quick clay. It is possible the results with the Bingham rheology would be better if the velocity was calculated based on studies on Norwegian sensitive clay. However, literature on such studies could not be found.

The Kråknes landslide developed retrogressively, at least in certain stages that were observed by the eyewitness and seen in the landslide morphology. It is known that DAN3D does not have the capability to simulate retrogressive landslide behavior, and therefore, the different blocks that slid out are simulated as one big progressive slide instead of several smaller slides. The fact that the landslide masses are initiated simultaneously in the simulations gives a lower velocity rate compared to the rate of several smaller moving masses and may therefore affect the run-out distance. This is probably why the run-out of the whole release area (above and below sea) stopped at the same place as the simulation in run 2. Another factor that may affect the DAN3D results is the fact the landslide occurred both above and below sea level, and DAN3D does not consider the hydrodynamic and buoyance effects on subaqueous flows that can increase the run-out distance of the landslide and affect the velocity.

Based on the bathymetric data the landslide might have had a longer run-out distance or at least erosion in the subsea channels reached further out into the fjord than the simulations did. The landslide masses from both simulations have failed, but it is not known for sure if the landslide was initially triggered below or above sea level. The model results give a decent representation of how the landslide masses may have moved compared to the bathymetric and terrain data, even though the different factors mentioned above may have reduced or exaggerated the run-out and impact area compared to reality. The empirical estimations for channelized terrain (given that it is a retrogressive landslide) give longer run-out distances

for both run 1 and 2. The velocity output for each of the situations is very high with increasing velocity from start to finish. Even though there are no records of velocities in sensitive clay landslides, the fact that the maximum rate is reached right before the landslide comes to a complete stop is considered unrealistic. However, this seems to be a common flaw as several other authors have also found the velocity output from DAN3D to be unreasonable (Cepeda, 2007; Gebremedhin, 2013; Issler et al., 2013).

It is clear that DAN3D needs improvements when it comes to modeling landslides in sensitive clay, especially if it were to be used in risk assessment for potential landslide events. For this study, the modeling is only used to give the reader an insight on how the landslides runout possibly developed and put together with geotechnical data and field observations recreate two possible scenarios on how the Kråknes landslide event may have occurred.

5.4 Possible scenarios

Landslide initiated below sea level

A possible scenario is that the landslide was initiated below sea due to the discussed failure mechanism of excess pore pressure and predetermined instability in the slope (weak layers) below water. This would be the same as if run 1 (Figure 87) was the initial landslide, followed by run 2 (Figure 88) shortly after.

The failure below sea level led to the failure on land in section C because of the loss of support from the failed mass below (Figure 93). Based on the sequence of events by the eyewitness (Figure 74), the landslide then continued to fail retrogressively sideways because of the sensitivity of the clay and the loss of support. In sections C and D, the landslide retrogression stopped when the back wall reached the bedrock and no further backward retrogression was possible. In section B, the cross-section B-B' shows a stair-like morphology, with a sub-scarp right below mean sea level, which could suggest that the failure in this section started below sea level and retrogressed backward on land. As block 8 failed on June 3rd, the back scarp in section B was established in the glaciofluvial deposits (material 6) at about 20 m asl. Water continued to seep into this section within the glaciofluvial deposits

and soil pipes in the back scarp and from surface streams along the E6-road, which eventually led to the failure of block 12 and 13 in the upper part of section B.

In the northern part of section D, the back scarp is mainly below sea level and the top of the back scarp can barely be seen during low tides. According to the eyewitness, block 10 (Figure 93) in this section slid out after block 8 on June 3rd, 2020. Cross-sections A-A' also has morphological suggesting retrogressive behavior. This is also the only area in which the geotechnical data show that there is the presence of quick clay layers in addition to several layers of sensitive clay (S_t= 20-50). The post-landslide cross-section suggests that this section started to fail below sea level along with what is interpreted as a sliding surface at 8 mbsl before it retrogressed backward on land.
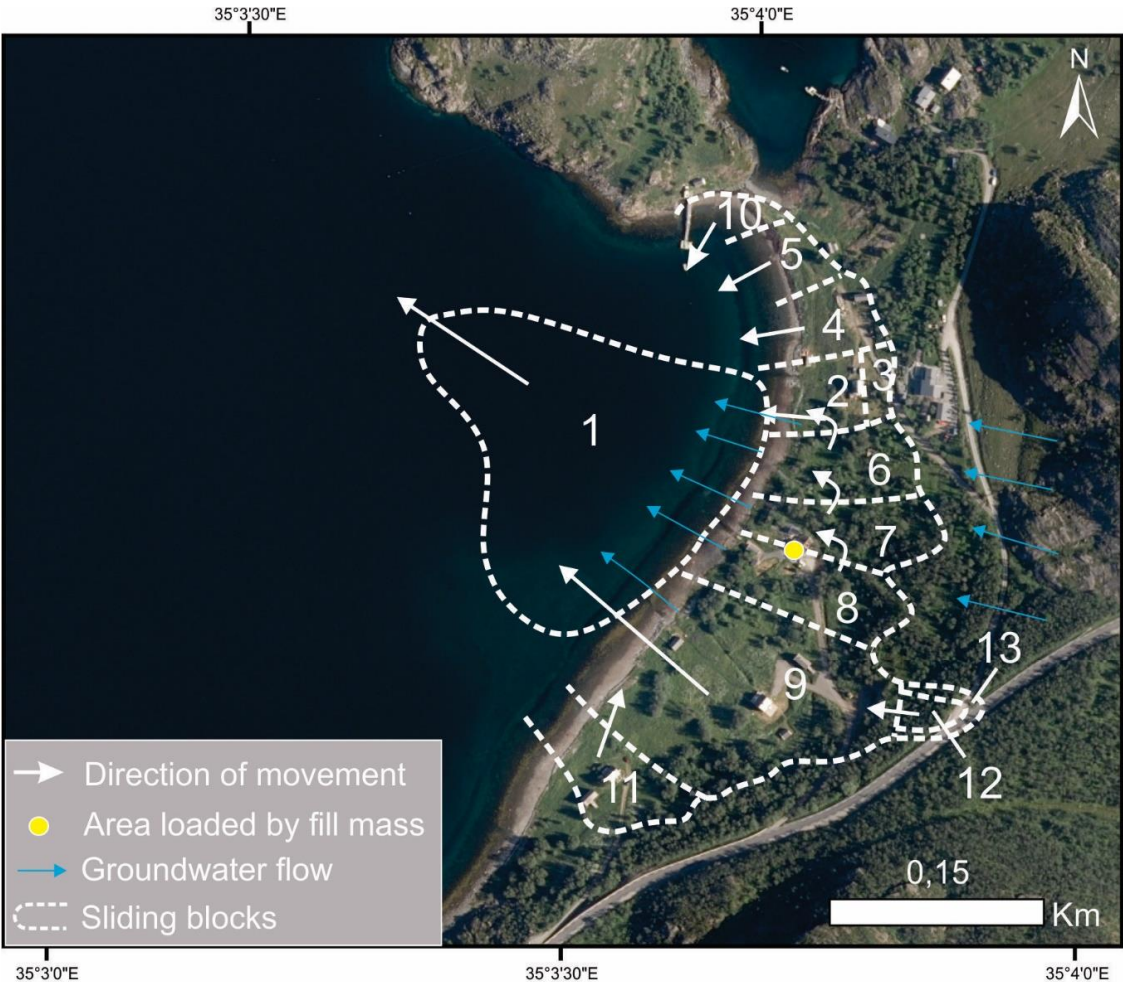

Figure 93 Sequence of events if the landslide was initiated below sea level.

Landslide initiated asl

Another scenario is if the landslide was initiated on land in section C (Figure 94), where run 2 (Figure 88) is followed by run 1 (Figure 87). The initial slide would likely be a progressive slide along a sliding surface created by strain-softening and triggered by the increased amount of meltwater. The initial slide would then cause a retrogressive failure in blocks 2-9 (Figure 94) as each block loses support when the buttressing mass below fails. The series of failures on land causes a rapid loading of landslide mass on the seafloor that eventually triggers a slide below sea level (Red circle in Figure 94). Based on the sudden descending water level explained by the coast guard, the slide below water is likely to have been triggered before block 11 in section A failed, one hour after the landslide was initiated. When the slide below sea level failed, the already sensitive block 11 failed due to the loss of support in the bottom of the slope.
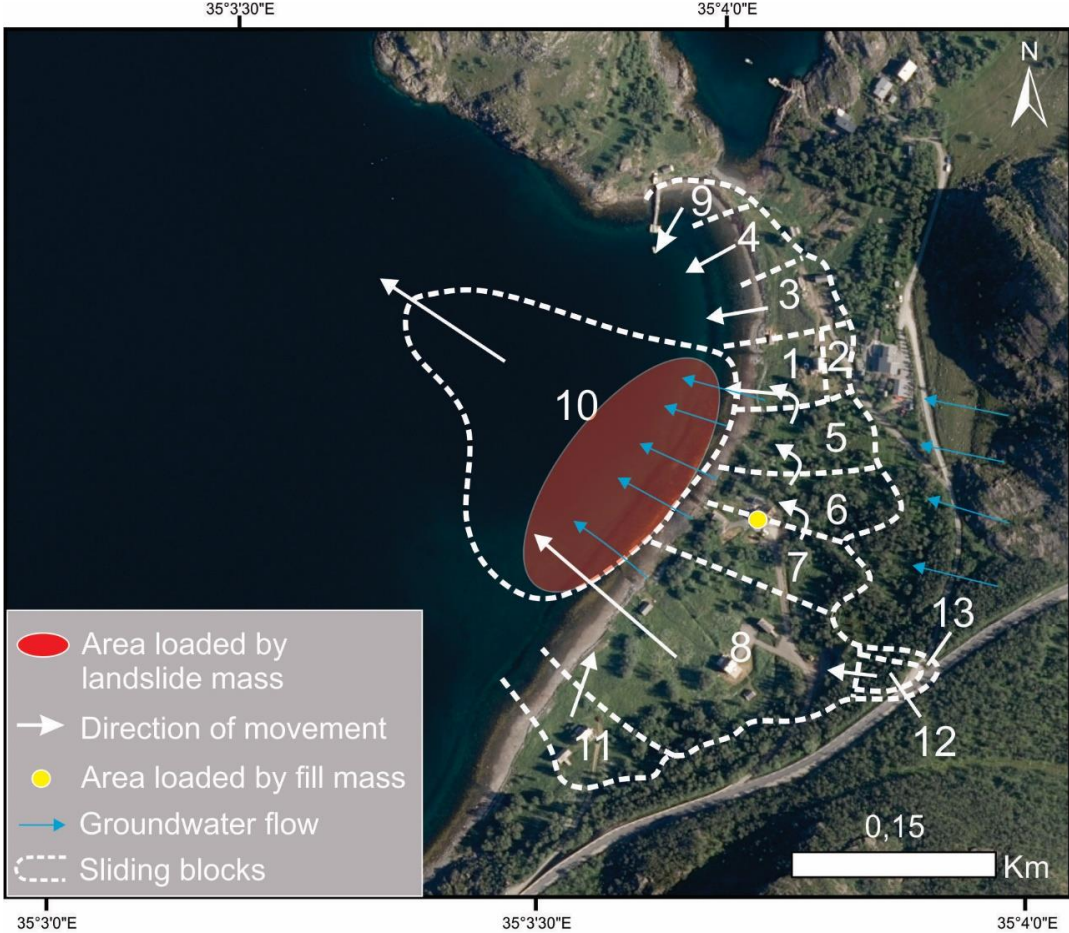

Figure 94 Sequence of events of the landslide was initiatied on land.

In the bathymetry, there is a sliding surface at 8 m bsl, which can also be seen in cross-section A-A'. Here the landslide deposits from block 11 are deposited on top of the sliding surface, supporting that the slide below sea was triggered before block 11 and supported by the stair-like morphology in cross-section A-A'. During the next two days after initiation, block 12 and 13 fail at the top of section B as explained in the first scenario.

5.5 Summary

Two different scenarios have been discussed to try and reconstruct the Kårknes landslide event based on modeling in DAN3D, geotechnical data and fieldwork. Based on the sudden descend in water level experienced by the coast guard after most of the landslide on land had already failed, in addition to the fact that there had not been observed any abnormal behavior at sea before the landslide, it seems most likely that landslide was initiated above sea level. Even though the sea slide is illustrated and modeled as one large slide, it is also possible that the failure below sea happened as several smaller events.

It might be questioned why DAN3d would not model a run-out for run 2 where the initiated landslide above sea level would trigger a slide below sea and that the whole landslide then would have a similar landslide run-out as run 2, which best fits the topography seen in the bathymetry. This could be explained by the fact that DAN3D does not account for multiple layers of different sensitivity. This means that there might be a presence of a layer of higher sensitivity below sea level (possibly a quick clay layer or weak layer), which works as a lubricating layer for the landslide mass deposited from land. That way the landslide deposits from land rides on top of the rapidly sheared quick clay and achieves a longer run-out distance.

6 Conclusion

In this study, the Kråknes landslide event that occurred in June 2020 has been reconstructed based on numerical modeling in DAN3D, geotechnical data and fieldwork. The modeling in DAN3D has helped illustrate how the landslide event may have unfolded based on the ge-

otechnical data that were put in. The model has several flaws that may have infected the re-sults of the modeling, but with the knowledge of its flaws from different literature together with observations during fieldwork, a reconstruction of the landslide and its failure mechanisms have been made. The essential findings in this study are as follows:

- The quaternary history and landscape development have created a topography and stratigraphy in the study area with sensitive clay that makes the area unstable and susceptible to pore water changes.

- Eighty truckloads of fill material added to one of the cabins in the study area caused an increase in pore water pressure and possibly strain-softening within a soil layer of little permeability, leading to the formation of a shear band and a possible sliding surface.

- After a winter of 90-300% more snow than normal, the study area was supplied with large amounts of meltwater through the glaciofluvial deposits in the ground in the days prior to the landslide event. This caused an increase in the groundwater levels and pore water pressure, which possibly led to failure in the already unstable slope.

- The landslide event was initiated in the slope above sea level (Section C) and cause a series of retrogressive and lateral failures on land. The landslide masses slid out along a sliding surface with the same orientation as the bedded stratigraphy (mainly to-wards the NW) and were deposited below sea.

- The rapid deposition of landslide mass on the seafloor initiated a slide below sea level because of the increase in total stress and pore water pressure in a weak layer due to the loading. The slide also caused failure further upslope on land due to the loss of support below sea level.

- The DAN3D software needs major improvements when it comes to simulating land-slides in sensitive clay, especially if it were to be used in risk assessment where an underestimated run-out may have severe consequences. For such work in retrogres-sive landslides, an empirical model may be more reliable.

Future work

Suggested future work would be a study on Norwegian sensitive clay to find better calcula-tions for their viscosity, similar to the work done on Canadian sensitive clay, which the vis-cosity equation provided by Locat et al. are based on (Eq. 8). Such viscosity calculation could be used for the Bingham model in DAN3D to see if there would be more satisfactory results in the run-out simulation of sensitive clay landslides. When it comes to the failure mecha-nisms at Kårknes, it would be interesting to study seismic data in the study area to see if a weak layer can be detected within the stratigraphy.

Reference list

Aarhaug, O. R. (1992). Geoteknikk [Geotechnics](1st ed.). *Vigmostad & Bjørke AS*, 109-379.

Aaron, J., Conlan, M., Johnston, K., Gauthier, D., & Mcdougall, S. (2016). Adapting and calibrating the DAN3D dynamic model for North American snow acalanche runout modelling. *International Snow Science Workshop, Breckenridge, Colorado, 2016*, 825–829.

Askheim, S. (2020). Altaelv*a*. Store Norske Leksikon. Retrived from https://snl.no/Altaelva

Aspaker, E. V. (2019). FylkesROS for Troms og Finnmark - Risiko- og sårbarhetsanaylse 2019-2021. *FylkesROS*.

Austefjord, S. W. (2016). Skred i strandsonen : Studie av skredet i Indre Sokkelvik [Landslides in the beach zone: Study of the landslide in Indre Sokkelvik], *NTNU.*

Bæverfjord, M. G. G., Bjaanes, E., & Vik, H. (2014). Leirskred - Skredmekanismer og farevurdering [Landslides - Landslide mechanisms and hazard assessment]. *Byggforskserien*.

Bjerrum, L. (1954). Geotechnical Properties of Norwegian Marine Clay. *Geotechnique*, *4(2)*, 49–69.

Bogaard, T. A., & Greco, R. (2016). Landslide hydrology: from hydrology to pore pressure. *Wiley Interdisciplinary Reviews: Water*, *3*(3), 439–459. https://doi.org/10.1002/wat2.1126

Brenner, R. P., Nutalaya, P., Chilingarian, G. V, & Robertson JR, J. O. (1981). Engineering geology of soft clay. In E. W. Brand & R. P. Brenner (Eds.), *Soft clay Engineering* (pp. 159–238). Elsevier Scientific Publishing Company.

Burland, J. B. (1990). On the compressibility and shear strength of natural clays. *Géotechnique*, *40*(3), 329–378.

Cepeda, J. (2007). The 2005 Tate's Cairn debris flow: back-analysis, forward predictions and a sensitivity analysis. *2007 International Forum Landslide Disaster Management. The Hong Kong Institution of Civil Engineers, Hong Kong*, 813–833.

Cissè, M. E. (2021, March 17). NVE: Snøsmelting og 80 lastebillass med stein utløste kvikkleireskred [Snowmelt and 80 truckloads with rocks triggered a quick clay landslide]. *Nrk.* https://www.nrk.no/tromsogfinnmark/grunnen-til-kvikkleireskredet-pa-kraknes-i-alta-var-snosmelting-og-hytteutbygging-1.15417904

Corner, G. D., Nordahl, E., Munch-Ellingsen, K., & Robertson, K. R. (1990). Morphology and sedimentology of an emergent fjord-head Gilbert-type delta: Alta delta, Norway. In *Coarse-grained deltas* (Vol. 10, pp. 155–168). International Association of Sedimentologists, Special Publication 10.

CustomWeather. (2020, Aug, 3). *Klima og gjennomsnittsvær i Alta, Norge (Climate and average weather).* Timeanddate.No. https://www.timeanddate.no/

De Blasio, F. V, Issler, D., Elverhøi, A., Harbitz, C. B., Ilstad, T., Bryn, P., Lien, R., & Løvholt, F. (2003). Dynamics, velocity and run-out of the giant Storegga slide. In *Submarine mass movements and their consequences* (pp. 223–230). Springer.

Dronedeploy. (2020, Oct.,15). *Dronedeploy*. https://www.dronedeploy.com/

Furseth, A. (2013). Skredulykker i nord [Landslide disasters in the North]. *Ottar*, *294*, 11–22.

Gebremedhin, D. (2013). *Numerical modelling of run-out of sensitive clay slide debris Daniel Gebremedhin* (Issue June). NTNU.

Gebreslassie, T. A. (2015). *Dynamic simulations of landslide runout in cohesive soils*. University of Oslo.

Geodata AS. (2020, March, 23). *SeNorge*. http://www.senorge.no/

Gregersen, O. (1981). The quick clay landslide in Rissa, Norway. *Norwegian Geotechnical Institute Publication*, *135*, 1–6.

Hansen, L., Høgaas, F., Sveian, H., Olsen, L., & Rindstad, B. I. (2014). Quaternary Geology as a Basis for Landslide Susceptibility Assessment in Fine-Grained, Marine Deposits, Onshore Norway. In J.-S. L'Heureux, A. Locat, S. Leroueil, D. Demers, & J. Locat (Eds.), *Landslides in Sensitive Clays: From Geosciences to Risk Management* (pp. 369–381). Springer Netherlands. https://doi.org/10.1007/978-94-007-7079-9_29

Hansen, L., L'Heureux, J.-S., & Longva, O. (2011). Turbiditic, clay-rich event beds in fjord-marine deposits caused by landslides in emerging clay deposits–palaeoenvironmental interpretation and role for submarine mass-wasting. *Sedimentology*, *58*(4), 890–915.

Highland, L. (2004). *Landslide types and processes*, USGS.

Highland, L. M., & Bobrowsky, P. (2008). The landslide Handbook - A guide to understanding landslides. *USGS Circular*, *1325*, 1–147. https://doi.org/10.3133/cir1325

Hoseth, K. A., Håland, G., & Kristensen, L. L. (2014). *Sikringstiltak mot skred- og flom Befaring i Troms og Finnmark høst 2012* (K. A. Hoseth (ed.)). Norges vassdrags- og energiforbund, Statens vegvesen & Jernbaneverket.

Hungr, O. (1995). A model for the runout analysis of rapid flow slides, debris flows, and avalanches. *Canadian Geotechnical Journal*, *32*(4), 610–623. https://doi.org/10.1139/t95-063

Hungr, O. (2010). DAN3D, Dynamic Analysis of Landslides in Three Dimensions (Beta Version 2) - User's manual. *O.Hungr Geotechnical Engineering.Inc*, 30.

Hungr, Oldrich, & McDougall, S. (2009). Two numerical models for landslide dynamic analysis. *Computers and Geosciences*, *35*(5), 978–992. https://doi.org/10.1016/j.cageo.2007.12.003

Indrevær, K. (2020). *Strukturgeologisk beskrivelse av Kråkneset Alta1 (002)*. NVE.

Issler, D., Cepeda, J. M., Luna, B. Q., & Venditti, V. (2013). *Back-analyses of run-out for Norwegian quick-clay landslides*, NVE

Janbu, N., Nestvold, J., & Røe, Ø. (1993). *Leirras–årsaksforhold og rasutvikling. Særtrykk fra Verdalsboka Ras i Verdal, bind B.(Clay slides, causes and development. Offprint from the book "Verdalsboka Ras i Verdal, bind B)*. ISBN 8–9909500–8-5.

Kalsnes, B., Gjelsvik, V., Jostad, H. P., Lacasse, S., & Nadim, F. (2014). Risk assessment for quick clay slides–the Norwegian practice. In *Landslides in Sensitive Clays* (pp. 355–367). Springer.

Kartverket. (2018). Retrieved from https://norgeibilder.no/

Koehl, J. B. P., Bergh, S. G., Osmundsen, P. T., Redfield, T. F., Indrevær, K., Lea, H., & Bergø, E. (2019). Late devonian–carboniferous faulting and controlling structures and fabrics in NW finnmark. *Norsk Geologisk Tidsskrift*, *99*(3), 1–39. https://doi.org/10.17850/njg99-3-5

L'heureux, J. S. (2012). A study of the retrogressive behaviour and mobility of Norwegian quick clay landslides. *Landslides and Engineered Slopes: Protecting Society through Improved Understanding - Proceedings of the 11th International and 2nd North American Symposium on Landslides and Engineered Slopes, 2012*, June, 981–987.

L'Heureux, J. S. (2012). *Characterization of historical quick clay landslides and input parameters for Q-Bing. NGI report nr 20120753-02-R*.

L'Heureux, J. S., Locat, A., Leroueil, S., Demers, D., & Locat, J. (2014). Landslides in sensitive clays– from geosciences to risk management. In *Landslides in Sensitive Clays* (pp. 1–12). Springer.

L'Heureux, J. S., Longva, O., Steiner, A., Hansen, L., Vardy, M. E., Vanneste, M., Haflidason, H., Brendryen, J., Kvalstad, T. J., & Forsberg, C. F. (2012). Identification of weak layers and their role for the stability of slopes at Finneidfjord, northern Norway. In *Submarine mass movements and their consequences* (pp. 321–330). Springer.

L'Heureux, J. S, Nordal, S., & Austefjord, S. W. (2017). Revisiting the 1959 quick clay landslide at Sokkelvik, Norway. In *Landslides in Sensitive Clays* (pp. 395–405). Springer.

L'Heureux, J.S., & Solberg, I.-L. (2013). *Utstrekning og utløpsdistanse for kvikkleireskred basert på katalog over skredhendelser i Norge*.

Landvik, J. Y., Bondebik, S., Elyerhoi, A., Fjeldskaar, W., Mangerud, J. A. N., Siegert, S., Salvigsen, O., Svendsen, J.-I., & Vorren, T. O. (1998). The last glacial maximum of Svalbard and the Barents Sea area: ice sheet extent and configuration. *Quaternary Science Reviews*, *17*(1), 43–76.

Lebuis, J., Robert, J.-M., & Rissmann, P. (1983). Regional mapping of landslide hazard in Quebec. *Rapport-Statens Geotekniska Institut*, *17*, 205–262.

Leroueil, S., Locat, A., Eberhardt, E., & Kovacevic, N. (2012). Progressive failure in natural and engineered slopes. *Landslides and Engineered Slopes, Edited by: Eberhardt, E., Froese, C., Turner, AK, and Leroueil, S., Taylor & Francis Group, London*, *3146*.

Locat, J., & Lee, H. J. (2002). Submarine landslides: Advances and challenges. *Canadian Geotechnical Journal*, *39*(1), 193–212. https://doi.org/10.1139/t01-089

Locat, J., Leroueil, S., Locat, A., & Lee, H. (2014). Weak Layers: Their Definition and Classification from a Geotechnical Perspective. In S. Krastel, J.-H. Behrmann, D. Völker, M. Stipp, C. Berndt, R. Urgeles, J. Chaytor, K. Huhn, M. Strasser, & C. B. Harbitz (Eds.), *Submarine Mass Movements and Their Consequences: 6th International Symposium* (pp. 3–12). Springer International Publishing. https://doi.org/10.1007/978-3-319-00972-8_1

Lowe, J. J., & Walker, M. J. C. (2015). *Reconstructing quaternary environments* (3rd ed.). Routledge.

Marthinussen, M. (1960). Coast and fjord area of Finnmark. *Geology of Norway*, *208*, 416–429.

Marthinussen, M. (1961). *Brerandstadier og avsmeltingsforhold i Repparfjord-Stabbursdal-området, Vest-Finnmark. En deglaciasjonsprofil fra fjord til vidde.*

Masson, D. G., Wynn, R. B., & Talling, P. J. (2010). Large landslides on passive continental margins: Processes, hypotheses and outstanding questions. *Submarine Mass Movements and Their Consequences - 4th International Symposium*, *28*, 153–165. https://doi.org/10.1007/978-90-481-3071-9_13

Mazzanti, P., & Bozzano, F. (2009). An equivalent fluid/equivalent medium approach for the numerical simulation of coastal landslides propagation: Theory and case studies. *Natural Hazards and Earth System Science*, *9*(6), 1941–1952. https://doi.org/10.5194/nhess-9-1941-2009

McDougall, S., & Hungr, O. (2004). A model for the analysis of rapid landslide motion across three-dimensional terrain. *Canadian Geotechnical Journal*, *41*(6), 1084–1097. https://doi.org/10.1139/T04-052

Metroligisk Institutt. (2020). *Yr.no: Sopnesbukt*. Retrieved from https://www.yr.no/nb/historikk/graf/5-92910/Norge/Troms og Finnmark/Alta/Sopnesbukt?q=2020

Mitchell, J. K., & Soga, K. (2005). *Fundamentals of soil behavior* (Vol. 3). John Wiley & Sons New York.

Nelson, S. A. (2015). *Mass Movements*. Tulane University.

Nesse W. (2012) *Introduction to Mineralogy* . (NO. 549 NES). Oxford University Press

New Zealand Geotechnical Society. (2005). Field description of Soil and rock. *Guideline for the Field Classification and Description of Soil and Rock for Engineering Purpose, December*, pp.3-38.

NGI. (1981). *The Quick Clay Landslide at Rissa - 1978 (English commentary)*. https://www.youtube.com/watch?v=3q-qfNlEP4A

NGI. (2011). *Kvikkleirekartlegging - Kartblad Alta (Quick Clay Mapping- Map sheet Alta) Report 20091762-00-1-R*.

NGU. (2015a). *Datasett og nedlastning [Datasets and downloads]*. Retrieved from https://www.ngu.no/emne/datasett-og-nedlasting

NGU. (2015b). *Marine Deposits and Landslides*. Retrieved from https://www.ngu.no/en/topic/marine-deposits-and-landslides

Multiconsult AS (2021). *Årsaksvurdering – Kvikkleireskredet ved Kråknes i Alta 3. juni 2020 [Cause assessment - The quick clay landslide at Kråknes in Alta 3 June 2020]*.

NVE. (2019). *Sikkerhet mot kvikkleireskred 1/2019 [Safety against quick clay landslides]*(Issue 1). NVE

NVE. (2020). *NVE Atlas 3.0*. https://atlas.nve.no/Html5Viewer/index.html?viewer=nveatlas

Ottesen, D., Dowdeswell, J. A., & Rise, L. (2005). Submarine landforms and the reconstruction of fast-flowing ice streams within a large Quaternary ice sheet: The 2500-km-long Norwegian-Svalbard margin (57–80 N). *GSA Bulletin*, *117*(7–8), 1033–1050.

Oven, D., Levanič, T., Jež, J., & Kobal, M. (2019). Reconstruction of landslide activity using dendrogeomorphological analysis in the Karavanke mountains in NW Slovenia. *Forests*, *10*(11), 1009.

Pierson, T. C. (1983). Soil pipes and slope stability. *Quarterly Journal of Engineering Geology and Hydrogeology*, *16*(1), 1–11. https://doi.org/10.1144/gsl.qjeg.1983.016.01.01

Raade, G. (2020). *Leirminerlaer*. https://snl.no/leirmineraler

Ramberg, I. B., Bryhni, I., Nøttvedt, A., & Rangnes, K. (red. . (2013). *Landet blir til - Norges geologi* (2nd ed.). Norsk Geologisk Forening.

Rankka, K., Andersson-Sköld, Y., Hultén, C., Larsson, R., Leroux, V., & Dahlin, T. (2004). *Quick clay in Sweden*.

Regobs. (2020). Retrieved 30.05.2020 from https://www.regobs.no/Registration/237480

Reite, A., Sveian, H., & Erichsen, E. (1999). Trondheim fra istid til nåtid-landskapshistorie og løsmasser (Trondheim form the ice age to the present). *Grasteinen*, *5*, 1–40.

Romundset, A., Akçar, N., Fredin, O., Tikhomirov, D., Reber, R., Vockenhuber, C., Christl, M., & Schlüchter, C. (2017). Lateglacial retreat chronology of the Scandinavian Ice Sheet in Finnmark, northern Norway, reconstructed from surface exposure dating of major end moraines. *Quaternary Science Reviews*, *177*, 130–144. https://doi.org/10.1016/j.quascirev.2017.10.025

Romundset, A., Bondevik, S., & Bennike, O. (2011). Postglacial uplift and relative sea level changes in Finnmark, northern Norway. *Quaternary Science Reviews*, *30*(19–20), 2398–2421. https://doi.org/10.1016/j.quascirev.2011.06.007

Sandnes, T. (2021). *Geotechnical investigation of the Kråknes landslide*, UiT.

Siegert, M. J., & Dowdeswell, J. A. (2004). Numerical reconstructions of the Eurasian Ice Sheet and climate during the Late Weichselian. *Quaternary Science Reviews*, *23*(11–13), 1273–1283. https://doi.org/10.1016/j.quascirev.2003.12.010

Sigmond, E. M. O., Bryhni, I., & Jorde, K. (2013). *Norsk geologisk ordbok [Norwegian geological dictionary]* Akademika.

Skempton, A. W. (1948). A study of the geotechnical properties of some post-glacial clays. *Geotechnique*, *1*(1), 1–16.

Skempton, A. W. (1953). The Colloidal "Activity" of Clays. *Selected Papers on Soil Mechanics*, 60–64. https://doi.org/10.1680/sposm.02050.0009

Sollid, J. L., Andersen, S., Hamre, N., Kjeldsen, O., Salvigsen, O., Sturød, S., Tveitå, T., & Wilhelmsen, A. (1973). Deglaciation of Finnmark, North Norway. *Norsk Geografisk Tidsskrift-Norwegian Journal of Geography*, *27*(4), 233–325.

Statens vegvesen. (2014). Labratorieundersøkelser [Labratory investigations]. *Håndbøker i Statens Vegvesen*, *Håndbok R210*, 112–146.

Statens Vegvesen. (1997). Feltundersøkelser- Retningslinjer[Field surveys- guidelines]. *Vegvesenets Håndbokserie*, *015*(022).

Strand, S.-A., Thakur, V., L'Heureux, J.-S., Lacasse, S., Karlsrud, K., Nyheim, T., Aunaas, K., Ottesen, H. B., Gjelsvik, V., & Fauskerud, O. A. (2017). Runout of landslides in sensitive clays. In *Landslides in Sensitive Clays* (pp. 289–300). Springer.

Svendsen, J. I., Astakhov, V. I., BOLSHIYANOV, D. Y. U., Demidov, I., Dowdeswell, J. A., Gataullin, V., Hjort, C., Hubberten, H. W., Larsen, E., & Mangerud, J. A. N. (1999). Maximum extent of the Eurasian ice sheets in the Barents and Kara Sea region during the Weichselian. *Boreas*, *28*(1), 234–242.

Terzaghi, K., Peck, R. B., & Mesri, G. (1996). *Soil mechanics in engineering practice*. John Wiley & Sons.

Thakur, V, Degago, S. A., Oset, F., Aabøe, R., Dolva, B. K., Aunaas, K., Nyheim, T., Lyche, E., Jensen, O. A., Sæter, M. B., Robsrud, A., Viklund, M., Nigussie, D., & L'Heureux, J.-S. (2014). Characterization of Post-failure Movements of Landslides in Soft Sensitive Clays. In J.-S. L'Heureux, A. Locat, S. Leroueil, D. Demers, & J. Locat (Eds.), *Landslides in Sensitive Clays: From Geosciences to Risk Management* (pp. 91–103). Springer Netherlands. https://doi.org/10.1007/978-94-007-7079-9_8

Thakur, V, & Nigussie, D. (2014). Run-out of sensitive clay debris: significance of the flow behavior of sensitive clays. *Geotechnical Engineering*, *45*(3), 22–31.

Thakur, V, Nigussie, D., & Degago, S. A. (2014). A preliminary study of rheological models for run-out distance modelling of sensitive clay debris. *Numerical Methods in Geotechnical Engineering*, *1*, 115.

Thakur, Vikas, Nordal, S., Viggiani, G., & Charrier, P. (2018). Shear bands in undrained plane strain compression of Norwegian quick clays. *Canadian Geotechnical Journal*, *55*(1), 45–56. https://doi.org/10.1139/cgj-2016-0443

Vorren, T. O., & Laberg, J. S. (1996). Late glacial air temperature, oceanographic and ice sheet interactions in the southern Barents Sea region. *Geological Society, London, Special Publications*, *111*(1), 303–321.

Walberg, Ø. (1993). *Verdalsboka - Ras i verdal [The book of Verdal- Landslides in Verdal] (Bind A)*. Verdal kommune v/bygdeboknemnda.

WGS. (2017). What are landslides and how do they occur? *Washington Geological Survey*. https://www.dnr.wa.gov/geology

Wiig, T., Haugen, E. E. ., Strand, S.-A., Gjelsvik, V., Gylland, A. S., Øiseth, E., & L'Heureux, J.-S. (2019). *Sikkerhet mot kvikkleireskred [Safety against quick clay landslides]*. NVE. http://publikasjoner.nve.no/veileder/2014/veileder2014_07.pdf

Zwaan, K. B., & Gautier, A. M. (1980). *Alta og Gargia Beskrivelse til de berggrunnsgeologiske kart 1834 I og 1934 IV -M 1:50000 [Alta and Gargia descriptions of geological bedrock map 1834]*. Universitetsforlaget.

Appendix

Appendix A: Geotechnical data

Borehole locations:
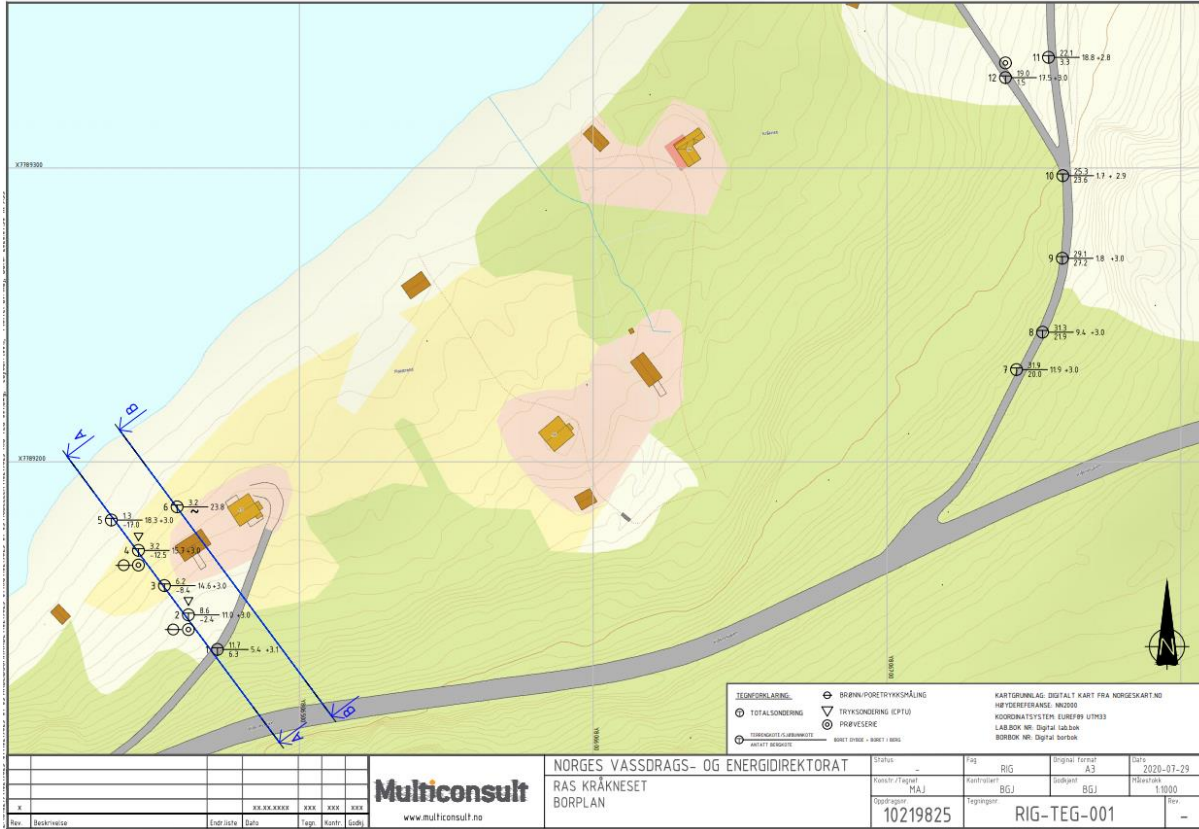
Core sample from borehole 2:

Dybde (m)	Beskrivelse		Prøve	Test	Vanninnhold (%) og konsistensgrenser	ρ (g/cm³)	Porøsitet (%)	Organisk innhold (%)	Udrenert skjærfasthet (kPa)	S_t (-)
		kt. 8,59			10 20 30 40 50				10 20 30 40 50	
	LEIRE	sand- og siltlag, enkl.gruskorn				1,92				16
5										
	LEIRE	sand- og siltlag, enkl.gruskorn				1,95				10 / 11
	LEIRE, siltig	forstyrret, sand- og siltlag, enkl.gruskorn		K		1,96			0,8	8
10	LEIRE, siltig	sand- og siltlag, enkl.gruskorn				1,98			1,3	12 / 16
15										
20										

Symboler:

Enaksialforsøk (strek angir aksiell tøyning (%) ved brudd)

- ○ Vanninnhold
- ⊢ Plastisitetsindeks, Ip
- ▼ Omrørt konus
- ▽ Uomrørt konus
- ρ = Densitet
- S_t = Sensitivitet

- T = Treaksialforsøk
- Ø = Ødometerforsøk
- K = Korngradering

ρs: 2,75 g/cm³
Grunnvannstand: m
Borbok: Digital
Lab-bok: Digital

PRØVESERIE

Borhull: 2

Norges vassdrags- og energidirektorat

Dato: 2020-06-25

Ras Kråkeneset

Multiconsult
www.multiconsult.no

Konstr./Tegnet: TEREZK	Kontrollert: MARTM	Godkjent: BGJ
Oppdragsnummer: 10219825	Tegningsnr.: RIG-TEG-200	Rev. nr.: 00

Core sample from borehole 4:

Core sample from borehole 12:

Appendix B: Grid-file preparations for DAN3D

Steps to create the path topography file for DAN3D in ArcMap 10.5 and Surfer golden software.

1. Open the post landslide DEM-file in ArcMap.

2. Convert the path topography file to a ASCII file by using the convert from raster tool in the Arctoolbox and save the ASCII file.

3. Open the ASCII file in Surfer and convert the file to (.dat) file by clicking: Grids → Convert. Select the ASCII file and save as (.dat) file.

4. Grid the (.dat) file by clicking Grid Data. Choose the Kriging method. Check that the (.dat) file is listed with X = X-coordinate, Y= Y-coordinate and Z= elevation.

5. Change the output as preferred, but make sure the path topography and the source topography have the same geometry.

6. See DAN3D user manual for more details on the output geometry of the grid file.

Steps to create the source topography file:

1. In ArcMap, subtracted the post-landslide DEM-file from the pre-landslide DEM-file with the raster calculator and a raster of the path topography will be created.

2. Convert the raster to an ASCII file and open in Surfer, OR convert both the pre and post-landslide DEM to ASCII and subtract using the Math tool in Surfer.

3. Open the ASCII file in Surfer and convert to (.dat) file as described in step 3 above.

4. Open the (.dat) file in Surfer or excel and replace the value zero (the area surrounding the landslide volume) with the no data value used in surfer (See DAN3D user manual) and save the file.

5. Grid the file by using the Nearest Neighbor method. Make sure it has the same geometry output as the path topography grid.